The University Of Sheffield.

The Cyclic Response of Mudrock

The University of Sheffield

Department of Civil and Structural Engineering

PhD Thesis

By:
Shaymaa Kennedy

Supervisors:
Dr Sam Clarke, Dr Paul Shepley

2019

Acknowledgements

Firstly, I would like to thank my supervisor Dr Sam Clarke, for being a source of constant guidance and advice throughout the period of this research. The quality of the work owes much to his dedication and attention to detail.

My thanks also go to Dr Paul Shepley for his guidance regarding the experimental setup and the departments technical staff for their support in the experimental work. Special appreciations to Mark Foster and Paul Osborne

Special thanks also go to the soul of my dearest father, his kindness and inspiration, and to my mother for her support during my PhD journey

Many thanks to Dr Nicoletta Sanvitale for her help support and kindness. Without her I could not have completed this thesis. I would also to thank all my family and friends.

This research project was made possible through support from the Iraqi Government.

Abstract

With the upcoming construction of High Speed Rail 2, (London to the 'North') a number of issues surrounding the construction technology and track design need to be answered. Previous experience in the UK rail industry has been based on ballasted track but this is not necessarily the most appropriate choice for new high speed rail construction. This project aims to investigate the use of different track types and the influence they will have on the underlying soil. In the case of this project that soil is mudrock, a weak prevalent rock which response under indicative loading of a high speed rail line is unknown. Ballastless track is a well established concept in Europe. This project aims to investigate the benefits of this form of construction due to its known savings in maintenance costs. In order to evaluate the behaviour of the underlying soil, physical tests will be conducted to assess the mechanical behaviour of mudrock under a range of dynamic loads which could be generated beneath different track constructions.

Some further parameters are required to frame the problem, including determining the stress change with depth and cyclic response to determine the cumulative strain which is of major concern. The shear strength of the soil highly depends on the stress-strain state during the passage of the axle load, which the study will aim to recreate in the laboratory.

Increasing water content, decreasing particle size and loading frequency were found to reduce the stiffness of the mudrock tested. Load frequency was found to have a positive effect on the performance of the soil. Inundation of the soil after a set of cyclic loading has been shown to significantly affect the performance by reducing the stiffness of the soil and increasing the settlement. Mudrock colliery spoil in the conditions simulated in this research can be classified as a medium stiffness subgrade. Settlement can be controlled with proper compaction and drainage of the material which will enable its use as a railway foundation subgrade.

Contents

List of Figures

List of Tables

Chapter 1

Introduction

With an increasing population, the shift in focus from London being the central hub of the UK economy can only be attained if transport links between London and the rest of UK and further afield are improved. To some extent High Speed 1 (London-Paris) pioneered this approach, with High Speed 2 (HS2) now on the horizon a very new engineering challenge is emerging. This involves combining the new technology which HS2 requires with known but undefined problem soils across the UK. With the focus of HS2 being on increased capacity, maintenance needs to be minimised to maximise this capacity. This in turn may lead the UK rail industry in the future to face a difficult choice, to continue using the tried and tested ballasted track system or to move to a more expensive but less maintenance heavy ballstless track (slip formed concrete). In order for the UK rail industry to make an informed decision on which track solution to use, the mechanical behaviour of the underlying soil must be known. For HS1 this was Clay and limestone, on which much research has been conducted. For HS2 other 'problem soils' use as areas of colliery spoil may have to be built on. This leads to a requirement to evaluate the behaviour of such soils. In this study an investigation into the performance of mudrock as a subsoil under high speed rail will be performed.

Soil is exposes to dynamic stress during life time; the sources for this load could be caused by seismic activity, passing traffic or vibrating machinery during installed structure and those which are generated by a waveform to soil which is dependent on the load source, in railway systems the waveform consists of a single frequency and that will need advanced test systems. High speed railway is one of the most important innovations affecting passenger transportation since the Second World War. During recent decades, completely new technology for high speed railway vehicles has been developed. This has led to new problems dealing with the interaction between the vehicles, track, and the underlying soil. In addition, dynamic effects which are associated with cyclic loading are generated due to train motion, this phenomenon can be reflected on the behaviour of soil

because its related with stiffness and the dissipation of energy (O'Reilly et al., 1991).

The UK has intended to design and construct high speed railway two (HS2) to connect with high speed railway one (HS1). This route will pass from London up to the Midlands as shown in Figure 1.1. This thesis will spot light on the sections of the HS2 line crossing over areas of colliery spoil near Sheffield which is part of the UK's mining legacy. This soil is made up of many types of rocks including: mudstone, siltstone, sandstone, claystone, ironstone and coal with a range of mineral species (Collins, 1976). It is already known that this type of soil has a tendency to settle which is dependent on factors such as moisture content, particle size distribution and soil state (Nahazanan, 2010). These studies until now, have been limited to static tests to determine behaviour. This study aims to investigate the performance of colliery spoil under dynamic loading with varying stress level and different water content and particle size distributions. This will involve in depth characterisation of the colliery spoil, adding to current knowledge base for this material. Furthermore, fluctuation of ground water level causes effective cyclic loading and that will be taken into consideration in this project.

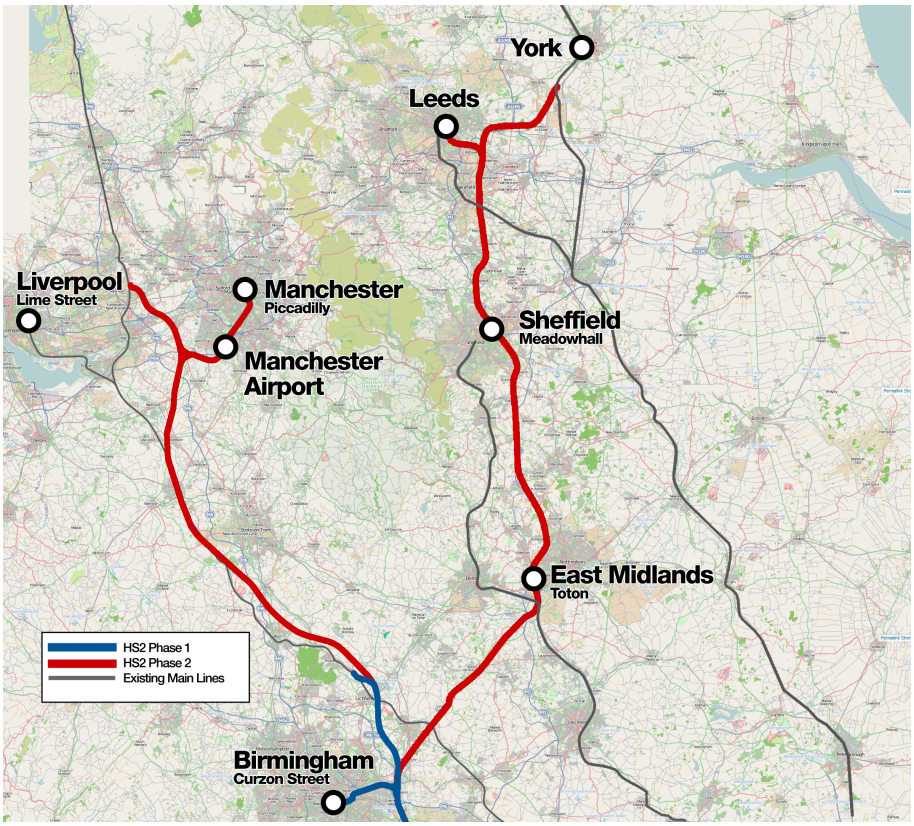

Figure 1.1: HS2 proposed route, downloaded from BBC

In studying the dynamic load behaviour of this soil, the different testing methodologies

will also be discussed, these include the triaxial cyclic loading test and standard triaxial test. A review of the relevant literature is presented in Chapter 2, with the definition of mudrock, typical characteristics and engineering properties being covered. Chapter 3 describes the detailed methodology and the programme of experimental work undertaken. Triaxial cyclic loading and traditional triaxial test apparatuses were utilised. The results of the testing are divided into two chapters. Chapter 4 discusses the effect of water content and grain size distribution on the cyclic behaviour of mudrock. Chapter 5 presents the effect of the stress level induced from train passage on the cyclic behaviour of mudrock. Chapter 6 summarises the work done and the discusses the apparent trends. Finally, Chapter 7 presents the conclusions and recommendations for future work.

1.1 The aim of the research

The performance of the railway track is based on the interaction between the subgrade and superstructure. Thus, appropriate track support is important for both ride quality and to reduce track and vehicle maintenance costs. To reduce maintenance costs a better understanding of the properties of the supporting soil (which includes both prepared soil and in situ conditions) are required. The resilient modulus or stiffness is an important parameter for the characterization of the supporting soil. This is defined as the interaction between the vertical displacement of the track and the applied load. In this project the stiffness of subgrade layers underneath the railway truck structure will be quantified, as this factor is essential to characterise the engineering properties with which to design suitable structures. In this project resilient modulus is measured at magnitudes and frequencies of loading applicable to field conditions, this will attained by:

1. Investigating the effect of water content on the stiffness behaviour by choosing different soil conditions: fully saturated, soil compacted at optimum moisture content (OMC), soil compacted at water content less than optimum moisture content and fully dry conditions.

2. Investigating the effect of particle size distribution as changing the particle distribution influences the wetting conditions.

3. Investigating the effect of stress state by simulating field condition under different track constructions and investigating how this may change with depth.

Chapter 2

Literature Review

2.1 Preface

The subgrade is an essential component of the track structure, and has an significant impact on the behaviour of the track. The engineering properties must be considered in order to effectively estimate the subsequent track quality. Thus, investigation of subgrade has been the aim of numerous investigations to prevent subgrade failure. Progressive shear failure and excessive deformation are major causes of subgrade problems due to repeated loading. This chapter is divided into two parts, the first part (Sections 2.2–2.4) presents the history of the material of study and characterisation. The second part (Sections 2.5 onwards) discusses the main literature that concentrates on the engineering properties for the structural elements of the track and the factors that have an effect on their performance.

2.2 Mudrock colliery spoil

Mudrock as a material description, covers a wide range of soil that have different properties, ranging from soils to strong rocks, commonly containing greater than 50% clastic grains of less than 60 µm. Hence, Dick and Shakoor (1992) describe it as having a broad range of lithotypes classified as poorly indurated low durability soil-like deposits to low-grade slates and argillites that rock-like properties. Whilst, Potter et al. (2005) defined the mudrock as a indurated terrigenous, fine-grained rock composed of 33–65% clay size constituents with stratification greater than 10 mm. According to Taylor and Spears (1981) if the material has a high degree of visible laminations, fissures or parting, it is a shale whilst if it is not fissile and wholly intact, it is a mudstone. In addition, the term of colliery spoil is used to describe sandstone, shale and coal laminated deposits that are found in large quantities in widespread areas of the UK, see Figure 2.1. These sedimentary strata,

commonly known as minestone were formed 296–315 million years ago, at that time similar coal measures in North America were formed. For early formation, most of Britain and much of Europe were situated between the Caledonia mountains to the north and shallow seas of the continental shelf to the south. Large populations of plants started to grow in wet coastal areas, and ground river, the debris of which eventually become coal. As a result of uplift and erosion, over time the coal measures is exposed and appears at the surface. This sequence is still preserved beneath a cover of later rocks that conceals the coal field area around the UK.

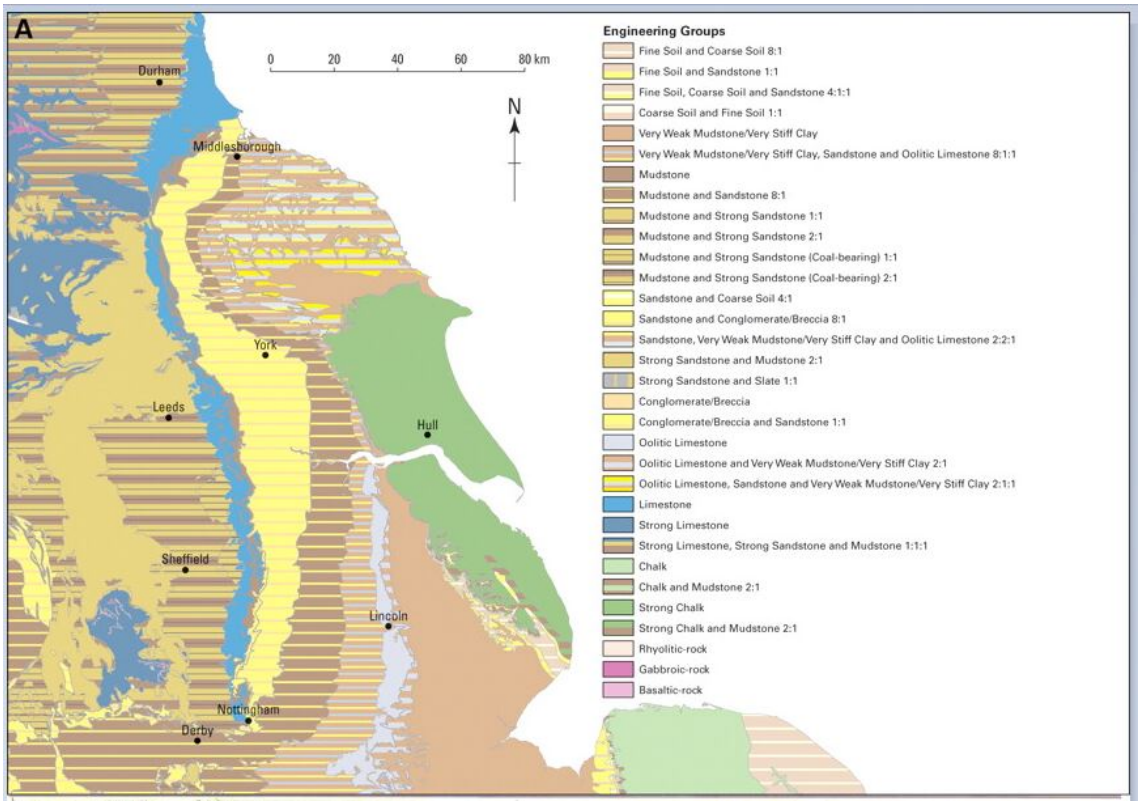

Figure 2.1: Engineering geology map of the UK, Dobbs et al. (2012)

2.3 Engineering properties of mudrock

Taylor and Spears (1970) and Cripps and Taylor (1981) found that the engineering properties for mudrock strongly depend on their mineralogy, shape and distribution of the grains size and structure, lithology and geological history. The shear strength for such rocks were categorized as very strong in dry situations and soft, friable soils as the water content increases. This leads to the breakage of inter-particles bonds, which in turn leads to increased deformability. The specific gravity for this rock is low comparing with the

other rocks and soil because of the organic content in the strata (Rainbow, 1987). They also concluded that South Yorkshire mudrock can be ranked as intermediate strength. Taylor and Garrard (1984) collated the results for thousands of specimens from around the UK and concluded that the effective angle of shearing resistance was from 22.5° to 46.5°. The mudrock in the UK is characterised as a shale or mudstone with less than 2/3 visible laminations and fissures, and with greater than 2/3 as a siltstone or sand. Taylor (1988) described the mudrock as durable and non-durable mudrocks depending on cyclic slake durability with value over 60% which was used to discern between durable and non-durable rocks. Franklin and Chandra (1972) first proposed the category for shale based on its durability index to become a standard test by measuring the slake durability of mudrocks in International Society for Rock Mechanics (ISRM). A slaking test is an essential test when evaluating rocks that have an ability to break down such as mudrock. In addition, other researchers have classified mudstone and shale based on their liquidity index (Morgenstern and Eigenbrod, 1974). Nahazanan (2010) found that the angle of shearing resistance of partially saturated and fully saturated mudrock are lower than that exhibited in dry conditions. This showed that the reduced shear strength and dilatant properties of mudrock were due to the presence of water. Furthermore, the results showed that the settlement behaviour is strongly influenced by initial water content, particle size distribution and soil state.

2.4 Mineralogy of mudrock

Mudrocks have a wide range of minerals due to diagenetic changes during the deposition process (Czerewko and Cripps, 2006). In the UK, X-ray diffraction (XRD) is widely utilised to distinguish between the minerals. However, there are other techniques such as optical microscope (OM), electron microprobe analysis (EPMA) and scanning electron microscopy (SEM), which also provide soil mineralogy. In Japan, Dhakal et al. (2002) used all the techniques mentioned above to investigate the composition and textural features of the rocks to understand the relationship between the mineralogy and durability of the rocks. It can be concluded that the argillaceous clastic rocks strongly affect the slake durability of the rocks as some minerals has ability to swell. The slake durability might also be impacted by changes to the rock mass by weathering, diagenesis and hydrothermal processes on a geological time record.

In some areas of the UK such as Worcestershire, Gloucestershire, Nottinghamshire and Leicestershire, Dumbleton and West (1966) found during the investigation of the mineralogical composition of Keuper Marl the clay minerals illite, chlorite and quartz present in all samples with variable percentage. The rocks are present in all samples with

Table 2.1: The average mineralogy of UK coal measures colliery spoils, Taylor (1988)

	Mineral	Proportion (%)
Clay minerals	Illite	27.0
	Illite-Smectite	17.0
	Kaolinite	20.0
	Chlorite	0.5
	Total	65.0
Non-clay minerals	Quartz	16.5
	Pyrite	2.5
	Organic Carbon	1.0
	Feldspar	0.5

varying percentage. The rocks present in colliery spoil are the same as those within the coal measures sequence, but spoil is extracted during underground working and these usually have highly variable proportions of rocks especially mudstone, siltstone, sandstone clay stone, ironstone and coal (Collins, 1976). The more common materials evolving in colliery spoil are quartz 20%, mica and clay minerals 75%, and lesser quantities of pyrites and carbonates of calcium, magnesium and ironstone or sulphates. In British coal measures Taylor and Smith (1986) reported that smectite is absent in their composition as a pure phase as presented in Table 2.1.

2.5 Track structure

Railway infrastructure consists of a track superstructure (rail, tie, fastener, turnout, crossing and diamond) and substructure (ballast, subballast, subgrade and drainage). Track components have been developed to become more durable and to optimise the use of materials, and use materials such as concrete and steel, for precautionary maintenance. Consequently, the stress transmitted into the ground due to the train loading leads to different track deformation performances.

There are two types of rail tracks: ballasted and ballastless. In the UK most tracks are ballasted, which notably also includes HS1. The options for HS2 currently include using a ballastless track to join London to the West Midlands. This would aim to create a maintenance-free railway, meeting the low deflection design criteria required of HS2, and may restrict the use of traditional ballast-based track beds. The performance of railway track depends on the behaviour of underlying subsoil over the life of the track. Thus, design of the structure of high speed railways needs to consider the mechanical properties of the subgrade soil in order to quantify the response of the soil under repeated wheel loading, and to find an adequate design against the deterioration of the track in the long

term (Brown, 1996). In addition, track performance has been found to depend on the stress path. and train speed, both lead to cumulative permanent deformation that will affect the behaviour of the track structure. This section describes some research that has studied the behaviour of railway track.

It is known that the maximum dynamic stress increases linearly with train speed, and the dynamic stress distribution is needed to identify the factors that affect the behaviour of the structure of the train such as wheel loads, material of underground soil, train speed, and depth (Gräbe and Clayton, 2009). The dynamic load, which is induced from the movement of the train can be considered according to a theoretical analysis of a stress wave penetrating into the soil. This load applied from the moving wheels generates stress pulses in the soil, each pulse includes three components: vertical, horizontal and shear causing rotation of the principal stress axes. The deformation response of soil under repeated loading, is defined by a resilient and a permanent deformation response. In other words, these layers expose a combination of resilient strains which are recovered after each load cycle, and permanent strains that control the total deformation after each load cyclic. For design purposes, it is important to consider how the materials involved in the design react and the how the resilient behaviour varies with changes in various influencing factors.

Hanazato et al. (1991) used numerical methods based on half space theory to simulate the stress wave which is generated by the train passing. However, direct in-situ measurements are required to calibrate the existing analytical model. This method is expensive but it gives a realistic assessment.

2.6 Design of ballasted track

Ballasted track is widely used throughout the world because it has a low construction cost, is easy to maintain, through this is frequent, and uses simple design and construction processes. However, there are disadvantages in using this type of track, such as degradation of the ballast and disruption of traffic during the inevitable maintenance operations causing a large problem in behaviour of the track system. Much research has been conducted in order to cope with these problems, particularly the differential settlement which results from the long term cyclic loads. The main parameters that affect track performance are explained in detail in the sections below.

2.6.1 Influence of stress change on the ground below rail structure

Generally, train movement generates stress cycles, and these stresses are transmitted into the ground below the track. The magnitude of the stress cycles decrease with depth due to the spread through the soil. This stress can be measured by the resilient modulus of

the underlying soil. The level of propagation is dependant on properties of the ground soil: strength, stiffness, deformation and failure due to transmitted loads. When the stress level is below the threshold for failure, this will represent a critical level of cyclic stress, while if the stresses exceed this level; plastic deformation will be higher, leading to failure. The estimation of these stresses is complex involving a cyclic rotation of the principal stress directions in some cases. In order to evaluate the performance of the underlying track structure during train passage, much research has been studied on the effect of stress paths which are induced by the movement of the train.

Most laboratory tests on railway foundations have been conducted using triaxial cyclic loading. The limitation of the triaxial cell means that tests do not impose the real scenario to account for the principle stress rotation. Some researchers have used the hollow cylinder apparatus (HCA) which allows the rotation of the major and the minor principal stresses to be taken into account. However, the permanent deformation and stiffness investigations tend to be based on triaxial cyclic loading because of the complexity of the HCA apparatus and limitation of its use (Gräbe and Clayton, 2009). Powrie et al. (2007) analysed the stress distribution by using 3D finite element analyses for each vertical and horizontal, normal and shear stresses. A geotextile layer over a prepared sub-grade was used to model experimental tests for wheel loads of 125 kN (being the maximum allowable static load in the UK). A typical loading scenario is shown in Figure 2.2, with a typical track structure being shown in Figure 2.3.

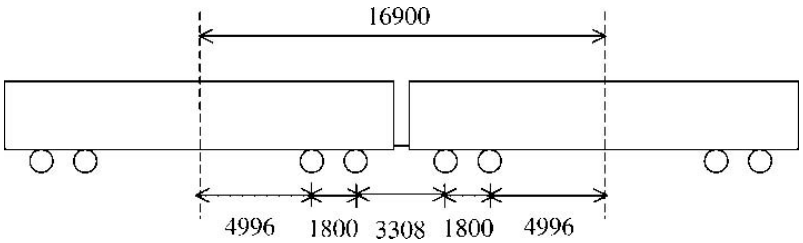

Figure 2.2: The configuration of wheel load that utilized by, Powrie et al. (2007)

In the Powrie et al. (2007) study, input parameters of geotechnical materials were modelled as linear elastic using Poisson's ratio and Youngs modulus as elements of soil below the track as shown in Table 2.2. Cyclic rotation of the principle stress directions are considered in order to find out the vertical strain by using hollow cylinder apparatus in which principal stress rotation is considered. They found both the magnitude and frequency of cyclic loading reduces with depth, because of the load propagation through the soil was changed from axial loading at $0.13S$ to bogie loading at $0.49S$ to wagon loading at $1.67S$ (Where, S = length of sleeper in mm). In Figure 2.4, it can be seen that vertical stress increases with depth.

Table 2.2: Soil properties used in finite element analysis, Powrie et al. (2007)

Soil description	Young's modulus (MPa)	Poisson's ratio	Unit weight (kN/m^3)	Observation
Prepared soil	100	0.49	19.6	
Natural soil	30	0.49	19.6	*E=30+mz (where m=4.5 MPa/m)

Notes: *E =Young modulus for natural ground.

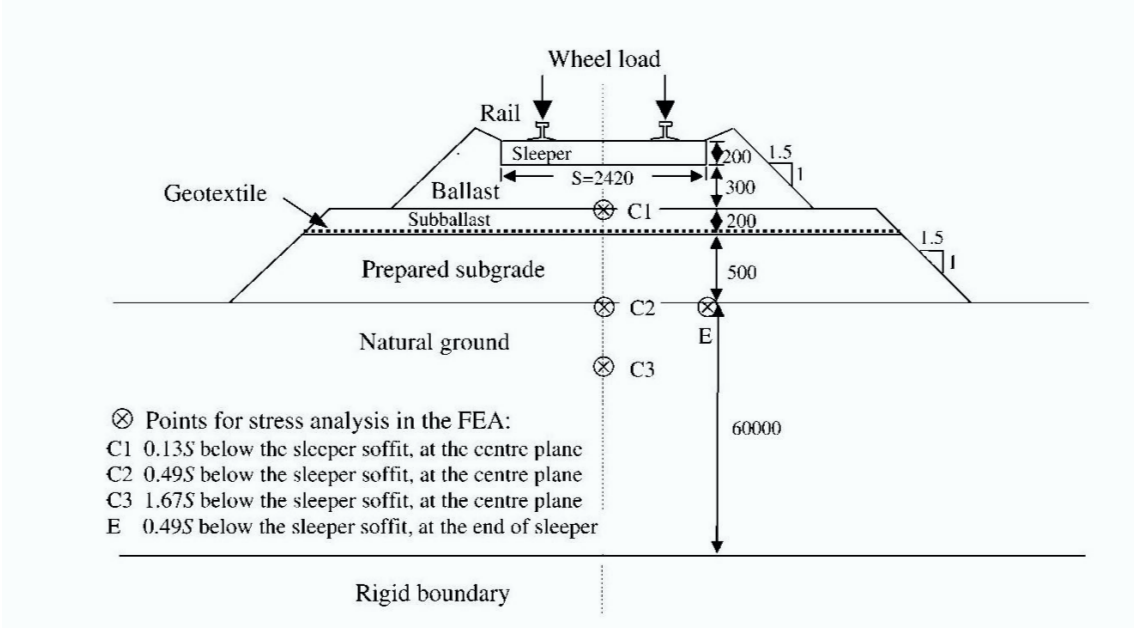

Figure 2.3: Diagrammatic cross-section of typical track structure, Powrie et al. (2007)

In addition, experimental results of stress path to the top of the natural soil layer set at depth $0.49S$ shown in Figure 2.5 is identified and simulated with central longitudinal plane, and modelled by application of an appropriate combination of initial axial load, inner and outer confining pressure and pore water pressure.

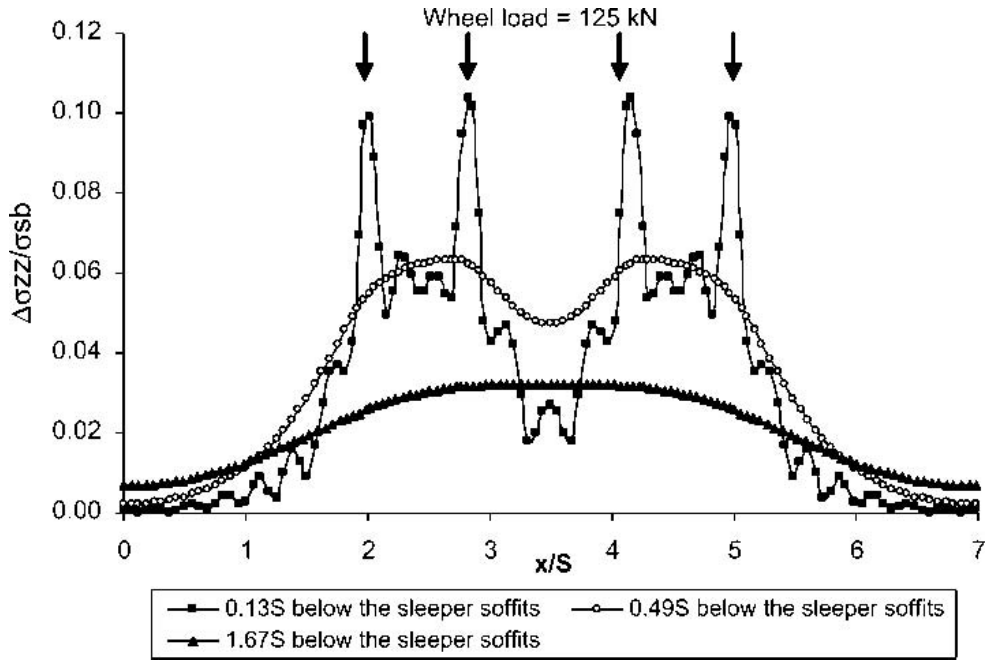

Figure 2.4: Incremental of vertical stress with depth, Powrie et al. (2007)

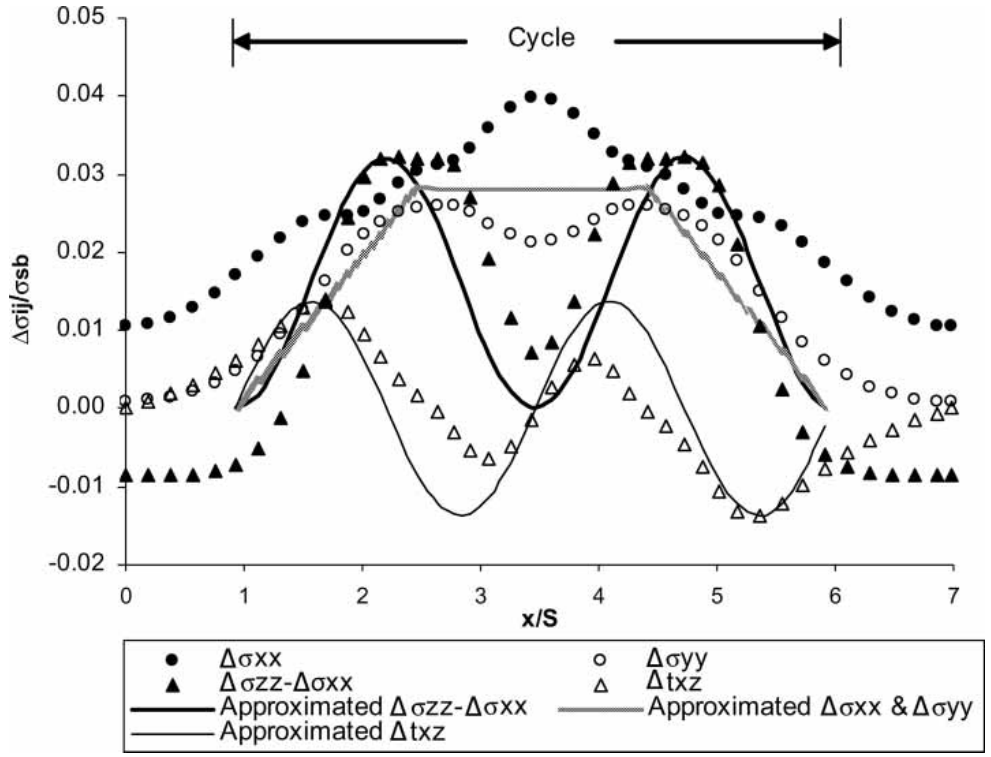

Figure 2.5: Estimation of stress path at the surface of natural soil at depth of 0.49S induced by train pass, Powrie et al. (2007)

Table 2.3: Soil properties used in finite element analysis, Yang et al. (2009)

Soil description	Young modulus (MPa)	Poisson's ratio	Density (kg/m^3)
A	143	0.3	2,100
B	118	0.3	2,100
Natural soil	27,000	0.25	2,300

Yang et al. (2009) studied a railway track at Boubank, 60 km south of Vryheid, South Africa using 2D dynamic finite element package Abaqus (ABAQUS, 2005). Natural ground was modelled as linear-elastic and assuming three typical wagons pass. Figure 2.6 shows the numerical mesh used where the subgrade has been modelled as three layers SSB, A and B with the natural soil below. The properties of modelled soil are shown in Table 2.3. Yang et al. (2009) normalized the relationship between the theoretical stress components and maximum surface stress, divided by sleeper area and ballast stress σ_{sb} with time to calculate the stress path at depths 0.45, 0.75 and 1.2 m. It was found that in these layers transmitted stresses below the track were larger than those at deeper depth. From Figure 2.7 it could be concluded that the displacement and shear failure are more probable at a shallower depths, as the load frequency will be higher .

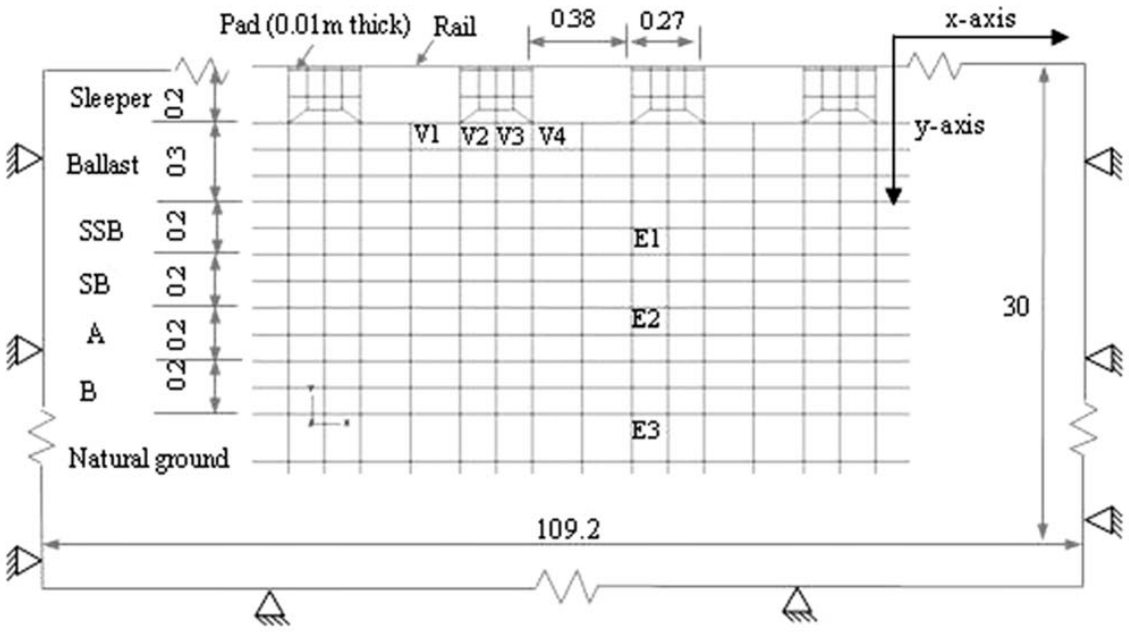

Figure 2.6: Analysis method of Bloubank test site by using finite element, Yang et al. (2009)

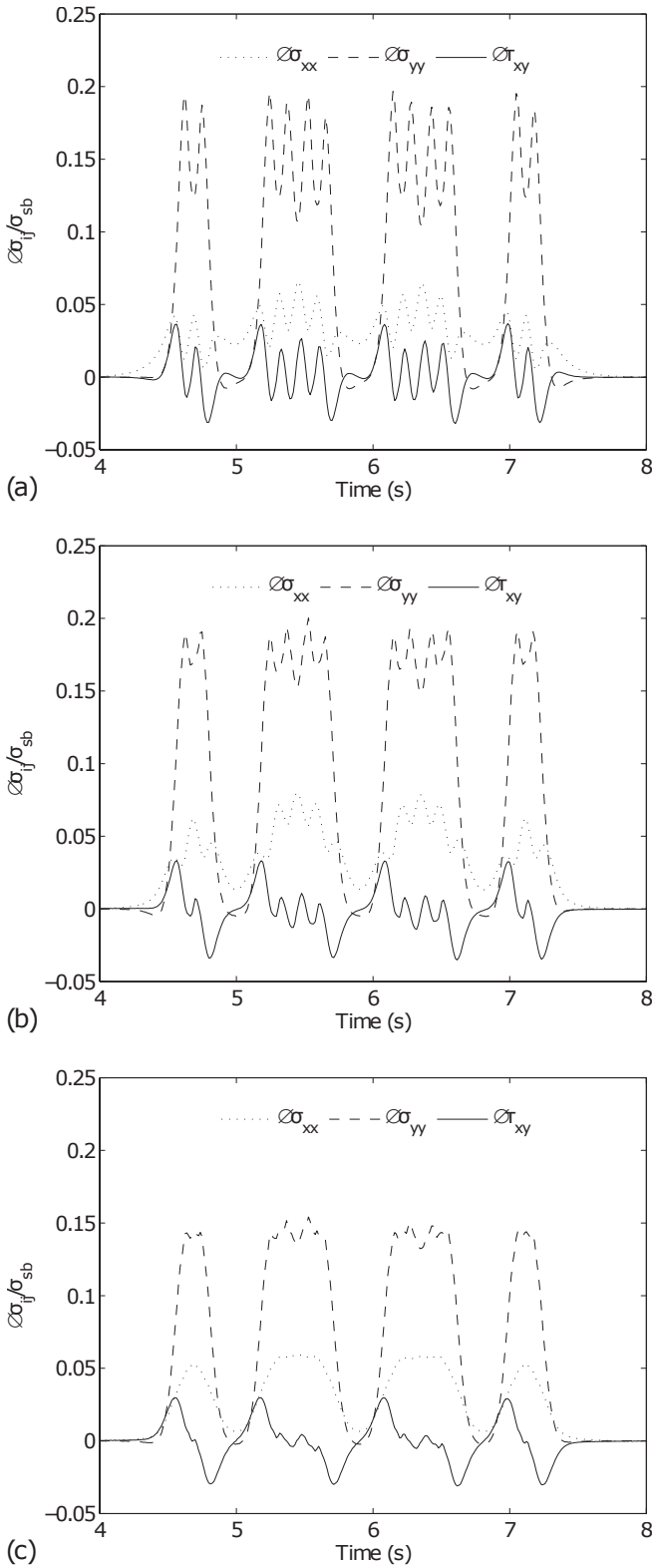

Figure 2.7: Transmitted stress underneath the track, (a) Layer SSB; (b) Layer A; (c) Natural soil, Yang et al. (2009)

Table 2.4: Velocities of compression waves and shear waves, Prakash (1981)

Soil	ρ (Mg/m^3)	vs (m/s)	vc (m/s)
Moist clay	1.8	155	150
Loess at natural moisture	1.67	800	260
Dense sand and gravel	1.70	480	250
Fine grained sand	1.65	300	110
Medium-grained sand	1.65	550	160
Medium-sized gravel	1.8	750	180

2.6.2 Influence of train speed on the stress path and ground movement

The magnitude of dynamic loading induced by passing high speed trains depends on train speed. This factor can distinct as a function of the surface wave which is travelled close to the surface of soil. These waves that comprise longitudinal and transverse motions that decrease exponentially in amplitude as distance from the surface are known as Rayleigh waves. Increasing speed is one of the most dynamic problems that impacts on the railway structure performance. If the wave velocity of the train exceeds the Rayleigh wave velocity, that would cause a large propagation of energy. In addition, the effects of train passage on the stress distribution with depth show an increase in the load cycling effect (Powrie et al., 2008). As a result the soil underneath the track passed by high speed train quickly develops a large permanent settlement if the track is not designed accordingly. According to Prakash (1981) the velocity of propagation of this wave can be calculated from Equation below:

$$\nu R = \frac{\lambda}{\text{vs}} \tag{2.1}$$

Where: vR is the Rayleigh wave, vs can be found in Table 2.4. For ν=0.5, R=0.9553 vs and for ν=0.25, R=0.9194 vs.

Field measurements are necessary in monitoring the train speed work system, as it has a significant influence on railway substructure's dynamic performance, especially for high speed trains passing on soft soils at high speeds (Priest and Powrie, 2009; Yang et al., 2009). In general, Rayleigh wave velocity can be approximated to be 500 m/s in stiff sub-grade (Madshus and Kaynia, 2000), whilst soft soil and peat this could be reduced to 40–50 m/s (Esveld, 2001). Dynamic loads start to be crucial to the performance of the track when the speed is train greater than 10% of Rayleigh wave velocity (Yang et al., 2009). The dynamic response of soil is most pronounced when the train speed approaches ν, leading to a higher stress states and a higher probability of failure with increased speed. Figure 2.8 plots the maximum shear stress (t) against effective stress (s). The results were following the stress path with varied rate of speeds. Thus, it can be concluded that failure is more likely as train speeds increase.

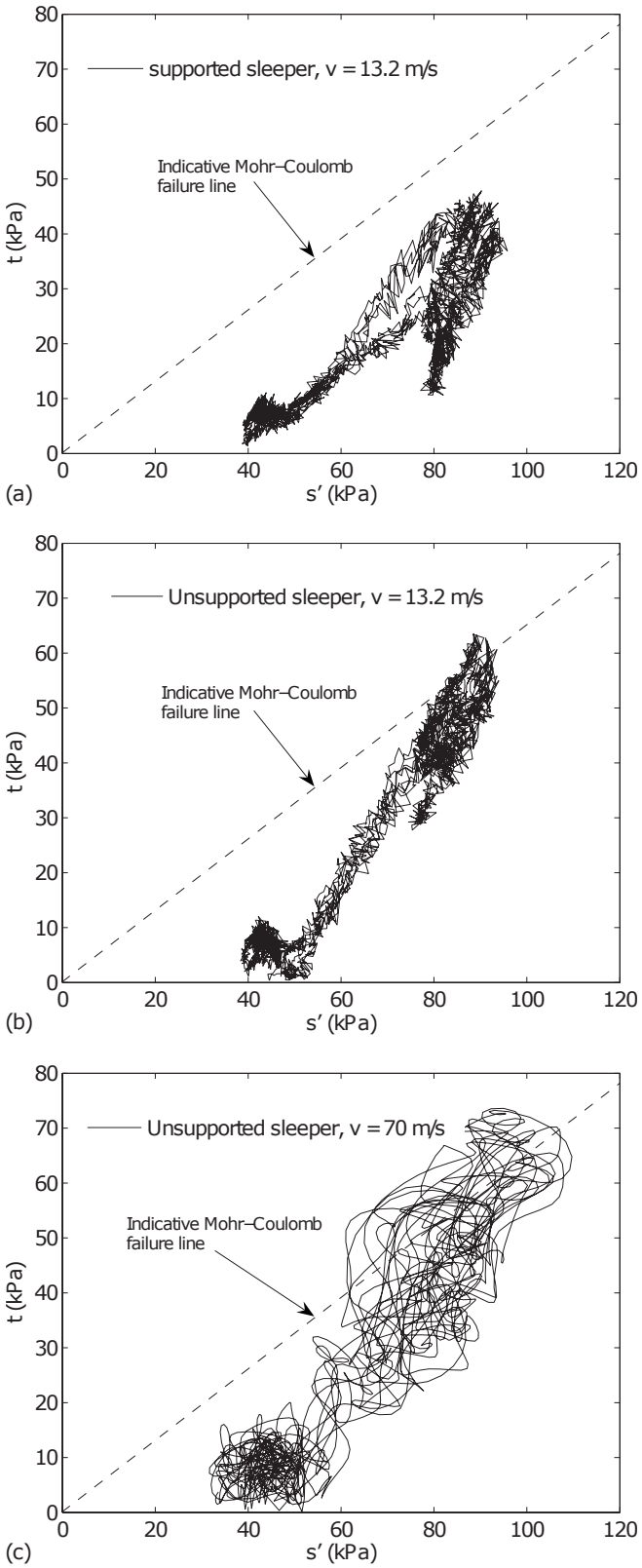

Figure 2.8: Stress paths at different speeds (a) ν=0.5νs (b) ν=νs (c) ν=1.25ν, Yang et al. (2009)

2.7 Design of ballastless track

Despite the construction of ballastless track having a high initial cost, the long service life, less disruption, low maintenance and high durability, mean these tracks have recently become more common as an alternative to traditional track (ballasted). Only a few references have paid attention to the dynamic load distribution under this type of construction, the detail of the effect are summarised below.

2.7.1 Influence of stress change on the ground below rail structure

The dynamic response strongly depends on the properties of individual elements of the track structure and the interaction between train movement and the underlying soil. In Germany experience has been gained in the application of 'slab' tracks instead of ballasted tracks to minimise maintenance. Kempfert and Hu (1999) reported that in situ measurements investigating the dynamic stress induced by railway traffic were found to depend on train speed, type of substructure, depth and also, the type of soil. It was found also that the rotation in principle stress is reduced with depth under ballastless track because the load is distributed over a wider area and hence there is a reduction of vertical stresses at depth see Figure 2.9.

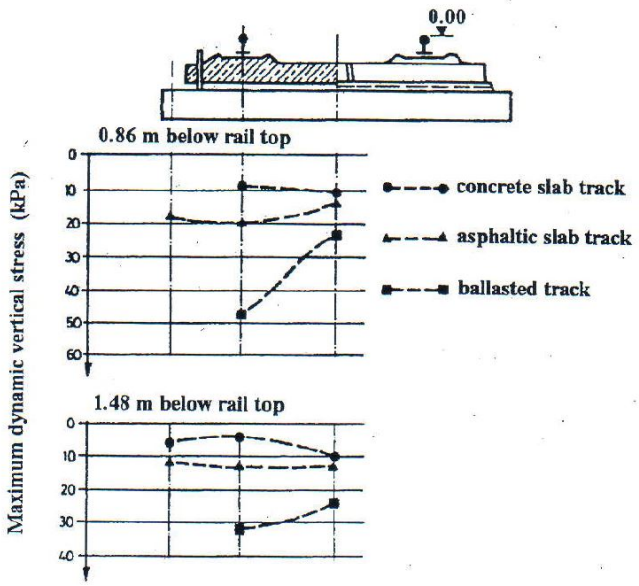

Figure 2.9: Stress distribution in substructure and subsoil, Kempfert and Hu (1999)

Bian et al. (2014) used a full scale model to compare the performance of ballasted and ballastless track by locating sensors under the track centre, the details shown in Figure 2.10.

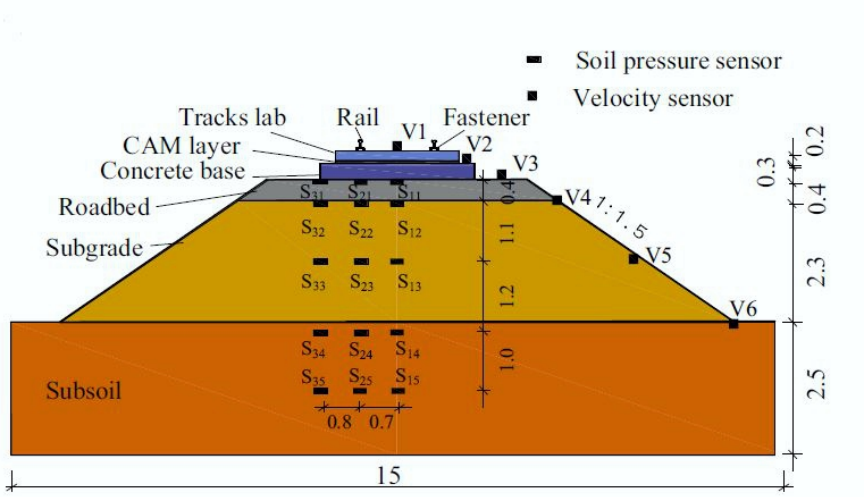

Figure 2.10: A diagram used of full-scale model of ballastless slab track in m, Bian et al. (2014)

Bian et al. (2014) found that the impact of dynamic stress on depth extends much deeper in ballasted tracks and that the stresses range between 50–100 kPa, whilst in the ballastless this is 13–20 kPa, this is summarised in Table 2.5 and shown in Figure 2.11. Furthermore, this study investigated the stress distribution for soil for both ballasted and ballastless shown in Figure 2.12. The attenuation coefficient is an important factor to represent the ratio of dynamic soil stress, it can be seen that the attenuation coefficient of dynamic soil stress of ballastless track is much lower than a ballasted track. Bian et al. (2014) also developed an empirical formula to describe the relationship between attenuation coefficients with depth for both types of tracks taking train speed into account:

$$\eta = 1 - z/(a + bz) \tag{2.2}$$

Where: η = attenuation coefficient, z = depth(m) from the surface, a and b parameters depends on track type and physical properties of soil. The relationship in Equation 2.2 could be given as a good estimation for the the amount of stress that propagates with depth and the evaluated differential settlement in the long term.

Table 2.5: Comparison between ballastless and ballasted, Bian et al. (2014)

Railways	Train type	Track type	Train speed (km/h)	Dynamic soil stress (kPa)
Wu-Gunge high speed railway	CRH-2	Ballastless	240–360	14.6–16.9
Cologne-Rhine new railway	ICE-3		140–326	15.0–20.0
Nuremberg-Ingolstadt railway	ICE-3		220–297	13.0–20.0
Testing loop at east suburb of Beijing	CRH-2		45–160	10.2–17.6
Full scale model testing	CRH-3		5.0–360	18.2–19.6
Qin-shen passenger line	DJJ2	Ballasted	200–330	50.00–100.0
Hannover-Wurzburg railway	ICE-V		10–400	70.0–100.0

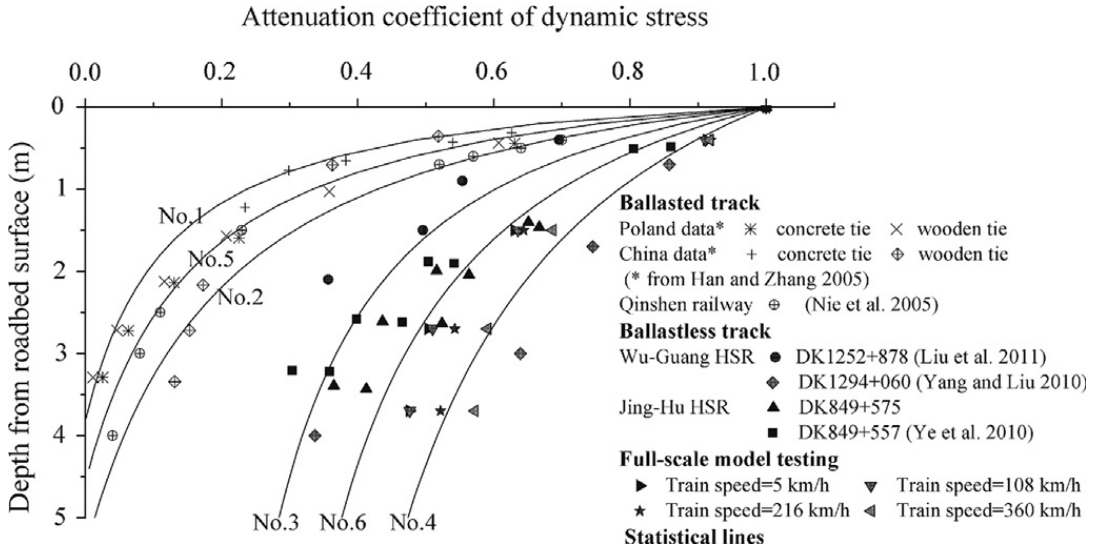

Figure 2.11: Attenuation coefficient of dynamic soil stress for different track structure, Bian et al. (2014)

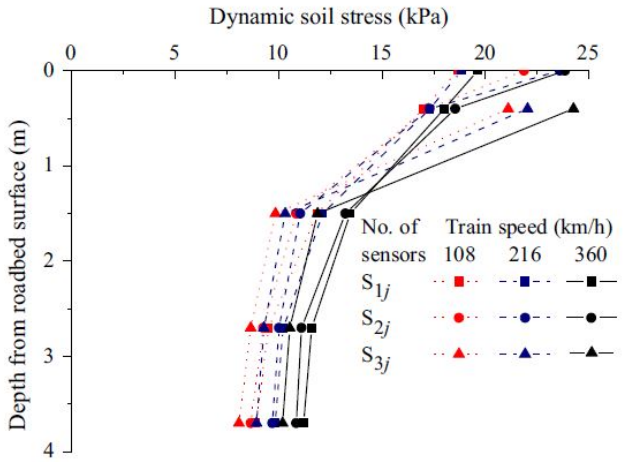

Figure 2.12: Distribution of dynamic soil stress, Bian et al. (2014)

Priest and Powrie (2009) described two techniques for the calculation of the dynamic track modulus, the dynamic axle loads increase with an increase of the speed of train about 20% and lead to an abatement in stiffness around 5%.

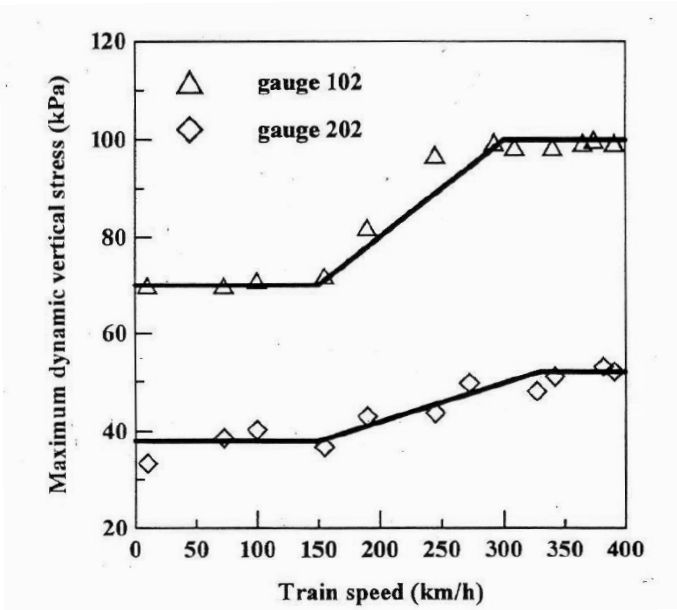

Figure 2.13: Effect of dynamic stress with increase train speed, Kempfert and Hu (1999)

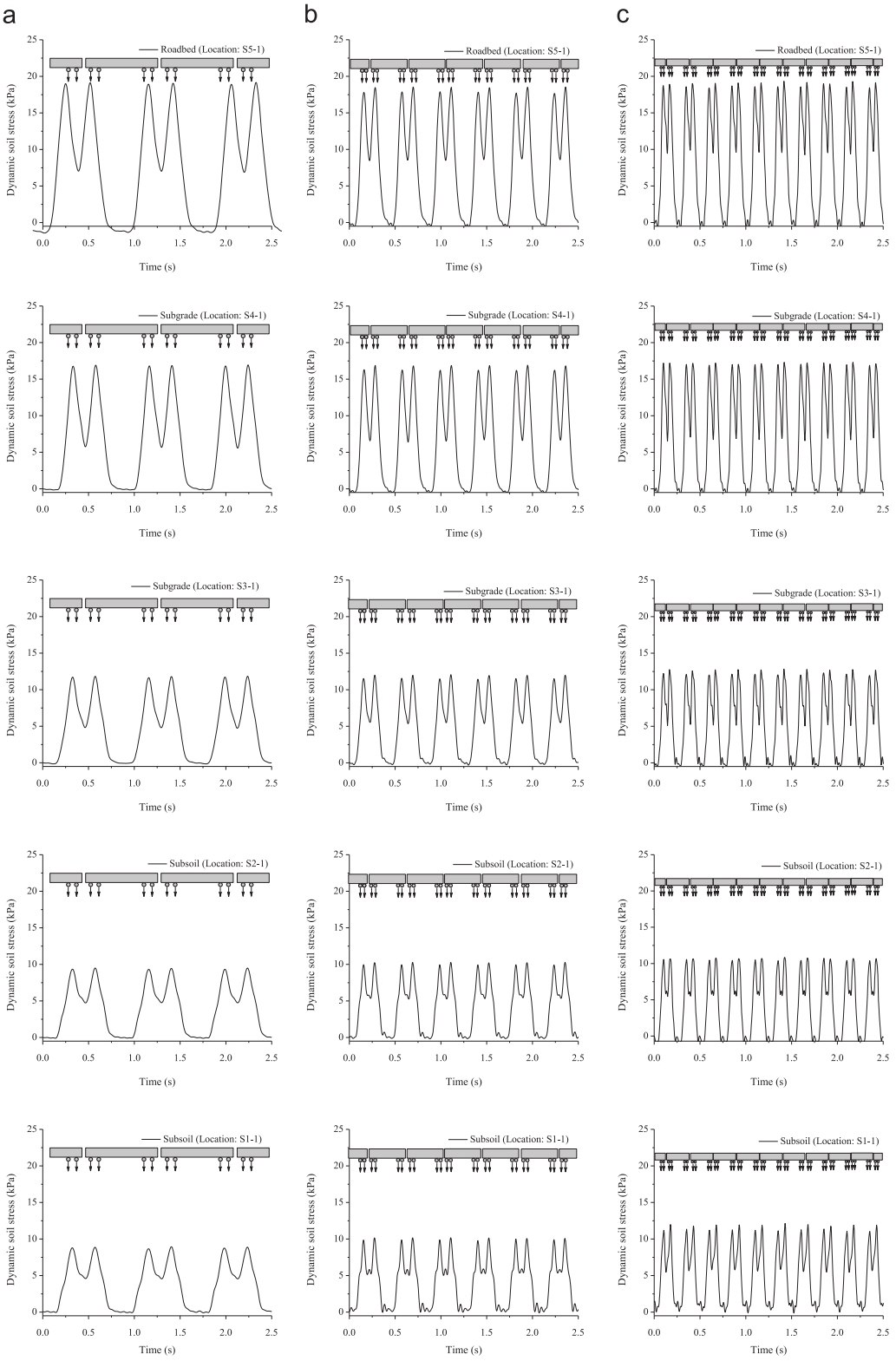

Figure 2.14: Time history of dynamic stress measured at different soil depths (a) 108 km/h (b) 216 km/h (c) 360 km/h, Bian et al. (2014)

2.7.2 Influence of train speed on dynamic load and ground movement

The transmission of dynamic load to the subsoil depends largely on train speed and its superstructure. As illustrated in Kempfert and Hu (1999), it can be observed that dynamic stresses increase between train speeds of 150–300 km/h for different pressure gauges (Figure 2.13). In addition, they used stress amplification factor k_{dyn} to better describe this dependency, which is defined as the ratio of dynamic stress σ_d to static stress σ_s. When k_{dyn}= σ_d / σ_s is 1.0 for train speeds up to 150 km/h, beyond this point the factor increases linearly with train speed till 300 km/h and then become independent of train speed.

In more recent work, Bian et al. (2014) studied the relationship between vibration velocity with different train speed under ballastless track shown in Figure 2.14. It can be concluded that the concrete slab construction can reduce the vibration induced by 75% which propagates into the subsoil, and this can possibly reduce the rotation in principle stress with depth. It can be concluded that the dynamic stresses recorded at shallow depths are affected slightly by an increase in the train speed.

2.8 Characterisation of the underlying soil

Soil under the track superstructure can be characterized by measuring the resilient modulus. The study of permanent deformation is also critical to the design and maintenance of a railway track. Understanding engineering properties for soil are required by studying those parameters. In the following section the main characterisation properties will be discussed.

2.8.1 Resilient modulus

The University of California first introduced resilient modulus to aid in the characterisation of the pavement layers to predict pavement behaviour under load cycling (Hveem, 1955). Seed and Chan (1958) defined the resilient modulus as a stiffness of the soil which is the ratio of the magnitude of repeated deviator stress to recoverable strains under repeated loading and unloading as illustrated in Figure 2.15. The AASHTO guide for the design of pavement structures proposed a characterisation scale for subgrade in terms of soil support value (SSV) in 1961 and then revised in 1972. The SSV has a scale ranging from 1 to 10, with a value of 3 representing the natural soil in the Road Test. In the revised 1986 AASHTO guide, the road bed resilient modulus, Mr, was selected to replace the SSV, because Mr has been recognized internationally as a method for characterizing materials for use in pavement design and evaluation, and the methods for measurement of Mr are described in Zaman et al. (1994), the latest being Andrei et al. (2004).

Most research has involved conducting experimental tests to identify the stiffness and strength of the subgrade soils. As a result, the resilient modulus has been found to be affected by several factors such as water content, percentage of fine particles, number of cycles and stress level (Brecciaroli and Kolisoja, 2006; Morgan, 1966; Barksdale, 1972; Lekarp, 1999).

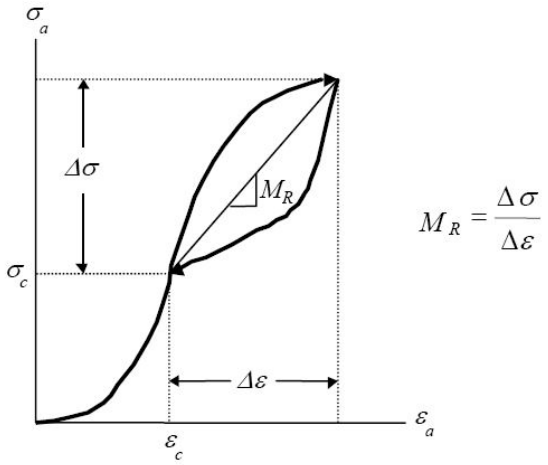

Figure 2.15: Definition of resilient modulus

Stress conditions are one of the main factors that impact the resilient modulus. A triaxial test is used to estimate the stiffness, and strength characteristics of the subgrade. Fredlund et al. (1977) proposed a theory between resilient modulus and stress conditions for cohesive subgrade soils and established the relationship between resilient modulus and stress state for specimens subjected to 100 cycles stress. Resilient modulus was found to be reduced by an increase in deviator stress and matrix suction (Figure 2.16).

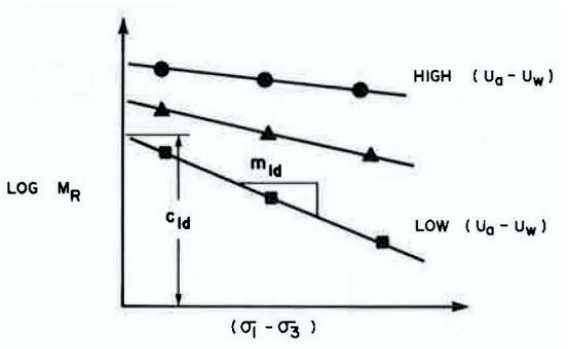

Figure 2.16: Effect of deviator stress on resilient modulus, Fredlund et al. (1977)

Duong et al. (2016) observed that for interlayer soils containing a high fines content has a better mechanical behaviour under unsaturated conditions. In addition, the higher

fines content leads to a significant degradation of the behaviour due to suction effect.

Liu and Xiao (2009) conducted experiments on the silt subgrade soil along the Beijing-Qinhuangdao and Beijing-Kowloon railway lines in China. Figure 2.17 shows that for the silt tested the resilient modulus decreases with increased water content and relative compaction, as a result the elastic deformation also increases and is affected by the train speed. As a consequence for such soils, methods to reduce the dynamic stress and load frequency induced during train passage should be enforced to minimise the degradation of the subgrade.

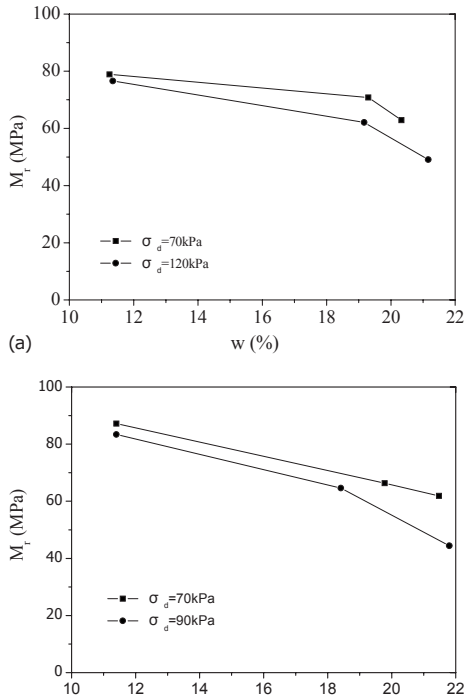

Figure 2.17: Effect of moisture content on resilient modulus at different dynamic stress, a) at relative compaction of 85%, b) at relative compaction of 90% Liu and Xiao (2009)

Thom and Brown (1987) highlighted the effect of water content on the behaviour of crushed limestone and found that the stiffness decreases with an increase in the percentage of fine content. In Figure 2.18, Specimens 1 and 2 were compacted dry at 2000 and 1995 kg/m^3 respectively, Specimen 3 was compacted at the optimum moisture content at 2006 kg/m^3. It can be seen clearly the effect of water on the stiffness especially when the conditions change from wet to dry for Specimen 2 as it wetted before the test and then dried.

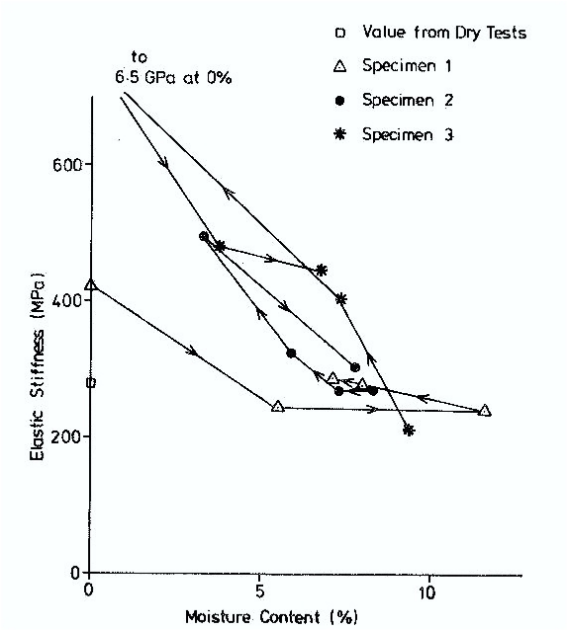

Figure 2.18: Elastic stiffness for British Type 1 subgrade material versus water content, Thom and Brown (1987)

Fredlund et al. (1977) investigated the performance of the cohesive of compacted subgrade soil with varied water content and found that the deviator stress has variable effect on the resilient modulus by increasing the value of Mr with increase the deviatoric stress. With increasing deviator stress the resilient strain increases, over repeated cycles this then decreases to reach a point of stabilization.

Previous studies have indicated that a large number of cycles are not required for certain to stabilize soil types (Duong et al., 2016) . At the start of a test, particle rotation and rearrangement produce the plastic strain. Thus, with high number of cycles the particle movements become limited and continued strain reduces due to the increased contact between particles. There is no particular number of cycles for stabilization. Stewart (1982) found stabilization after 1000 cycles for a typical ballast material, whilst Lackenby (2006) indicated that stabilization set at 50–100 cycles for granular materials, depending on type of material, water content and stress level.

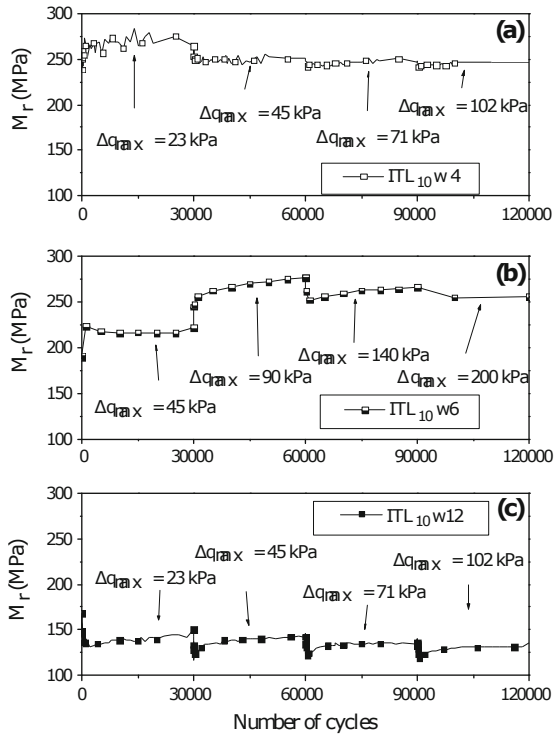

Figure 2.19: Effect of deviator stress increases during testing for varying water contents: (a) 4% (b) 6% (c) 12%, Duong et al. (2016)

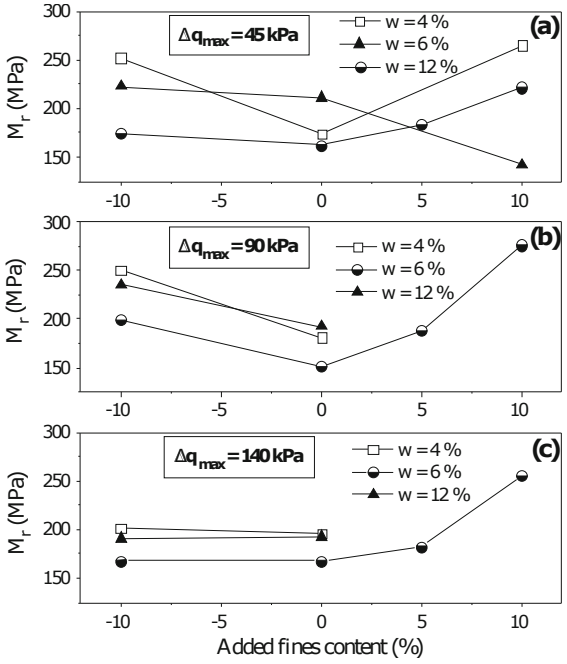

Figure 2.20: Effect of fines content on resilient modulus with varying deviator stress: (a) 45 kPa (b) 90 kPa (c) 140 kPa, Duong et al. (2016)

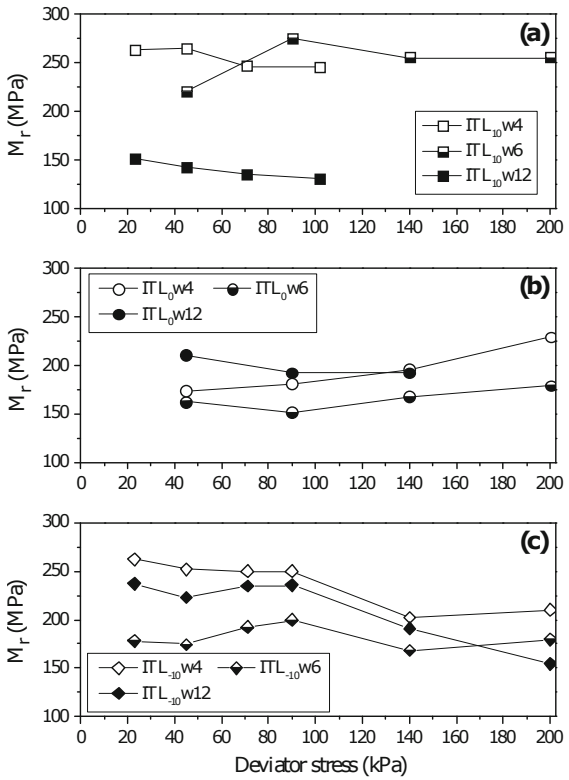

Figure 2.21: Effect of deviator stress on resilient modulus for varying water contents: (a) 4% (b) 6% (c) 12%, Duong et al. (2016)

Duong et al. (2016) conducted tests identifying the effect the interlayer soil (which is defined as a layer between ballast and subgrade soil) has on performance, using a large scale triaxial cyclic apparatus. Different stress levels were applied to this layer with adding of 10% of fine to the sample, and also different water content to evaluate the effect on the resilient modulus. In Figure 2.19 presents the development of resilient modulus after changes in water content to the stabilization state of recoverable strain. Figures 2.21 and 2.20 plot the end-stage resilient modulus with deviator stress at three water contents ($w =$ 4, 6 and 12%) and three different added fine content(-10,0, 10% subgrade) added 10% fine content causes an increase in Mr. The results show that a decrease in resilient modulus with increasing water content.

Li and Selig (1998) developed a new design method for granular layer thickness. The purpose of this design was to prevent the excessive deformation and progressive shear failure in subgrade materials.

2.8.2 Permanent strain

Permanent strain is defined as the total strain that is generated by each load cycle, leading to a gradual increase in cumulative stain with an increasing number of cycles. This can

also lead to failure. Many studies have focused on understanding the resilient strain. The growth of permanent strain is impacted by same factors that effect Mr. Water in the soil has negative influence as it increases the amount of permanent strain as pore water pressures are generated. Several other studies have investigated unbound granular materials and found that the permanent strain is related to the stress ratio (the ratio between maximum deviator stress to maximum of confining pressure).

Duong et al. (2016) found that the resilient strain developed with increase number of cycles and deviator stress as shown in Figure 2.19. This shows that the resilient strain goes up after each increment of deviator stress after which it then decreases to reach the equilibrium state.

The loading generated by high speed trains is known to induce larger settlements, as the dynamic loading generates higher stresses in the ground. As the number of load cycles increase so the settlement of substructure occurs and is the main cause of the deterioration of track performance. This can cause large cumulative strains over the long life of the tracks and leads to deterioration and irregularities of the track level.

Significant research has been done to assess factors which affect the permanent deformation of the track foundation for different materials (Shackel, 1974; Brown et al., 1975; Monismith et al., 1975; Wood, 1980; O'Reilly et al., 1991; Li, 1994). The studies found that large dynamic loads caused progressive permanent deformation. In addition, principle stress rotation has a direct effect on the accumulation of plastic strain in granular materials and that increasing numbers and magnitude of repeated loading, leading to increased cumulative plastic deformation. Increases in train speed also cause an increase in the dynamic loading and frequency. For a silt subgrade Liu and Xiao (2009) found that permanent strain rises with increased water content, and is more the soil likely to fail in a fully saturated state (Figure 2.22).

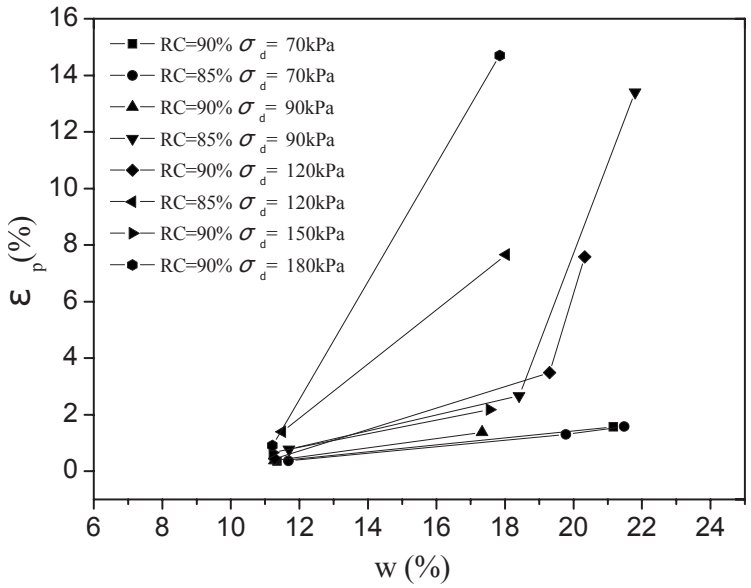

Figure 2.22: Effect of water content on plastic strain, Liu and Xiao (2009)

The major problem for railway track is excessive subgrade plastic deformation and failure under repeated cyclic loading. Plastic strain is essential to determine which is a relationship between stress and plastic strain under repeated loading as express in Equation by Pappin and Brown (1980).

$$\varepsilon_p = f(N)\iota(\eta)^l rt \tag{2.3}$$

Where: ε_p = plastic strain, $f(N)$ = function of the number of load cycles, t, l, r and ι = are material constants and η = stress ratio ($\eta = q/p$).

Thom and Brown (1988) noted that permanent shear strain was related to the stress ratio. Many factors impact the capability of predictive models of strain state such as soil stress state, number of repeated loadings, soil type, soil state, particle size distribution, and water content. (Li and Selig, 1996). Thus, there were many studies done to minimise maintenance costs and traffic high load quality. Li and Selig (1998) used a 3D 'Geotrack' model to estimate cumulative plastic strain for fine grain subgrade soils under repeated loading, and developed the relationship between cumulative plastic strain and number of repeated deviator stress represented in Equation below:

$$\varepsilon_p = \alpha(\beta)^m N^b \tag{2.4}$$

Where: α, b and m parameters are dependant on type and properties of soil and stress state. $\beta = \sigma_d/\sigma_s$ and N = number of cycles.

Results indicated that differential subgrade settlement along the track was caused

basically by the non-uniform distribution of the subgrade soil strength due to variations in moisture content and the deviatoric stress generated within the soil.

Gräbe (2002) examined cyclic tests on particular materials in South Africa which were consolidated from slurry to pre-consolidation pressures up to 300 kPa with and without cyclic stress rotation. Shear stresses on the horizontal plane were cycled between ±7 kPa, results are presented in Figure 2.23. It can be said that those materials were stable under cyclic vertical load, whereas plastic strain started to accumulate with principle stress rotation in long term.

Obviously, plastic behaviour for the materials differs with particle size distribution. The permanent deformation increased for more well graded materials Kamal et al. (1993). It is observed that deflection increased with increased the percentage of the fine contents.

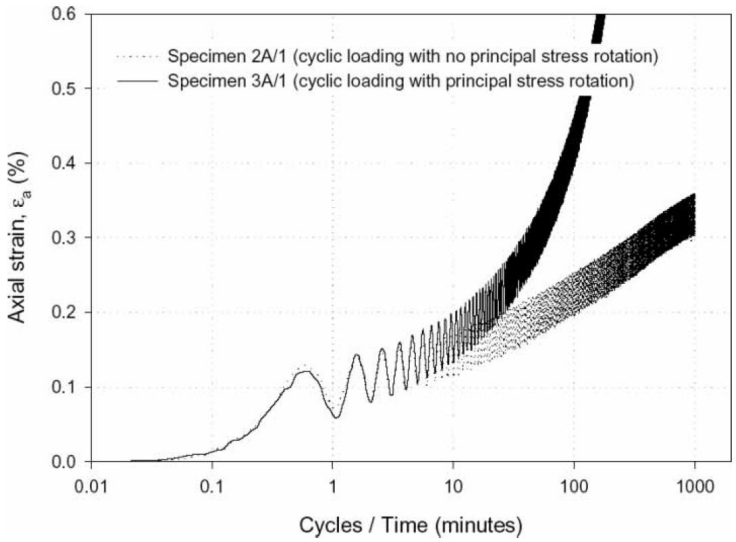

Figure 2.23: Cumulative strain of principle stress rotation, Gräbe and Clayton (2009)

Gräbe and Clayton (2009) looked at effects of principle stress rotation (PSR) during cyclic loading on the permanent deformation in a series of hollow cylinder tests in coal line in South Africa, with and without principle stress rotation, axial strain find increase with increase the peak of effective stress ratio, and under PSR rises up to become larger than with no PSR (Figure 2.24).

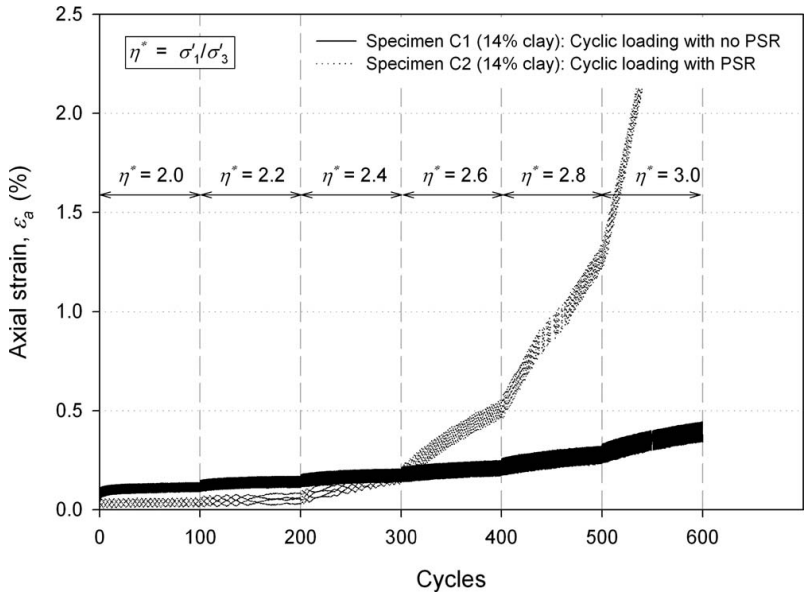

Figure 2.24: Effect of rotation on axial strain versus the number of cycles at different peak effective stress ratio for material with 14% clay, Gräbe and Clayton (2009)

2.9 Breakage of particles due to repeated loading

In dynamic loading it is observed that the breakage of soil particles is likely to occur. This can significantly degrade the original particle size distributions leading to changes in the mechanical characteristics of granular soil Lade et al. (1996) and Indraratna et al. (1998). In general, particle breakage negatively affects the drainage and filtration efficiency and also the soil strength. Marsal (1967) and Carrera et al. (2011) found that more particle breakage would occur in soils with a relatively low coefficient of uniformity and high void ratio. Donohue et al. (2009) conducted drained cyclic triaxial tests on loose, uniformly graded samples of Dogs Bay carbonate sand. It was observed that particle breakage is dependent on stress level, cyclic stress ratio, and creep and is directly related to volumetric strain. Drained cycling increases volumetric strain and therefore more breakage occurs when larger numbers of cycles are imposed.

Drained cyclic triaxial tests were performed on samples of artificially crushable material by Liu et al. (2016) to explore particle breakage in the cyclic loading process with a frequency of 1.0 Hz. They found that the particle breakage resulting from the cyclic loading process is mainly affected by the confining pressure, maximum cyclic deviatoric stress and number of cycles and contributes greatly to the volumetric change of the samples. The cyclic deviatoric stress, number of cycles and confining pressure all influence the internal frictional angle and number of cycles of failure, which is related to the formation of force chains, transition of loads, fabric adjustments and the deformation mechanism

at the mesoscale under cyclic loading conditions. McDowell et al. (1996) found that the probability of particle breakage depends on applied stress, particle size and reduction of contact with neighbouring particles and shape of particles.

2.10 Modelling plastic strain and resilient modulus

The prediction of resilient modulus has to take into account the factors that effect the response such as: stress state, soil type and physical state of soil. Reducing excessive deformation due to high speed train loading has been the aim of numerous studies. Varied models have been presented for predicting the cumulative plastic strain. The most commonly used model is the following power law developed by Monismith et al. (1975) and Knutson et al. (1977), in Equation below.

$$\varepsilon_p = A(N)^b \tag{2.5}$$

Where: ε_p = cumulative plastic strain (%), N = number of cycles, and A and b are two material constants which depend on soil type, soil properties and stress state.

This model has been used to estimate the relationship between the cumulative plastic strain and the number of repeated deviator stress applications. However, this model has limited practical use as with most models in this section it is merely a curve to be fitted to experimental data rather than a true predictive tool.

Li and Selig (1996) created an improved method to calculate the plastic deformation of the fine grained subgrade and to design the thickness to reduce the plastic settlement. This model attempts to represent the relationship between cumulative plastic strain and the number of cycles whilst also considering the deviator stress which is the most important stress factor. Water content and dry density are taken into consideration in this model by soil static strength. Multiple layers could also be considered.

For resilient modulus, as mentioned earlier, the most significant factors that impact on the magnitude of resilient modulus are stress state, soil type, and physical state of soil. Many constitutive models have been generated to estimate the effect of deviator stress on the resilient modulus. But as for the plastic strain much test data is required to populate these models (Thompson and Robnett, 1976; Fredlund et al., 1977; Drumm et al., 1990; Moossazadeh and Witczak, 1981; Li, 1994; Seed et al., 1962).

Chapter 3

Methodology

This chapter presents the material of study, including particle size distribution, compaction and slaking tests, and XRD results. In addition, the equipment that was adopted for use in the experimental programme is described in detail in this chapter. Triaxial cyclic loading is the main apparatus used in this project and the testing procedure is described in detail in this chapter. Standard triaxial testing was performed using a GDS triaxial stress path apparatus.

3.1 Physical properties of mudrock

The material of study, mudrock colliery spoil, was collected from Kellingley Colliery on the 10th of August 2015. This has been stored in a covered crate outside the research laboratory at the University of Sheffield since collection. This material can be described as a weathered dark grey mudrock and has a variety of particles sizes to a maximum of 50 mm (Figure 3.1). Particle size distribution tests were undertaken, showing that the spoil can be classified as poorly-graded base on the results shown in (Figure 3.2). The maximum particle size for the analysis has been taken to be 14 mm due to sieve availability. The values of D_{10}, D_{30}, D_{60} are 4.6, 8 and 10.4 mm respectively. The coefficient of uniformity (C_u=D_{60}/D_{10}), and the coefficient of curvature (C_c=$(D_{30})^2/(D_{60}\times D_{10})$) are given in Table 3.1 (and a visual example is shown in Figure 3.3). The soil consists of large angular particles and can be classified as poorly-graded for the $<$ 10mm samples and well-graded for the $<$ 5mm samples. The permeability values calculated for this material are based on the empirical relationship given by Carrier III (2003):

$$k = 552D^2[e^3/(1+e)] \tag{3.1}$$

Where: D is the effective particle size in mm and k is the permeability and e is the void ratio.

Following Equation 3.1, the permeability for the compacted particles passing through a 10 mm sieve is 0.0337 m/s and for particles passing through a 5 mm sieve is 0.0203 m/s. Hence, the soil can be classified as being semi-pervious or having a moderate permeability (Powrie, 2013).

Table 3.1: Particle size distribution classification

Particle size	D_{10}	D_{30}	D_{60}	C_u	C_c
$<$ 10 mm	2.25	4.4	7	3.1	1.22
$<$ 5 mm	0.5	1.5	3.2	6.4	1.40

Figure 3.1: Natural material of study (indicated length is 30 mm)

3.2 Specific gravity

The specific gravity of this soil was tested according to BS1377: Part 2 (Head and Epps, 1986). The specific gravity, G_s, was found to be 2.75.

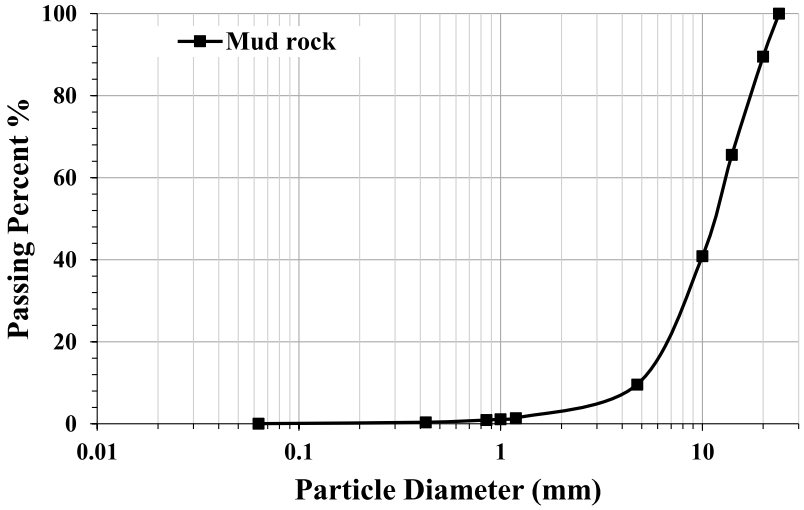

Figure 3.2: Natural particle size distribution of mudrock colliery spoil

Figure 3.3: Particle size distribution that used for compaction in < 10 mm tests

3.3 Compaction

The compaction characteristics of soil were first described by Proctor (1933). In the compaction process soil particles are packed more closely together by reducing the air voids to a minimum to increase the density of soil mass. In this project ordinary compaction tests were conducted according to Head and Epps (1986). The compaction technique in

this method is to divide the soil into three layers, each layer subjected to 25 blows manually in a mould of 100 mm diameter and 200 mm length using a 2.5 kg rammer dropped from a hight of 45 cm to apply maximum effort of compaction with the same energy as standard compaction test as shown in Figure 3.4. Two particles sizes have been investigated in the current study to enable the influence of this degradation on performance to be quantified:

1. Particles passing through a 10 mm sieve.
2. Particles passing through a 5 mm sieve.

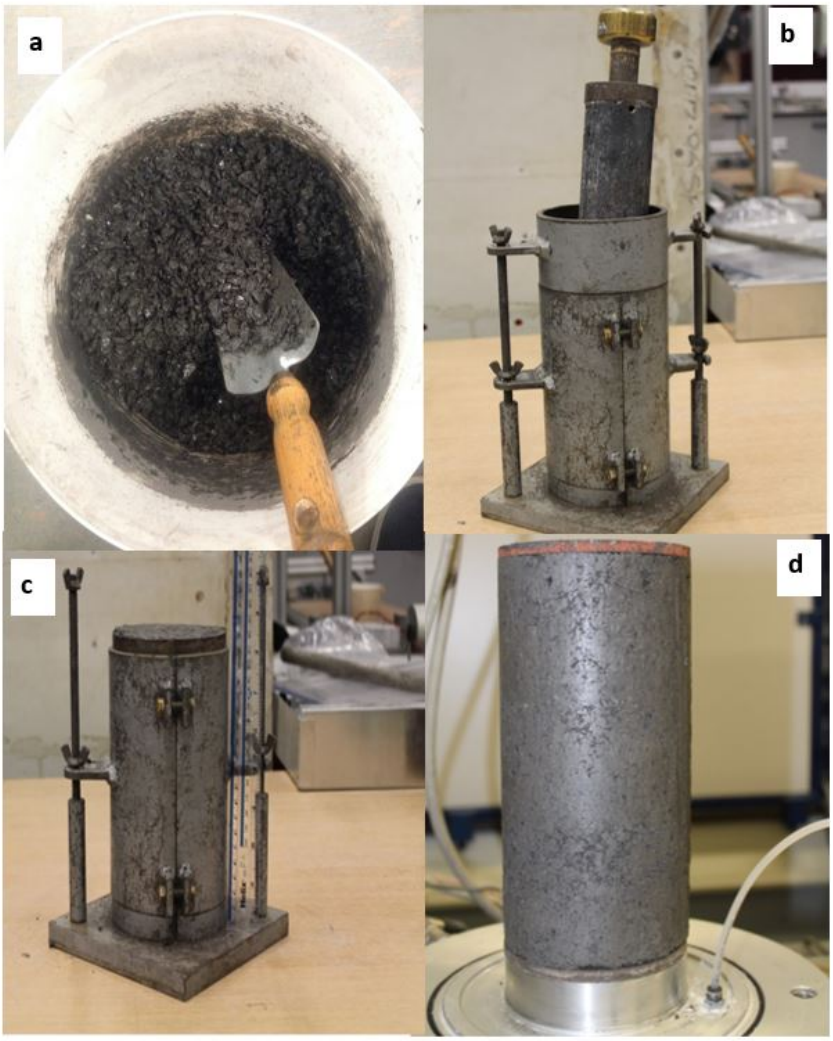

Figure 3.4: Compaction test preparation (a) mixing mudrock at a given water content, (b) compaction mould, (c) compacted soil inside the mould, (d) specimen after compaction

The compaction results are shown in Figure 3.5. The optimum moisture content for particles smaller than 10 mm is 11% giving a maximum dry density of 2.04 Mg/m^3, whilst

for the particles passing through 5mm the maximum dry density 2.1 Mg/m^3 and optimum moisture content is 8.6%.

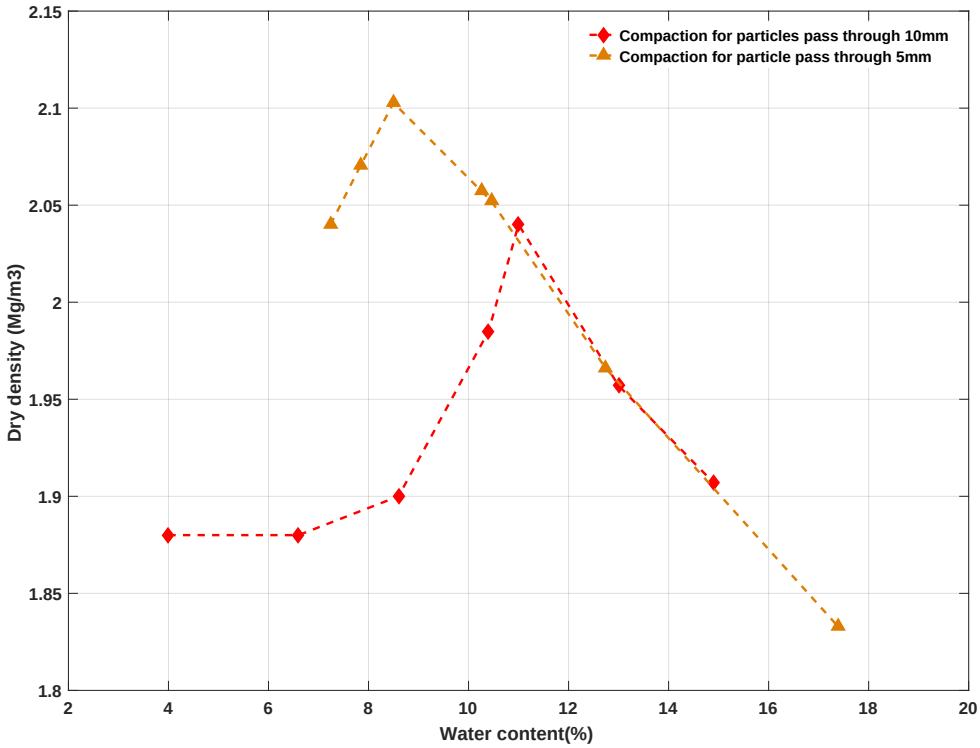

Figure 3.5: Determination of the optimum moisture content for < 5 mm and < 10 mm specimens

According to the triaxial cyclic load testing protocol given in ASTM (2013), the maximum particle size allowed in a test is 1/6 of the diameter of the triaxial cell to be utilised. In the current testing a 100 mm diameter cell is to be used which gives a maximum particle size of 16 mm. However, in this experimental programme, the particles passing through a 10 mm sieve were selected for testing to meet the ASTM limit and equipment at Sheffield University. The particles bigger than 10 mm were removed due to their angular shape which led to difficulties when compacting specimens. Figure 3.6 displays the effect of compaction and cyclic testing on the degradation of the material. It can be seen that there is a change of particle distribution after compaction, also there is a slight different for particles after each test due to the continued particle degradation which is explored by slaking tests in Section 3.5. All tested specimens were compacted according to the information given in Table 3.2. Each saturated specimen is saturated prior to testing representing a worst case scenario that could occur due to fluctuation in the groundwater table. The dry case is taken into consideration to estimate the effect of water content and the breakage of particles on the stiffness of soil, this condition the relative density has been tested and the samples compacted at maximum density Table 3.3. The specimens

Table 3.2: Compaction properties for mudrock

Test	Dry density (Mg/m^3)	Degree of saturation (%)	Void ratio
Particles passing through 10 mm sieve			
Dry-side	1.98	53	0.969
OMC	2.04	79	0.61
Saturated	1.98	100	0.46
Particles passing through 5 mm sieve			
Dry-side	2.065	58	0.781
OMC	2.11	77	0.55
Saturated	2.05	100	0.32

Table 3.3: Relative density for dry case of mudrock

Test	$\rho_{max}(Mg/m^3)$	$\rho_{min}(Mg/m^3)$
10 mm	1.80	1.68
5 mm	1.89	1.71

were tested under different conditions. The load frequencies used in this study are 4 Hz (4 cycles each second) and 1 Hz (1 cycle each second).

Figure 3.6 displays the effect of compaction and cycling on the degradation of the mudrock. The mudrock has been sieved to prepare for compaction and then compacted to be ready for the test. Specimens after compaction were dried in the oven and sieved again. It can be seen that the change of particle size distribution after compaction was 56% at D_{30}, also the material that has been sieved after cyclic loading showed again a further reduction in particle size.

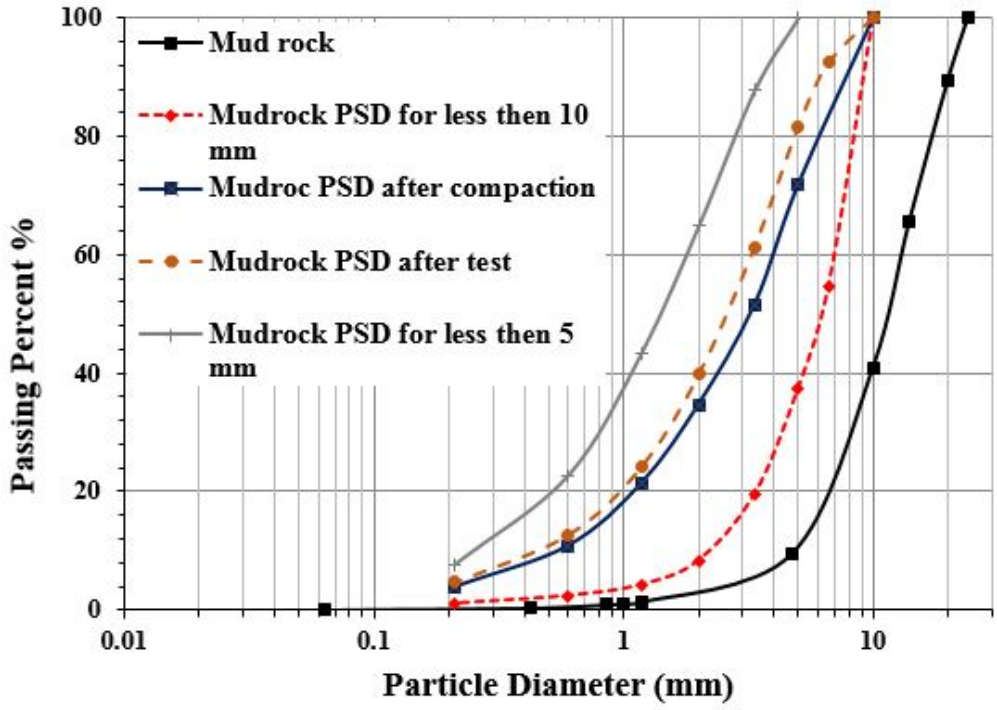

Figure 3.6: Particle size distribution of mudrock colliery spoil before and after compaction

3.4 Mineralogy

A number of techniques are appropriate for identifying the mineralogical composition of mudrock such as X-ray diffraction (XRD) analysis, optical microscopy and scanning electron microscopy. In this project XRD was used to investigate the mineralogical composition by using powder of mudrock. This test conducted in the Department of Materials at the University of Sheffield. The result is shown in Figure 3.7, which identified the materials as mainly quartzite, chlorite, mixed layer of illite-smectite, calcite, plagioclase feldspar and siderite. Swelling clay minerals were absent from the composition of the mudrock such as pure smectite and montmorllonite.

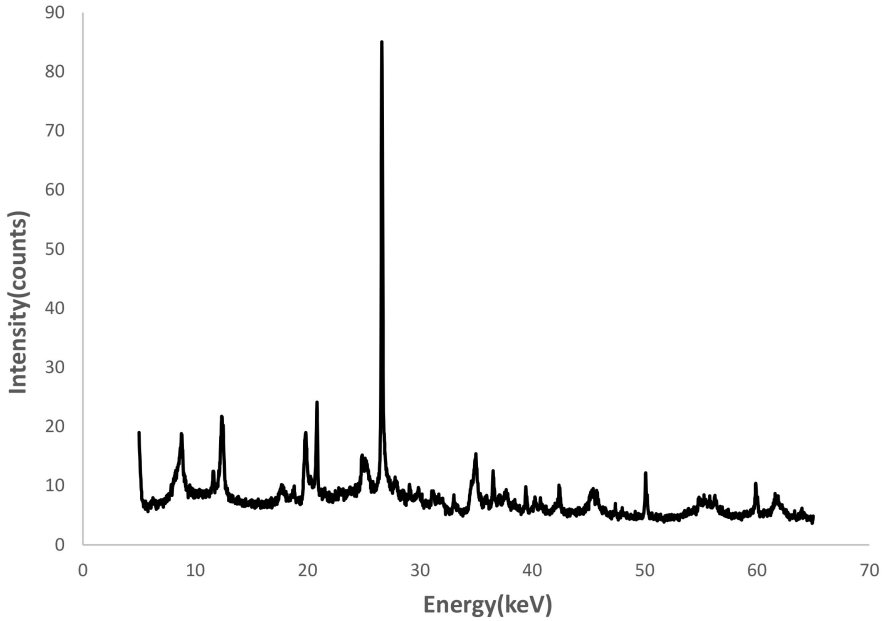

Figure 3.7: XRD result for mudrock

3.5 Slake durability

This method is used to estimate qualitatively the durability of weak rocks which helps identify the effect of existing discontinuities together with bedding planes, faults, joints, laminations, and fractures under atmospheric conditions. Slake durability parameters are used extensively as a stability indicator to analyse the susceptibility of intact rock to brief time period deterioration when subjected to a simulated rapid weathering approaches. The slake durability index for mudrock is determined after two drying and wetting cycles with abrasion according to Franklin and Chandra (1972) from the formula below:

$$I_d = \frac{W_{f2}}{W_{f1}} \times 100 \tag{3.2}$$

Where:
I_d = slake durability index,
W_{f1} = mass of dried particles after first cycle,
W_{f2} = mass of dried particles after second cycle.

This test method consists of placing pieces of mudrock with a particle mass of 20 mm, and mass 40–60 grams each in a wire mesh drum mounted in an apparatus where the drum is partially submerged in a trough filled with distilled water (Figure 3.8). The specimens in the drum are rotated in the water for two cycles. Each cycle includes rotation with

speed of 20 rpm for 10 minutes. At the end of the first cycle, the specimen is oven dried and the total mass of specimen retained in the drum being recorded. Then, a second cycle with the same speed and time period as the first one is performed. The retained total mass of specimen from the second cycle is recorded. The slake durability index is calculated based on both measured total masses of test specimen retained in the drum per each cycle.

Figure 3.8: Slaking apparatus

From the results of testing, the durability index was found to be $I_d = 72.59\%$ (Table 3.4). The soil of study can be classified as having medium slake durability according of the classification of Franklin and Chandra (1972). Subsequently, the visual view of the soaked fragments with water fragments started to breakage to small pieces shown in Figure 3.9.

Table 3.4: Slaking durability index, Franklin and Chandra (1972)

Slake durability, I_d (%)	Classification
0–25	Very low
25–50	Low
50–75	Medium
75–90	High
90–95	Very high
95–100	Extremely high

(a) Before slaking

(b) After slaking cycle 1

(c) After slaking cycle 2

Figure 3.9: The effect of slaking on mudrock

3.6 Cyclic triaxial equipment

The triaxial testing system was manufactured by ELE International, UK, and Industrial Process Controls Ltd. The actuator supplies a controlled force and was modified after purchase by Higuchi (2002) at the University of Sheffield. The system consists of a triaxial cell, a loading frame fitted with a double-acting actuator connected to a pneumatic servo valve, and a Control and Data Acquisition System (CDAS) linked to a computer. The axial strain was obtained by using an LVDT. A pressure regulator was also included in the system to ensure that the pressures supplied were consistent throughout the test, which is crucial for the servo valve. The whole cyclic triaxial system is shown in Figure 3.10. Details of the development and modifications to the ELE cyclic triaxial system can be found in Higuchi (2002) and Meca (2005). The details of the triaxial cyclic load control software can also be found in Feeley (1994).

Figure 3.10: Triaxial apparatus

3.6.1 System control

This section describes the details of the pneumatic system, the principles of servo valve control, and the concept of open-loop control. The feedback controlled cyclic triaxial test applies cyclic loading to soil specimens. This form of loading simulates the conditions produced by high-speed railways. The wave shape for the loading pulses used in the current testing is sinusoidal. The UTM CDAS software allows the operator to enter the initial specimen measurements, specimen test condition, load cell width. Displacement, pore water pressure, volume change and pressure transducers are used to monitor the behaviour of the specimen during each test. A test will continue to cycle until the test termination cycle count is reached or the strain level is exceeded.

3.6.2 Control and data acquisition system

The CDAS consists of a number of panels as listed below:

- Acquisition panel:
  This comprises of a load cell, axial LVDT, pore pressure transducer, confining pressure transducer, back pressure transducer, volume change measurement and actuator displacement LVDT.

- Acquisition hardware:
  The UTM CDAS is a compact, self-contained unit that provides all critical control, timing and data acquisition functions for the test frame and transducers. The CDAS is linked to a computer via a serial link. All control, communication and transducer cables terminate in connectors located on the front panel of the CDAS.

The CDAS comprises a power supply module, a microprocessor module, an analogue input/output module, and a closed-loop digital signal processing module. It is a compact, self-contained unit that provides all critical control, timing and data acquisition functions for the testing frame and transducers. The CDAS is connected to a personal computer on which is installed the cyclic triaxial testing software provided by ELE International Ltd.

For feedback control operation, the CDAS has three normalised input channels. One was dedicated to the position of the actuator, the second was dedicated to the actuator force, and the third was a general purpose input for on-specimen transducers etc. Each of these three channels fed into the control module and were buffered and brought out to a connector for optional data acquisition. The CDAS automatically controls the operation of the loading frame for each types of test. The CDAS directly controls the servo valve to apply the requested loading rate as well as a wave form. It can also apply a voltage via the Digital to Analogue Converter (D/A) to alter the air pressure to the required level for tests requiring confining stress. While the specimen is being subjected to cyclic loading forces. The CDAS captured data from the transducers and transferred these, via a RS232 serial link, to the PC for processing for feedback, display, and storage (Figure 3.10).

3.6.3 Hardware components

- Loading frame and actuator:
  The loading frame was manufactured by ELE International Ltd. This incorporates a flat base plate, supported on four plane screws. Two bolts hold a cross-head beam which was of heavy construction to limit the deflection and vibrations of the frame which could affect the accuracy of measurements during repeated cyclic loading. The actuator mounted on the cross-head beam was a low friction, double acting, and high-speed design with a very high-frequency response of up to 70 Hz.

- Modified triaxial cell:
  The triaxial cell manufactured by ELE could place a specimen having dimensions of up to 200 mm height and 100 mm diameter. The cell was rated to a maximum confining pressure of 1700 kPa.

- Pressure reservoir:
  A pressure reservoir was used to maintain a stable air pressure provide to the high precision servo valve. For practical use, the air pressure was maintained at 5 bar throughout the test. The reservoir has two water/oil traps at both inlet and outlet ports to ensure that the air was clean.

- Cell pressure:
  The cell pressure system contains an electro-pneumatic servo valve, a pressure transducer, a bladder type air/water pressure assembly, and a pressure gauge. The air pressure regulated by the servo valve was supplied to the air/water pressure assembly, which in turn pressurised the water in the assembly. Thus, the pressure transmitted into the triaxial cell from the servo valve which was manufactured by Festo Co. The output range of a pressure supplied is 0–1000 kPa for an input range of 0–10V. The pressure transducer manufactured by ELE was located next to the output port of the servo valve. The required pressure could be monitored on a computer screen through the software.

- Back pressure and volume change unit:
  The system of the transducer in back pressure unit was the same as used for the cell pressure. The continuous measurement of the volume change was supplied by connecting the water outlet of the air/water interface tank to the volume change measurement apparatus, and then to the cell base used to apply back pressure to the specimen. The volume change unit used was manufactured by ELE. A piston fitted with a Bellofram, and an LVDT. The lower chamber of the cylinder was connected to the air/water pressure unit whereas the upper chamber was connected to the cell base. The LVDT attached to the piston was used to monitor vertical displacement association with the area of the piston.

- Pore pressure transducer:
  The measurement of pore water pressure was done by using a pore pressure transducer manufactured by ELE. The transducer had a range. The signal from the transducer was amplified by an in-line gain amplifier manufactured by Industrial Process Controls Ltd.

- Submersible load cell:

The compression was controlled and monitored by employing a submersible load cell manufactured by Wykeham Farrance. The load cell had a load range of 5 kN, with a final resolution of ±2.5 N. The load cell was calibrated using a Bundenberg Dead Weight Tester together with a load cell calibration frame.

- Deformation transducer:
  In order to measure the vertical deformation of the specimens the LVDT manufactured by ELE was clamped to the loading piston the top of the triaxial cell while its post and bracket were During testing. The LVDT had a linear range of 50 mm and a resolution of ± 0.01 mm. The deformation data were collected by the CDAS and was displayed, monitored, and recorded by the personal computer for further analysis. The LVDT was calibrated before use by using a 0.001 mm resolution Mitutoya digital micrometer.

- Top platen loading cap and connecting device:
  The top platen loading cap and connecting device were made in-house. It was designed to have a fixed connection between the loading piston and the top cap. The loading piston consisted of a loading rod connected to the submersible load cell. The load cell was attached to a steel truncated-cone shape. The connection to the top cap was a socket-like rubber protrusion designed to just fit and surround the steel. The fixed connection was achieved when a full vacuum was applied through the hole in the top of the cone while it was inserted into the rubber.

3.6.4 Principle of operation

Servo testing systems are used for cyclic triaxial tests because they provide accurate control and measurement of the deformation and force applied to a soil specimen. Within the servo testing system, the energy was transmitted to a specimen using hydraulic fluid acting on the actuator which was coupled to the specimen through the reaction loading frame. The flow of hydraulic fluid was controlled by the servo valve. The servo valve had small electric currents which were used to open and close the control spool of the valve. Because such valves have very high power amplification, large specimens as well as large rates of work can be easily controlled by just controlling the electric current input. Typically transducers such as load cells and strain gauges are mounted on the system for measuring the parameters required. These transducers not only convert the mechanical movement into standard electronic signals via the CDAS but also provide the output display on a computer user interface screen.

There are four ports on the side of the triaxial cell base plate. The confining fluid fills, or is drained from the cell through one port which is also used to apply the confining stress

to the specimen, another two ports provide access at the base of the specimen for either pore pressure or volume change measurement. The fourth port is used for drainage at the top of the specimen and flexible tube with fittings is supplied for the additional port are machined into the base of cell for cable access of the internal on specimen transducers.

3.7 Specimen preparation

All specimens tested in optimum moisture content and saturated states were compacted at same optimum moisture content and maximum dry density. Specimens at dry side were compacted at lower water contents and reached lower dry densities as shown in Figure 3.5. Specimens were then placed on the platen. A latex membrane was placed over the specimen and sealed with o-rings at the base. Any excess air was removed from between the membrane and the specimen and the membrane was sealed with o-rings to the top cap. At this point, the specimen was sealed, and the chamber was filled with water and would be ready for testing in a conventional test.

Before the test the de-aired water in the cell and back pressure GDS was replaced, and the pipe work flushed along with the pore pressure transducer. The cell pressure cylinder was left at the lowest limit of its range to allow for the increased volume change required to drive excess air in the cell into solution. The back pressure cylinder was positioned centrally to allow water to flow both into and out of the specimen. The top cap was positioned inverted with its top level at the specimen mid-height. The back pressure cylinder was emptied to form a thin film of de-aired water on the inverted top cap, the zero of the back pressure and pore pressure transducers was then set. The application of a confining pressure was accomplished immediately after the triaxial cell was full. In order to prevent damage the specimen, the back pressure line left open to the pressure controller. The stepper motor driven controller was capable of holding a constant volume. To ensure no movement of the back pressure a B-check type test was programmed into the GDSLAB software. The cell pressure stage increase in stages until the pore pressure reading was a stable value. By this method, an estimate of the initial effective stress of the specimen could be obtained (Burland and Maswoswe, 1982).

A B-check was then performed to check the degree of saturation of the specimen by applying an increase in cell pressure while maintaining the specimen volume. A B-value of 1 indicates a perfectly saturated soil while lower values relate to lower degrees of saturation. Small changes in saturation, Sr, could cause a large change in B-value.

3.8 Test procedures

3.8.1 Test assembly

1. Created a remoulded specimen by compacting soil at optimum moisture content and maximum dry density into a mould for the wet test, whilst in dry specimen soil compacted at relative density of 75 % that base one table 3.3.
2. Removed the assembled compaction mould from the specimen and place top and bottom porous discs on specimen, then placed the specimen inside the triaxial cell.
3. Top cap should be enclosed by the membrane which was put by the stretcher and sealed with o-rings.
4. Connected the drainage line between the top cap and the base plate with small nylon pipe.
5. Measured the dimensions of the specimen using micrometer and average which is taken from the top, bottom and the middle.
6. Triaxial cell was assembled and secured.
7. The loading piston was dropped slowly to touch the top cap, then connected to the drainage line between the top cap and outer base plate.
8. Drainage line was connected to the water tank to fill the cyclic triaxial cell.

3.8.2 Preparing for the test

1. Cyclic triaxial control programme was opened on the computer.
2. Balance of actuator was adjusted at the middle, then the actuator valve was shut off, lowered, attach and screw the actuator to the piston with the universal joint.
3. LVDT was attached and set to a central displacement.
4. Cell pressure connected and drainage lines connected.
5. Specimen information was inserted as well as cyclic deviator stress to be applied.
6. Zero displacements for the transducers in software.
7. Close the level screen, now the actuator valve can be opened.
8. Click start, enter a file name to be saved.
9. The dialogue box pops up; click reset, to reset all pressures and loads to be zero.

3.8.3 Achieving saturation (if required)

1. Begin saturation by clicking the saturation button.

2. Test designated cell pressure was applied.

3. Test designated back pressure was applied.

4. B-value was checked by closing back pressure valve and applying next increment of cell pressure, then increment of back pressure and open back pressure valve, Note: when B-value ≥ 0.95 indicates full saturation, otherwise the specimen is discarded.

3.8.4 Consolidation

1. Begin consolidation by clicking consolidation button.

2. Set initial effective stress in kPa. First cell pressure was increased.

3. Watch volume change to get stable value, by the opening valve in the software and then opening back pressure valve manually.

3.8.5 Cyclic load

At this stage specimen is already consolidated, number of cycles, constant cell pressure and frequency have been chosen during the programming of the test. Thus, begin with cyclic button and wait till the test terminates having reached the required number of cycles, and then press unload to end the test.

3.9 Monotonic triaxial test

A hydraulic GDS triaxial apparatus for controlling stress path testing was utilised in this project to study the stress-strain response for large displacements. In this system both stress and strain rates are capable of being controlled in the tests (Bishop and Wesley, 1975). A GDS standard triaxial advanced pressure/volume controller (ADVDPC), the pressure supply was provided to the lower chamber cell, and back pressure by a GDS advance pressure/volume controller. These provided pressure up to 2 MPa by use of a microprocessor controlled screw pump and had a volumetric capacity of 1000 cm^3 for cell pressure and lower chamber, while a 200 cm^3 volume was provided on the back pressure.

3.10 Experimental program

Numerous repeated loadings are applied to the track and subgrade as the train passes on a railway track. This would cause induce cyclic stress pulses with varying duration of time between sub sequent pulses depending on train speed as seen in the literature. The response of the superstructure to the cyclic loading varies depending on different parameters such as: shape, duration, train speed, weight of train and the total numbers of pulses. In this project long-term tests are utilised. The cyclic loading was applied to the subgrade and calculated according to the following assumption made in high speed rail way which can be shown in the equations below:

$$\sigma_{cyc} = \frac{\text{axle load of the train}}{\text{sleeper base area}} \tag{3.3}$$

Note: the maximum axle load permitted on the UK network is 125 kN.
The area of sleeper base in HS1 was 2.42 m $\times$ 0.24 m, giving a maximum theoretical load of 430 kPa. This is then reduced by the track superstructure to the levels seen in the literature.

$$q = \sigma_1 - \sigma_3 \tag{3.4}$$

$$p' = \frac{(\sigma'_v + 2\sigma'_h)}{3} \tag{3.5}$$

However, the calculation of weight of track which consists of ballast, sub-ballast and prepared subgrade depends on the unit weight of materials which can be calculated in terms of the formula below:

$$\sigma_v = \gamma d \tag{3.6}$$

Where: d is the depth from the surface in metres and γ is the soil unit weight in kN/m^3. A schematic diagram for the cyclic loading is shown in Figure 3.11.

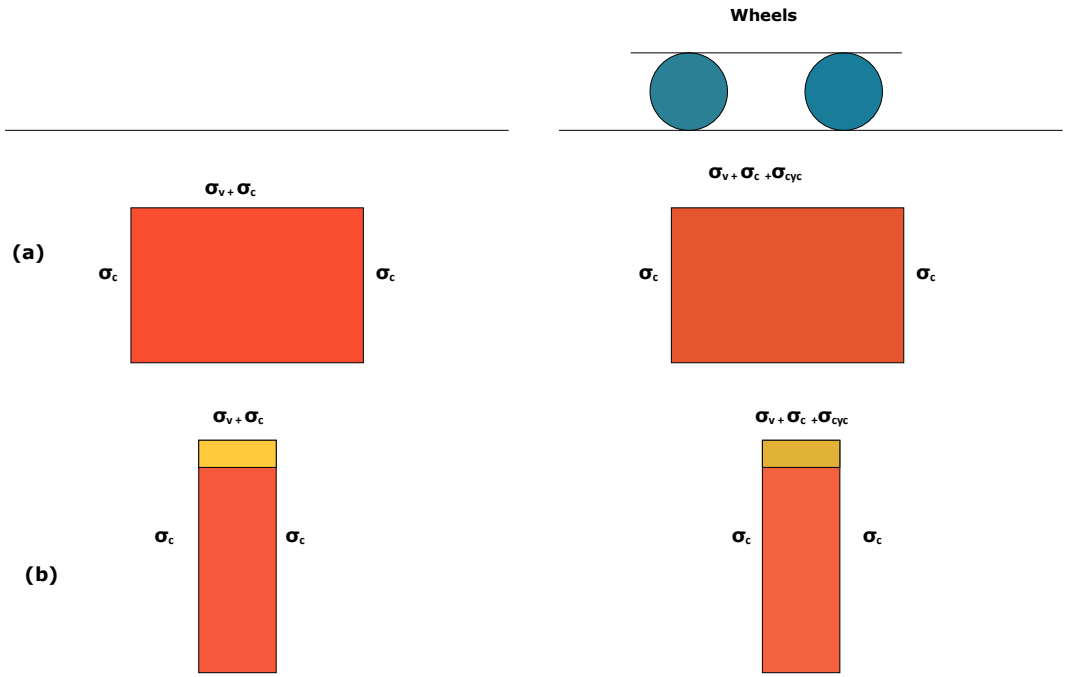

Figure 3.11: Axial symmetric stress state (a) stress state in the field (b) stress state in the laboratory

3.11 Test programme

The axle load considered in this study is that of the British acceptable load, 125 kN. The characteristic of actual dynamic load, confining pressure and initial axial stress were assumed on specimen. The programme of tests are shown in Table 3.5, the measurement of the stress state for both ballasted and ballastless according to the schematic cross section that is shown in Figures 3.12 and 3.13. The vertical stress has been calculated according to depth until 4 m assuming a density of 2.14 Mg/m^3, beyond which the Δq is assumed to be zero (in the ballastless track), as shown by Bian et al. (2014). All specimens have been tested under drained conditions due to the long duration of the tests. In the partially saturated and dry tests, the pressure inside the system was kept equal to the atmospheric pressure by keeping the valve connected to the atmosphere open and shutting off the valve connected to the back pressure chamber. In the saturated condition the valve to the water source of back pressure was kept open, in this case the pore water was allowed to freely drain during loading. The stresses applied at each depth have been taken from the literature review and are given schematically in Table 3.5.

Table 3.5: Test programme overview

Depth (m)	σ_c (kN/m^2)	σ_v (kN/m^2)	σ_{cyc}* (kN/m^2)	σ_{cyc}** (kN/m^2)	q (kN/m^2)	p' (kN/m^2)	S.R.*	S.R.**
1	18	20	40	20	2	18.67	2.14	1.07
2	27	40	30	10	13	32	0.93	0.31
3	40	60	20		20	46.67	0.43	
4	55	80	10		25	63.33	0.158	

Notes: * = ballasted, ** = ballastless, S.R. = stress ratio.

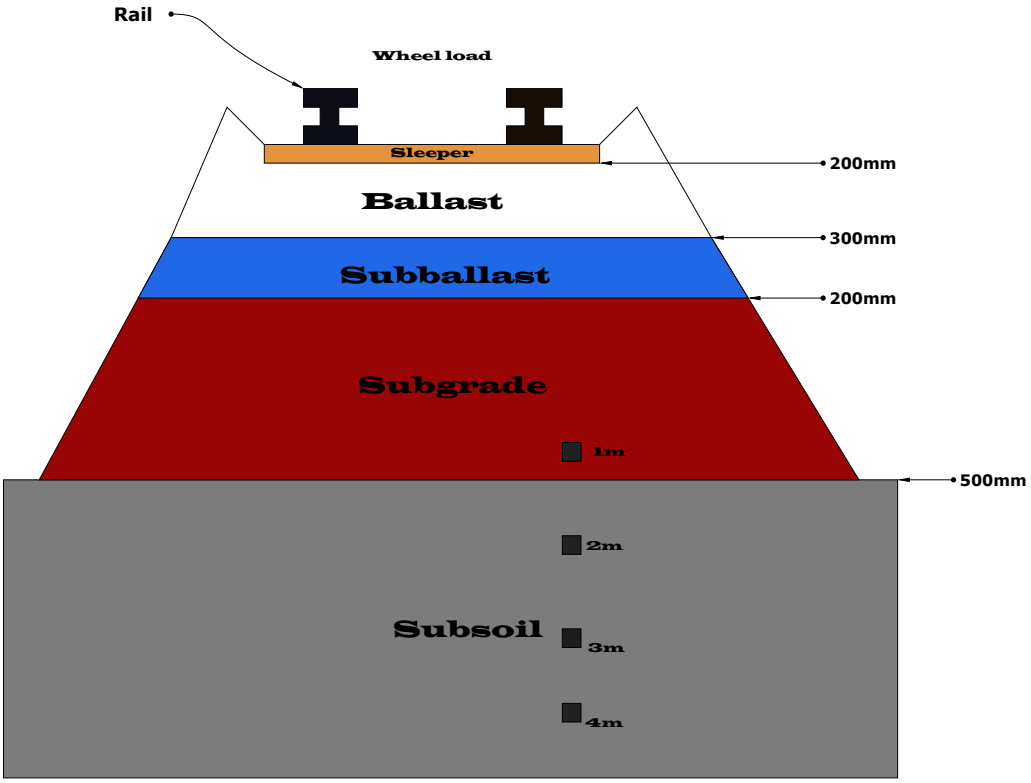

Figure 3.12: Schematic cross section of ballasted track

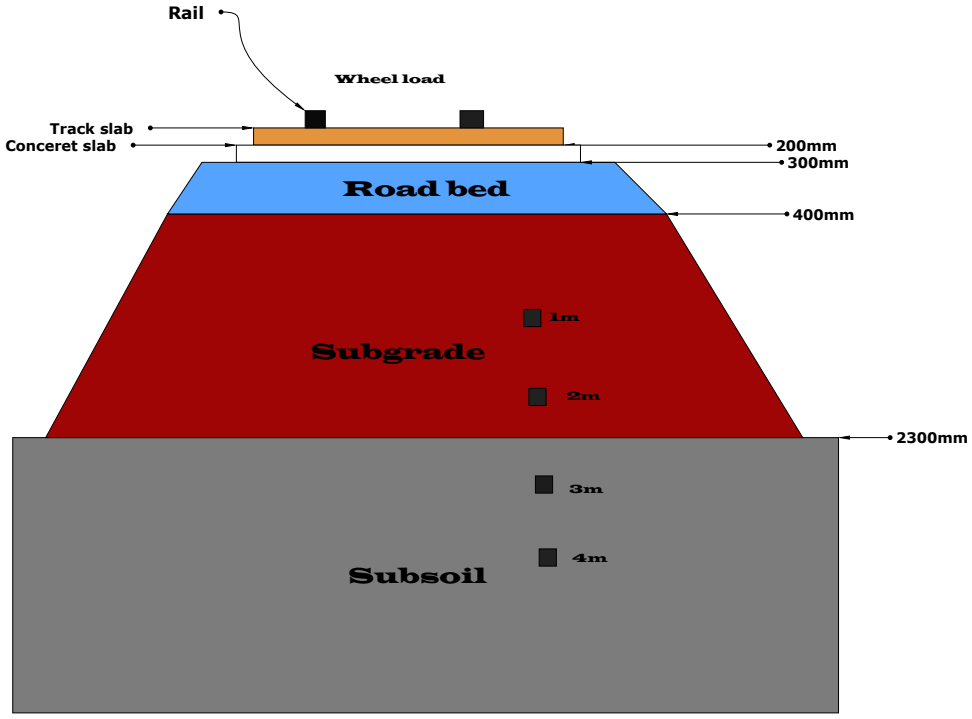

Figure 3.13: Schematic cross section of ballastless track.

3.12 Load frequency

Load frequency plays an important role on the influence of the cyclic stress and cumulative strain and hence the behaviour of the subgrade soil under track. The load frequency of moving train depends upon the train speed, carriage length, number of bogies and axle distance. In the UK transportation pattern high speed railway (HS1) trains run at speed between 230 km/h (143 mph) to 300 km/h (186 mph) with length 108 m. In this study load frequencies of 1 and 4 Hz were used for testing and are indicative of the frequencies induced by HS1.

3.13 Validation checks for the apparatus

A cyclic test was carried out to validate the apparatus. In this method a specimen made from insulation (phenolic) foam, was tested as it exhibits elastic behaviour under compression until it reaches its yield point at 120 kPa. The specimen was made with dimensions 100 mm diameter and 200 mm length. 70 kPa initial confining stress and 40 kPa cyclic stress were applied under three different frequencies.

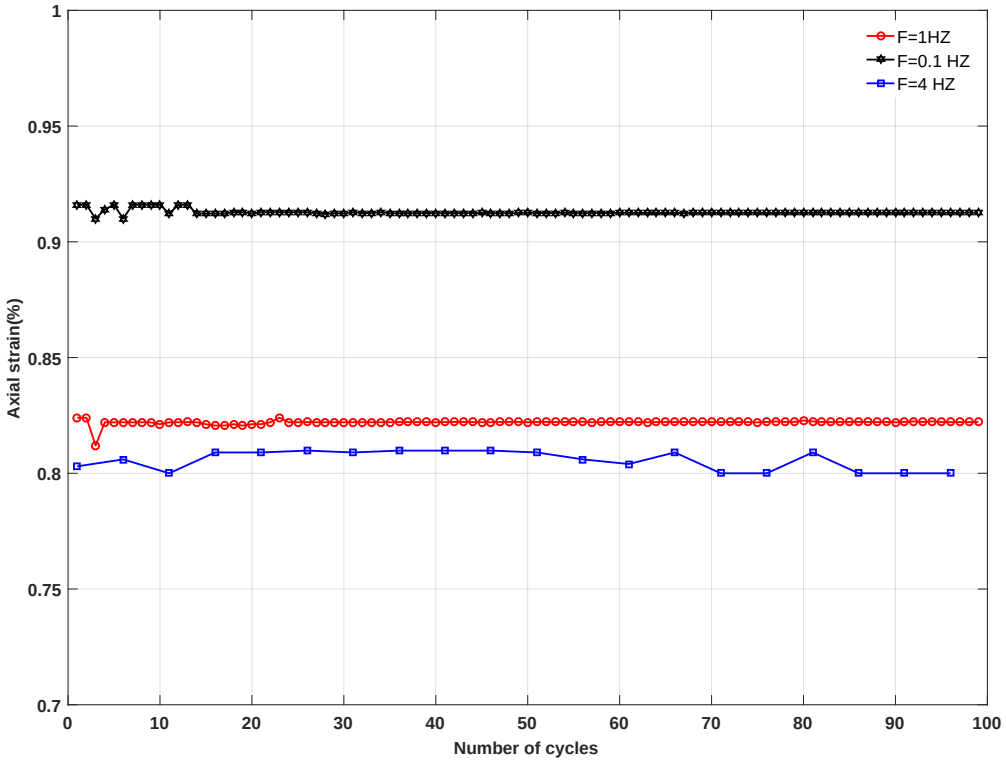

Figure 3.14: Axial strain for phenolic foam insulation

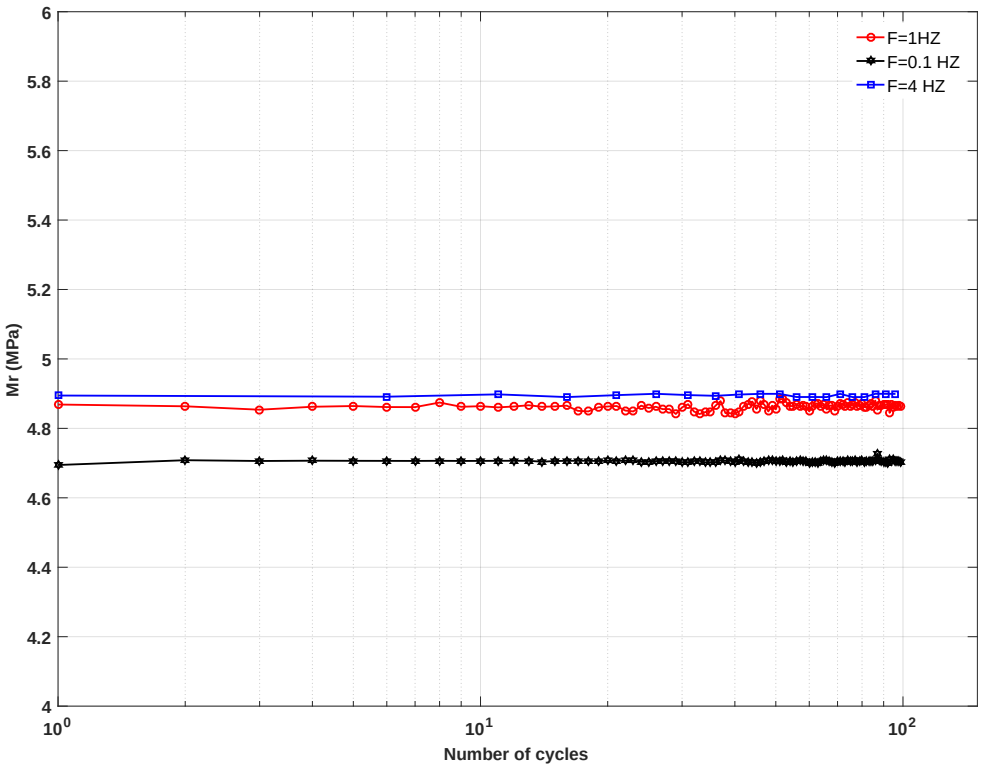

Figure 3.15: Resilient modulus for phenolic foam insulation

The resilient modulus was determined and the results of axial strain are shown in Figures 3.14 and 3.15 these results show that the resilient strain was constant for the duration of the test, as would be expected for a material undergoing elastic deformation. This test was essential to illustrate that the measurement of vertical strain and the calculation of the resilient modulus are reliable.

3.14 Repeatability of the apparatus

In ideal conditions repeated tests are required to be able to accurately assess any given material. With the current test programme having many possible variables and each test being a long duration test to in 10^6 cycles, it was critical that the requirement for repeats could be eliminated. Hence, repeated test were conducted for two test conditions (4 specimens) under triaxial cyclic loading. The results are presented in Figures 3.16–3.19. Specimens 1 and 2 had $<$ 10 mm particles and were tested under saturated conditions, with σ_{cyclic} = 40 kPa and σ_c = 18 kPa. Specimens 3 and 4 had $<$ 5 mm particles and were also tested under saturated conditions but with a σ_{cyclic}= 20 kPa and σ_c= 40 kPa. It can be seen that in both cases the specimens behave almost identically in terms of both resilient modulus and cumulative strain. Hence, in the current test series repeat tests will not be conducted, allowing a wider set of test variables to be examined as shown in Table 3.6.

3.15 Experimental issues

With the current cyclic system, loading is applied continuously until either the termination strain level is exceeded or it is stopped manually by the operator. To apply a always compressive sinusoidal load, the loading pulse wave shape was set in the UTM software to be haversine. The information in the binary file (*.bin) stored all the test parameters and test data results. This data could also be converted into an ASCII file (*.csv), a readable data file which is generated by the system and can be read by spreadsheet programs. The run time data capture file(*.txt) is used to capture all the cyclic test data during the cyclic test phase of the procedure. The wave shape function stored 512 loading points per cycle and was used by the DSP controller to time the output steps of the 512 entries that constitute the desired wave shape.

The storage of information in the UTM software depends on the loading rate and loading sequence. For a test consisting of 10^6 cycles the software only stores 626 data points. This is hard programmed into the software and is not user configurable. The software was originally designed for slow cycles taking many seconds, not for thousands

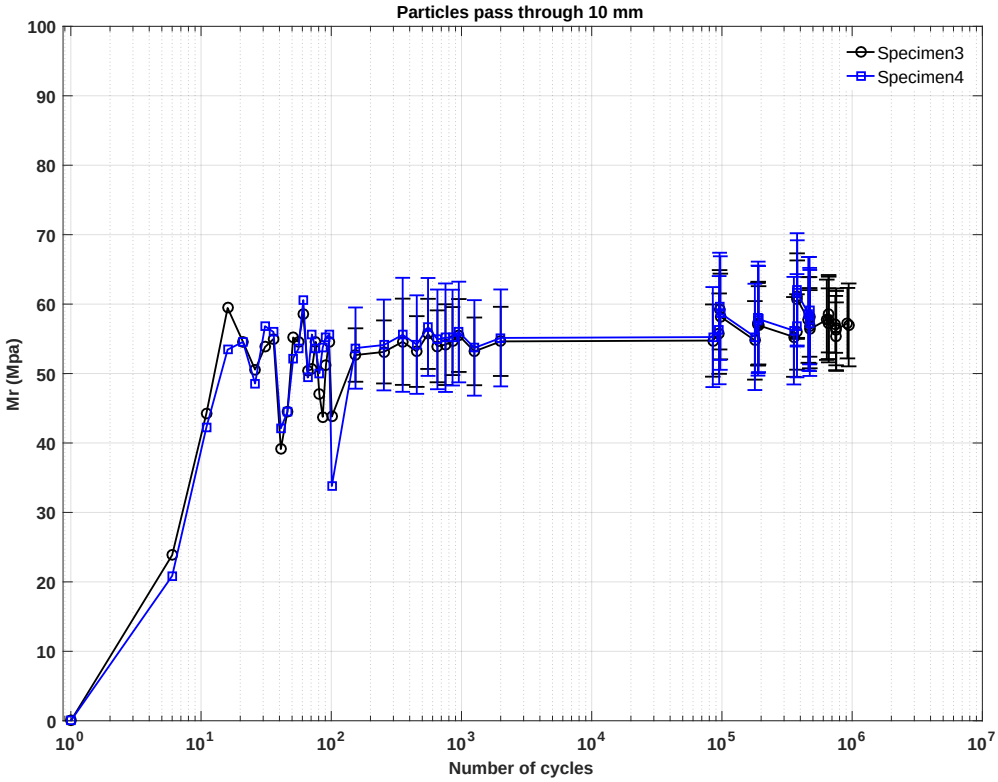

Figure 3.16: Resilient modulus for two identical saturated specimens, $\sigma_{cyclic} = 40$ kPa

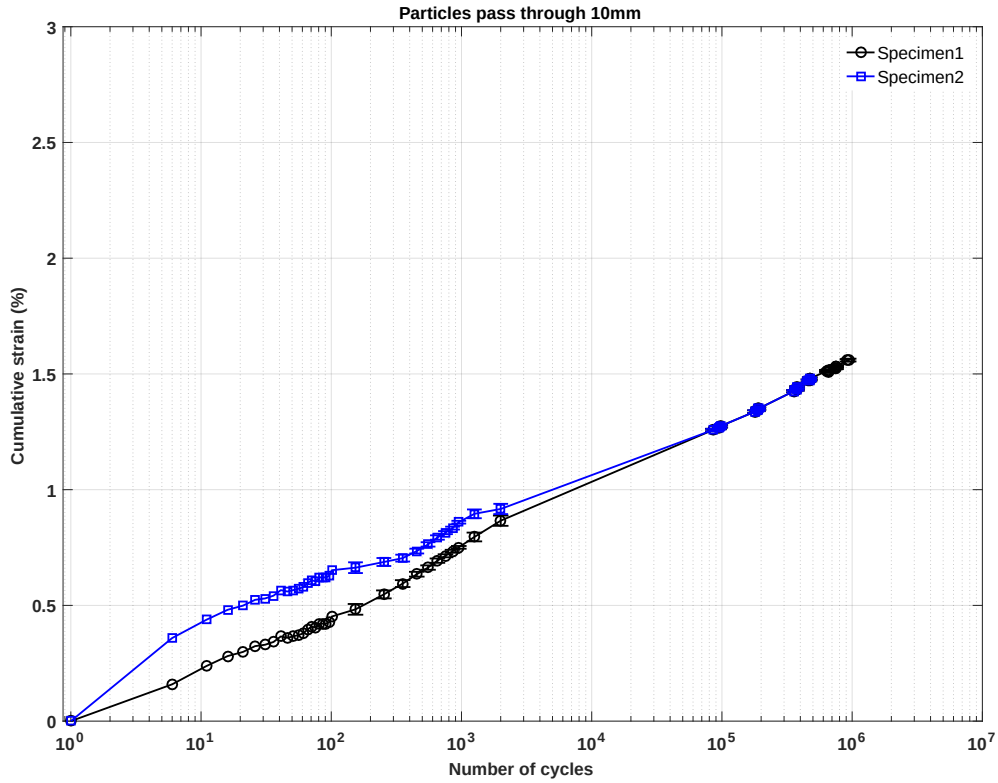

Figure 3.17: cumulative strain for two identical saturated specimens, $\sigma_{cyclic} = 40$ kPa

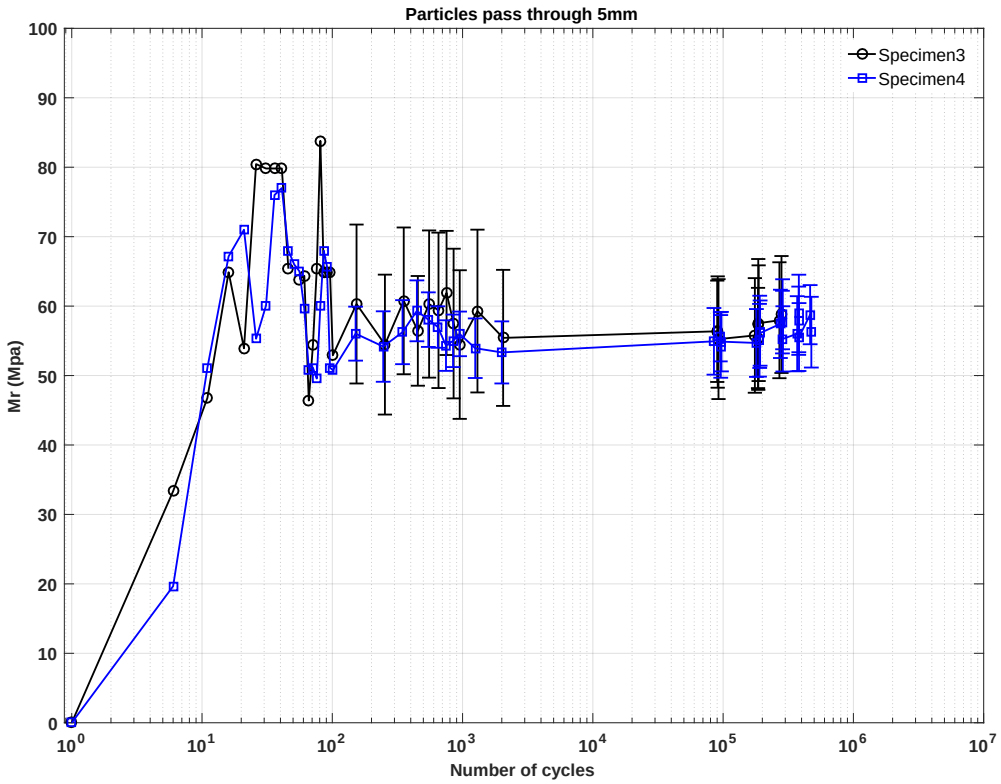

Figure 3.18: Resilient modulus for two identical saturated specimens, $\sigma_{cyclic} = 20$ kPa

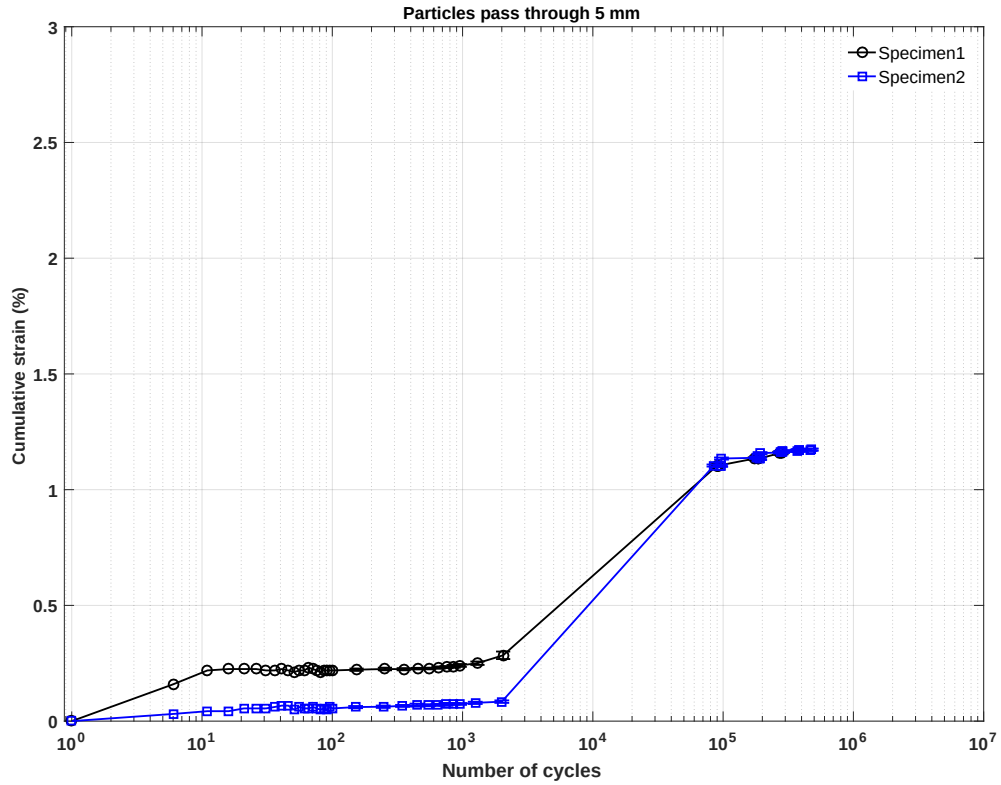

Figure 3.19: Cumulative strain for two identical saturated specimens, $\sigma_{cyclic} = 20$ kPa

of cycles at high frequency. In order to collect as much data as possible, 10^5 cycles were applied, for two different frequencies. For the frequency of 4 Hz each data point represents the average of 5 cycles, this is maintained for the first 2496 cycles, then data kept from 80156 to 10^5 cycles with each data point representing 160 cycles as shown in Figure 3.20. In order to analyse the data in this case after first sequence of cycles the cumulative stain was measured and resilient modulus was calculated. Firstly, the first hundred data points of resilient modulus were plotted. Secondly, from 106 to 2496 cycles the average with standard deviation(error bar) were plotted and from 80156 until 10^5 data again the average with standard deviation were plotted. For the next sets of 10^5 cycles the average between 1 to 2496 and 80156 to 10^5 were plotted to complete the whole figure (Figure 3.21).

In the 1 Hz tests the first 500 cycles were captured each being represented by a single data point, the data is then not stored until 64128 cycles at which point each data point from cycle 64128 to 10^5 represents an average of 128 cycles, shown in Figure 3.22. Similar to the 4 Hz data scheme, the specimen that was tested at 1 Hz, the first 100 data point of resilient modulus versus number of cycles have been plotted and then for the rest of the data points represent the average and standard deviation (error bar) for each 1000 data points as shown in Figure 3.23.

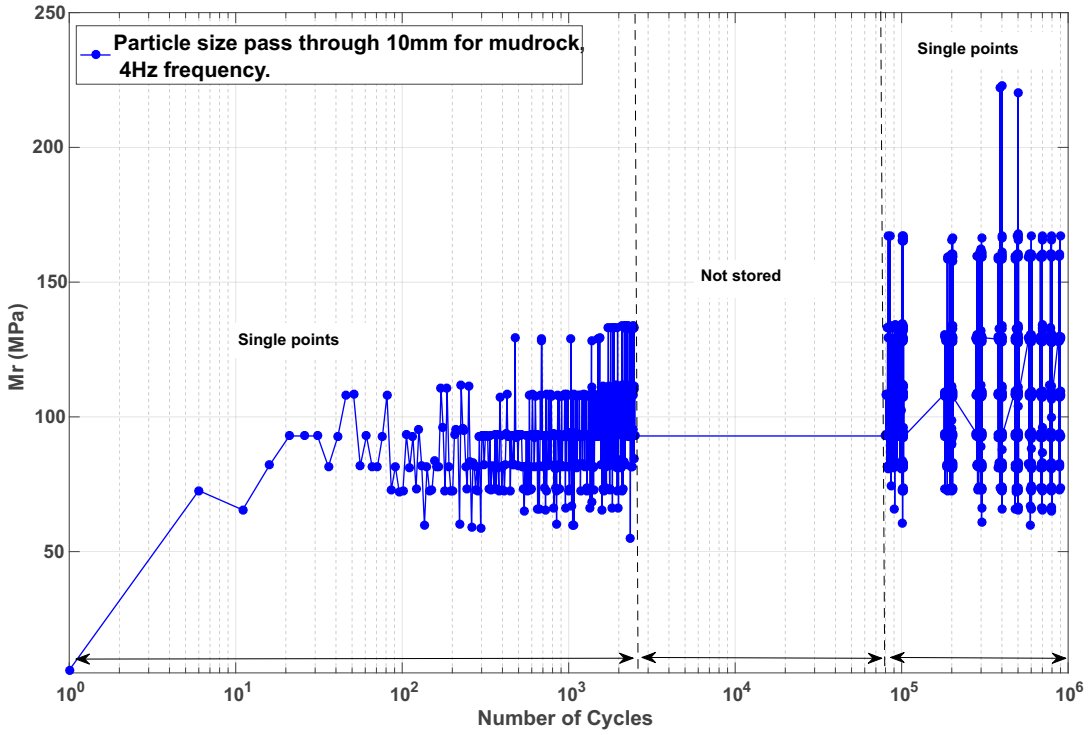

Figure 3.20: Data recorded during a test with 10^6 cycles, 4 Hz

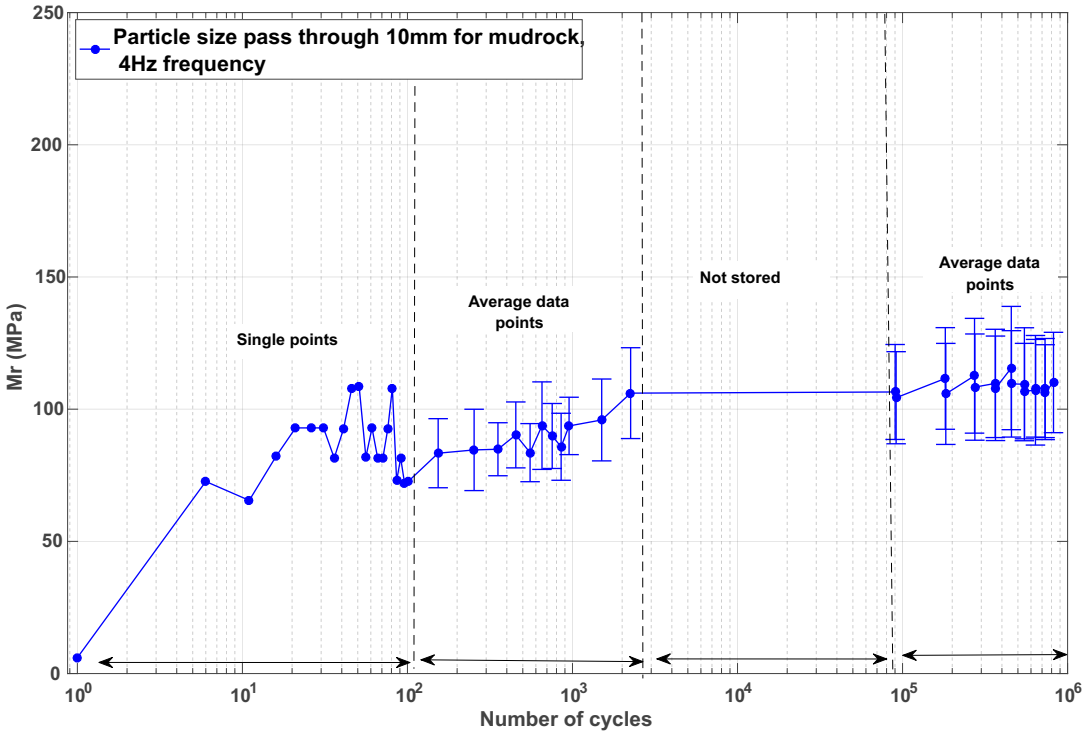

Figure 3.21: Processed output data scheme, 4 Hz

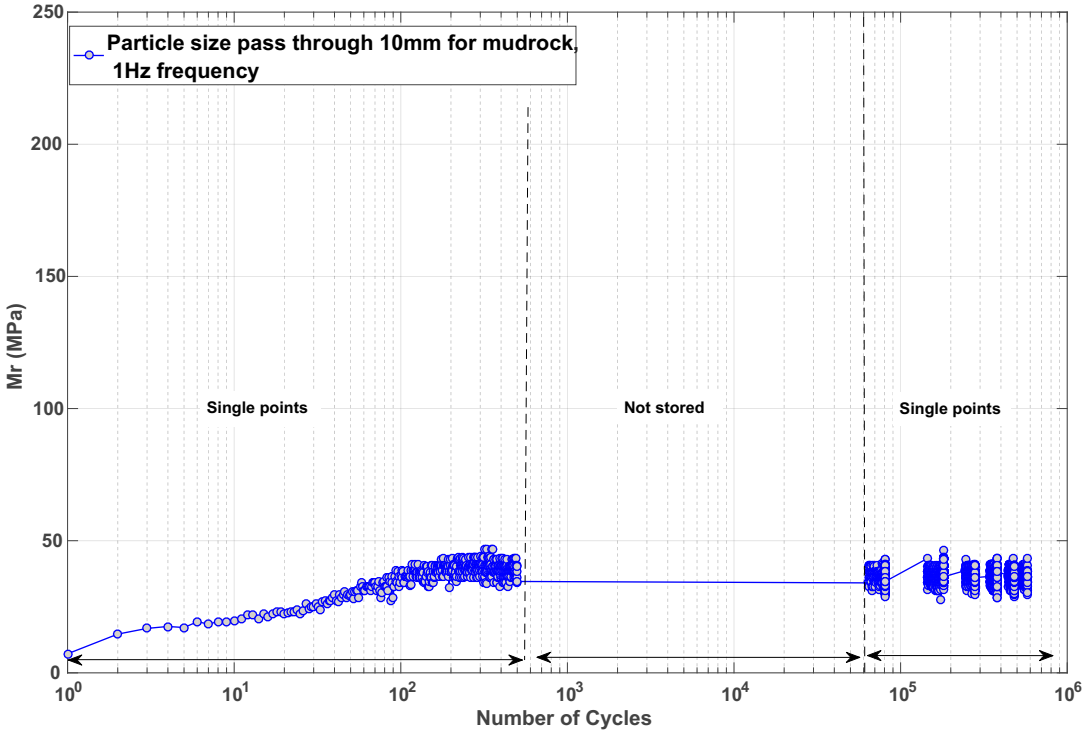

Figure 3.22: Data recorded during a test with 10^6 cycles, 1 Hz

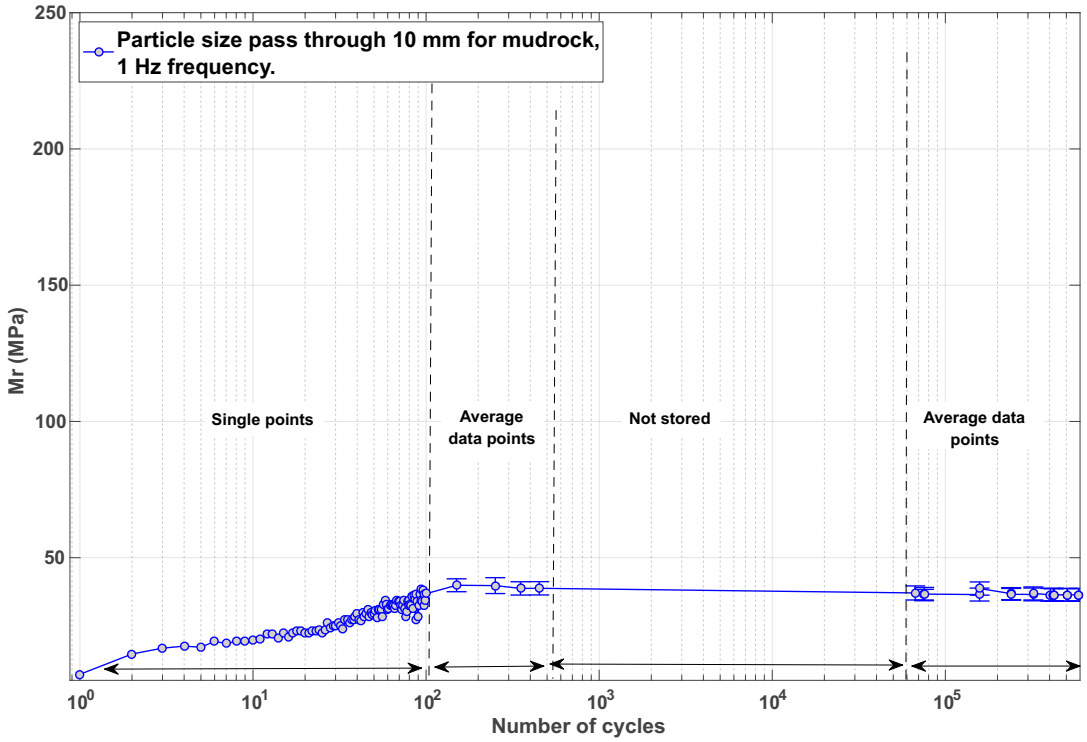

Figure 3.23: Processed output data scheme, 1 Hz

3.16 Stress-strain characteristics of mudrock

Two specimens of mudrock with particles less then 10 mm were compacted at optimum moisture content. The specimens were saturated and isotropically consolidated before been sheared under confining pressure of 30 and 58 kPa. The purpose of this test was to investigate the effect of stress on the strength of the soil and determine the failure envelope. A shearing rate of 15%/h was chosen for both tests. The results are shown in Figure 3.24 and Figure 3.25. The end point for each of each shear test can be refereed to as being on the critical state line. It can be observed that the gradient of the critical state line (M) decreases with decrease the confining pressure. This equates to a friction angle between ϕ= 32.7° and ϕ= 36.9° for this material under stress conditions tested.

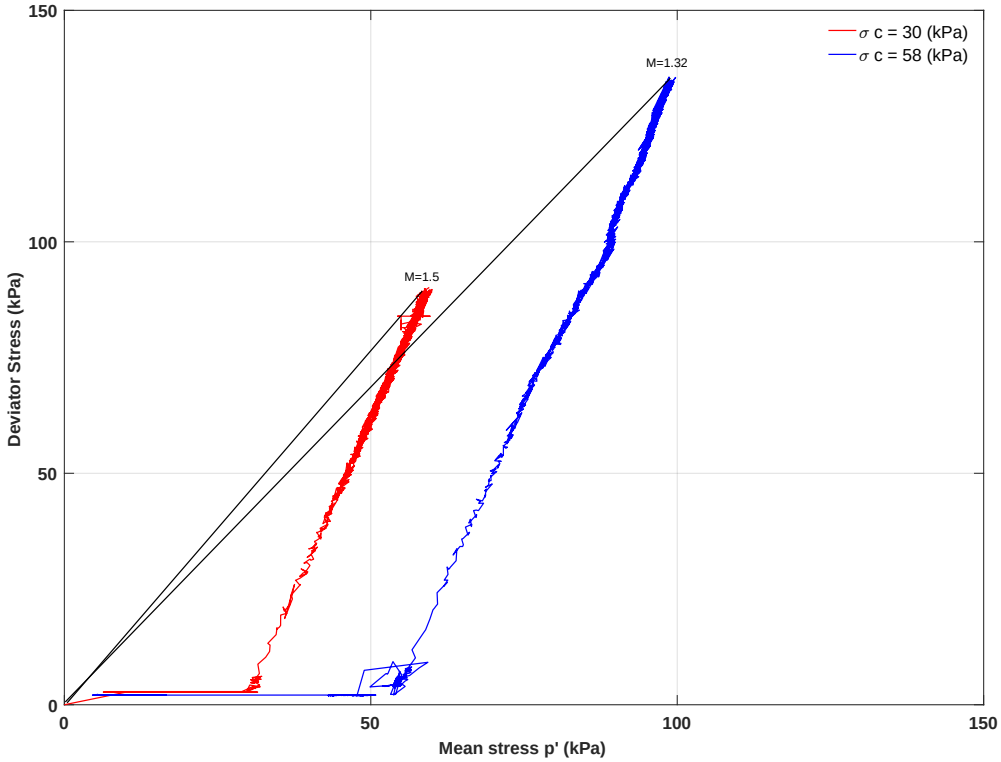

Figure 3.24: Determination of critical state for 30 and 58 kPa confining pressure triaxial compression tests

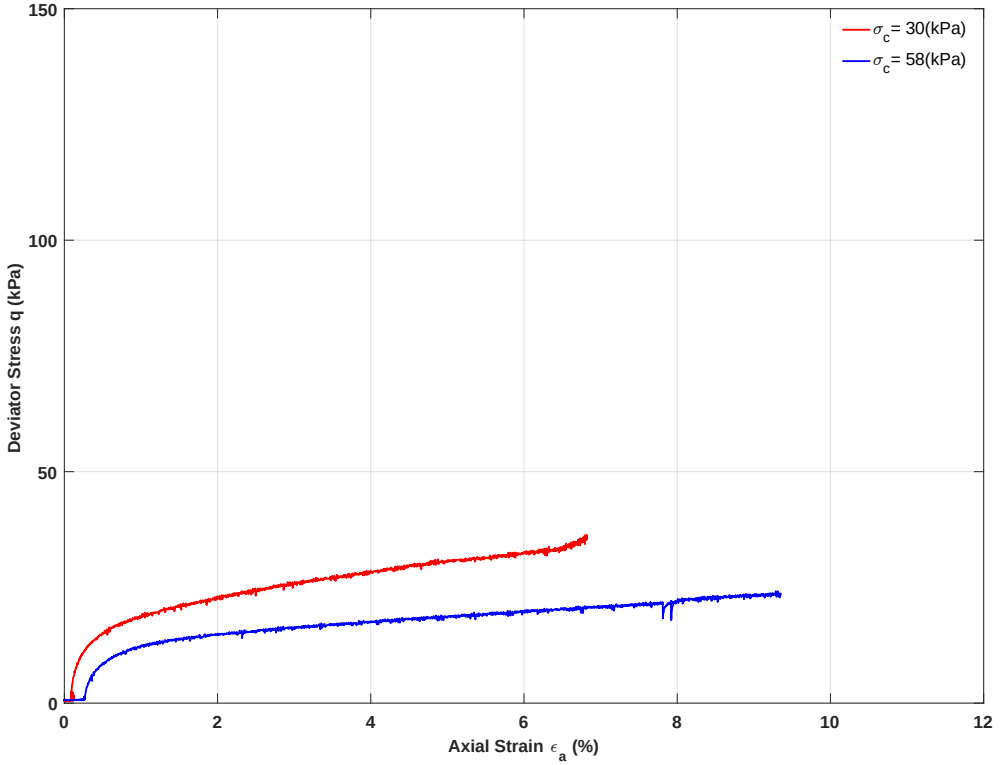

Figure 3.25: Stress-strain data for 30 and 58 kPa confining pressure triaxial compression tests

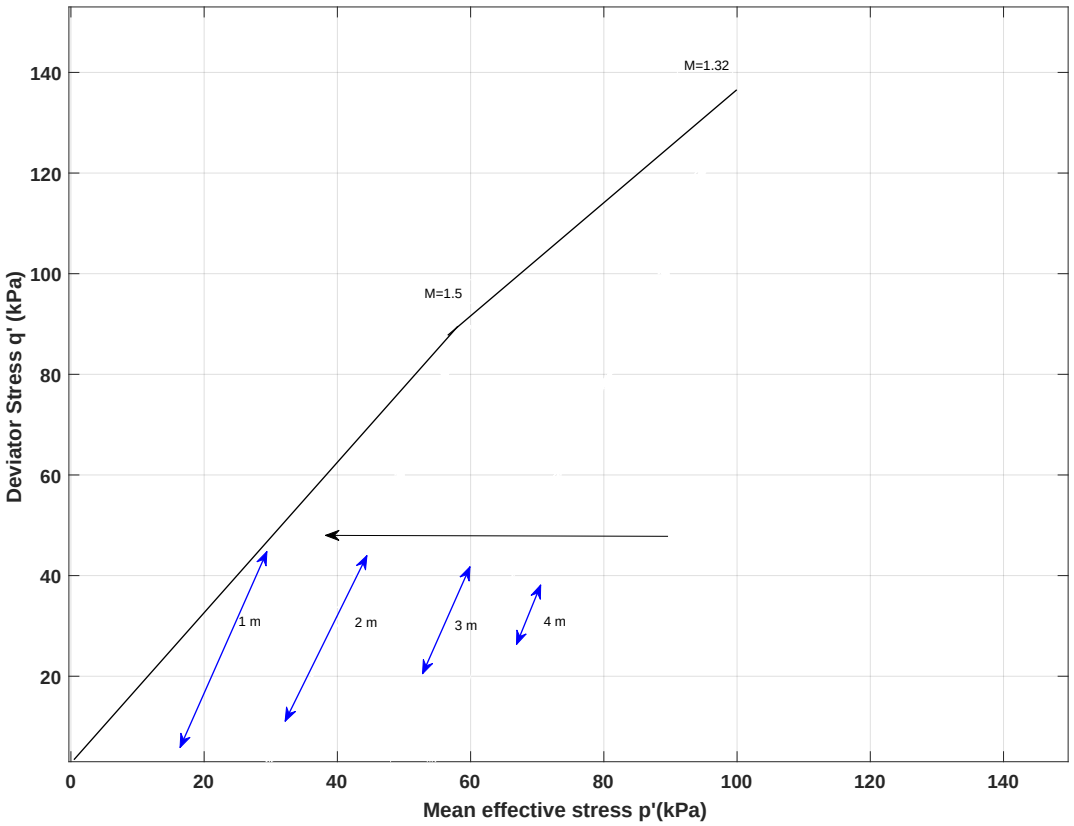

Figure 3.26: Expected stress paths for the experimental programme

Figure 3.26, plots the expected stress paths from the test programme (Table 3.5 on page 51) onto an extrapolated failure envelope. This shows that the soil is not likely to fail under the conditions of the experimental programme.

3.17 Summary

This chapter has described the methodology that will be used in the test programme below. 54 samples have tested based on the literature tests will be conducted with under different conditions of water content, stress level and loading frequency. The conditions of each planned test is shown in Table 3.6. The method for specimen creation has been tested to ensure consistency across the test programme. The physical properties of the material have been shown above in order to understand the behaviour of mudrock, and it found that properties of mudrock in this study are in the same range of that reported by Nahazanan (2010) and Blanchfield (1998). In addition, both specimen preparation and apparatus have been validated. The results have shown that the apparatus is capable of producing repeatable tests. Thus, each condition will be tested once allow a larger

parameter space to be explored.

Table 3.6: Detailed test programme, with numbers of samples tested

Soil conditions	σ_{cyc}= 40 kPa σ_c= 18 kPa	σ_{cyc}= 30 kPa σ_c= 27 kPa	σ_{cyc}= 20 kPa σ_c= 40 kPa	σ_{cyc}= 10 kPa σ_c= 60 kPa	σ_{cyc}= 20 kPa σ_c= 18 kPa	σ_{cyc}= 10 kPa σ_c= 27 kPa
Particles < than 10 mm, 4 Hz						
Saturated, ρ=1.96 Mg/m^3	1	1	1	1	1	1
P.S. <OMC, ρ=1.98 Mg/m^3	1	0	0	0	0	1
P.S. at OMC, ρ=2.04 Mg/m^3	1	1	1	1	1	1
Dry, ρ= 1.80 Mg/m^3	1	0	0	0	0	1
Particles passing less than 5 mm, 4 Hz						
Saturated, ρ=2.05 Mg/m^3	2	1	1	1	1	1
P.S. < OMC, ρ=2.065 Mg/m^3	1	0	0	0	1	0
P.S. at OMC, ρ=2.11 Mg/m^3	1	1	1	1	1	1
Dry, ρ_{max}=1.89 Mg/m^3	1	0	0	0	1	0
Particles less than 10 mm, 4 Hz						
Saturated, ρ=1.96 Mg/m^3	2	1	1	1	1	1
P.S. at OMC,ρ=2.04 Mg/m^3	1	1	0	0	1	1
Dry, ρ= 1.80 Mg/m^3	1	0	0	0	1	0
Particles less than 5 mm, 1 Hz						
Saturated, ρ=2.05 Mg/m^3	1	1	0	0	1	1
P.S. at OMC, ρ=2.04 Mg/m^3	1	1	1	1	1	1
Dry, ρ= 1.89 Mg/m^3	1	0	0	0	1	0

Notes: OMC= Optimum moisture content, P.S.= Partial saturated,
= Cyclic stress, σ_c= Confining pressure.

Chapter 4

Effect of particle size and water content on Resilient modulus

The subgrade soil in railway track substructures is subjected to high numbers of loading cycles every day. The stresses such soil would be exposed to have been recreated in the laboratory. Triaxial cyclic loading was carried out to study the resilient modulus Mr of the mudrock under variations of water content and particle size including dry, partially saturated at dry side, partially saturated at optimum moisture content and in saturated conditions, as the resilient modulus is the key parameter for the engineering pavement design. Both frequencies of 1 and 4 Hz are also considered. The results and discussion of this work are contained within in this chapter.

4.1 Particle size distribution and water content

Different particle size distributions and water contents have been chosen in this programme, as these factors are changed by fluctuations in the natural water table. Tests were conducted on compacted specimens under 20–25 kPa of initial vertical stress and cyclic loading of 20–40 kPa, 18 kPa confining stress which was held constant and 1 and 4 Hz frequencies to simulate the impact of train bogie loading under 1 m depth, a large number of cycles were then applied (10^6 for most tests).

4.1.1 Particles passing through 10 mm sieve

Figure 4.1 shows a semi-log plot of the test results, plotting the resilient modulus as a function of number of cycles under different water content conditions at 4 Hz. This figure shows that at the beginning of each test there is an increase in Mr and then a more stable region with an increasing number of cycles that can be attributed to the rearrangement

and breakage of particles. The resilient modulus, develops to 110 MPa at 2×10^{6} cycles. The is a general trend that Mr decreases with increasing water content. It can be observed that the Mr in the partially saturated OMC test tends to decrease after 2×10^{3} cycles to become 16% less than the fully saturated stiffness. It is known that particles tend to rearrange themselves to become more dense to reach equilibrium, and this depends on the soil conditions. As a result of this rearrangement, permanent slips occur at the contacts between particles and permanent dislocation of particles leading to unrecoverable strain (see Section 4.2).

Similarly, Figure 4.2 shows the results of the same tests conducted at 1 Hz to highlight the effect of frequency on the response. It can be seen that with the reduction of loading frequency, the resilient modulus also lowers whilst keeping the same moisture content trends. Under saturated conditions the soil Mr increases sharply after first cycle then reaches an early equilibrium. In the partially saturated specimen this increase in Mr is much more gradual, becoming stable after 10^3 cycles, with the magnitude being equal to the saturated state.

Structural breakage and rearrangement leading to densification of the specimens is likely in these high number of cycle tests. This phenomenon is likely to increase the scatter for Mr due to the high frequency of the repeated load. Saturated and unsaturated conditions are considered to account for the effect of water content on resilient modulus. It can be seen that the Mr is higher at low degrees of saturation (dry side), due to the lower amount of moisture having a beneficial impact as water inside the soil structure causes a lubricating effect and leads to reduced friction (Thom and Brown, 1987).

At water contents higher than optimum, the voids are mainly filled with water and matrix suction would be low in this case. Thus, the soil is likely to lose some mechanical development of strength (Duong et al., 2016). For degrees of saturation lower than optimum, Mr was higher and increased with number of cycles. This is likely due to the air voids present in the soil. The specimen tested at the optimum moisture content behaved the same as the specimen at full saturation for the first of 2500 cycles and then diminished slightly possibly due to internal pore pressures; in this case, the effective stress may not be equal to the total stress for partially saturated case. Whilst in the dry case the total stress and the effective stress are the same (Hicks and Monismith, 1971). In addition, in the saturated state, the effective stress in the specimen under repeated loading decreases due to the development of excess pore pressure. It could be argued that it is influenced by the response of deformation, as well as causing a reduction in both strength and resilient modulus (Dawson et al., 1996).

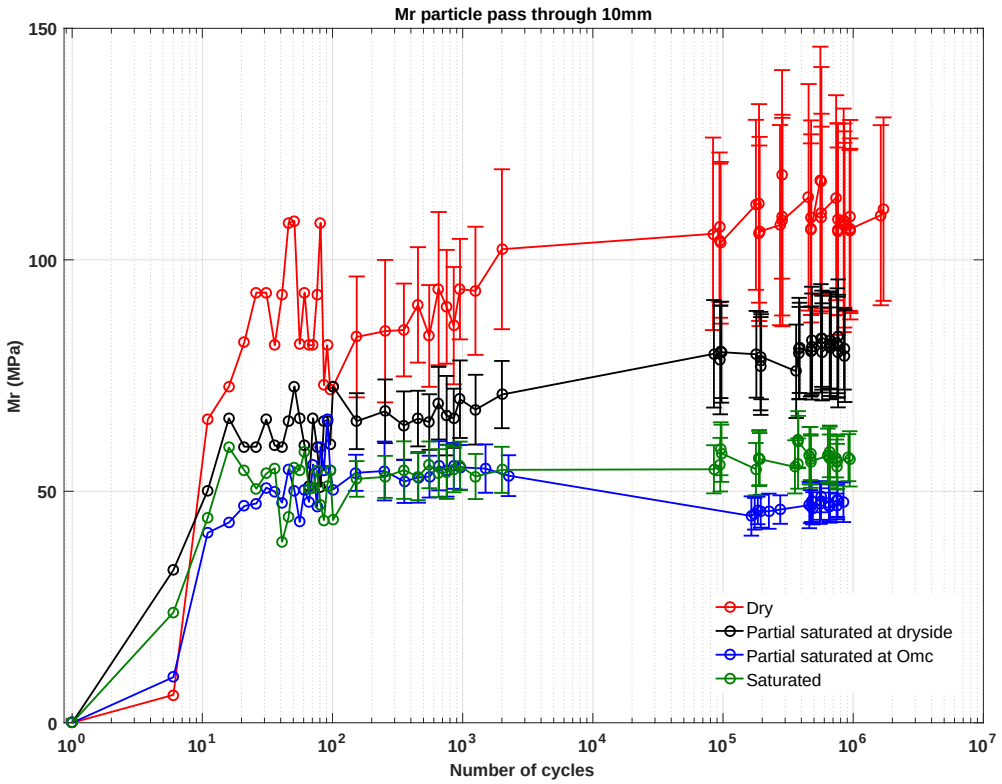

Figure 4.1: Resilient modulus with different water conditions for particles < 10 mm, 4 Hz.

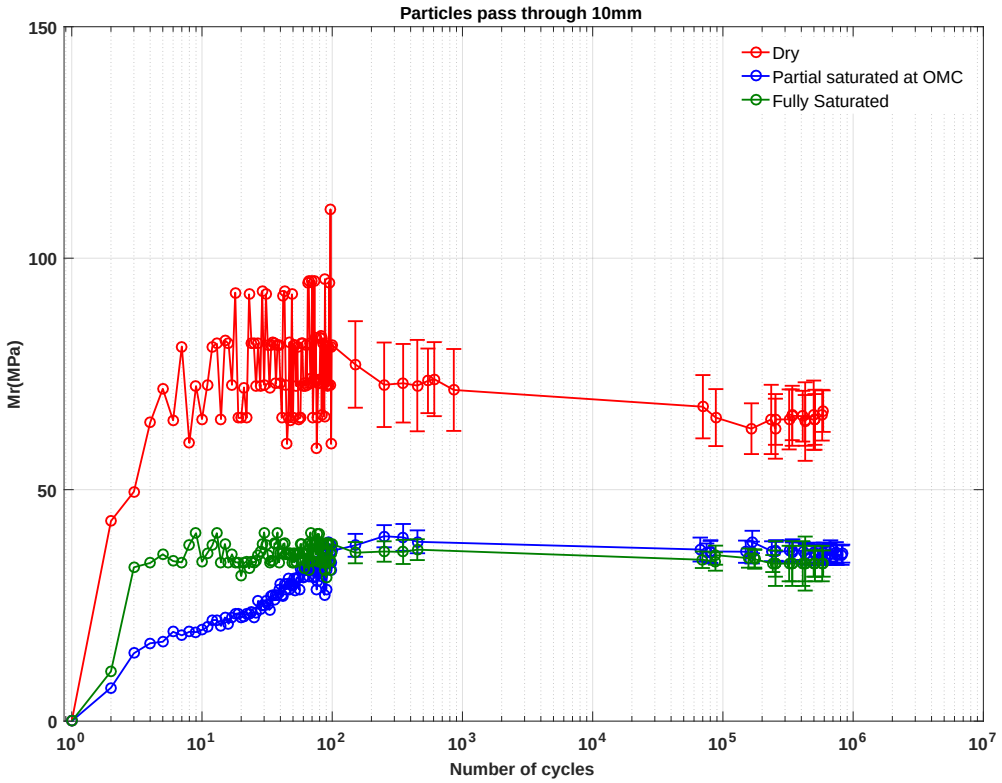

Figure 4.2: Resilient modulus with different water conditions for particles < 10 mm, 1 Hz.

4.1.2 Particles passing through 5 mm sieve

Figure 4.3 shows the results for each specimen tested under the same loading and water conditions of the specimens in Figure 4.1, to show the effect of reducing the maximum particle size. In this figure, partially saturated at optimum and fully saturated specimens reach stability in the early stages of the cyclic test, again the partially saturated case is less stiff than the saturated case (6%). In the unsaturated at dry side specimen a plateau is reached which lasts to around $2{\times}10^3$ cycles, then diminishes to reach a final resilient modulus 13% higher than the saturated state. It can be observed that an increase in fines content leads to a decrease in the resilient modulus whilst keeping the same pattern of water content influence. This agrees with the results shown by Kamal et al. (1993) for soils consisting mostly of coarse grained fractions. However, in the saturated case the excess pore water pressure develops under the rapidly applied loading, resulting in a reduction in the resistance to deformation of the soil. Generally, there is a combined effect from water and fines content, as a reduction in the resilient modulus accompanies increase in water and fines content.

A loading frequency of 1 Hz was also applied for compacted mudrock specimens in same conditions that the $<$ 10 mm particles were tested under. The results are shown in Figure 4.4 and show the same progression as seen in the $<$ 10 mm tests. In general, the patterns of resilient modulus with variations in moisture content conditions exhibit the same trends with an overall reduction in resilient modulus. Mr is reduced in the saturated and partially saturated specimens with a sharp decline in final modulus from the dry specimen. The Mr of the dry specimen also increases linearly with the increasing number of cycles. For specimens tested under the higher cyclic frequencies there would be a shorter resting time for the loaded specimen to rebound elastically between the pulse loads. If the specimen does not rebound completely, the total recovered strain would be lower and the determined resilient modulus would be higher.

Generally, at the beginning of each test the cyclic stress did not return to the original level and this could hasten the development of permanent axial strain, with an increasing number of cycles. In addition, the vibration induced by the cyclic loading causes rotation and rearrangement of the particles producing plastic strain. The $<$ 5 mm specimens show a similar form of response in the 4 Hz frequency testing, with the specimens tested in dry conditions giving the highest resistance as with the lower 1 Hz testing frequency. Specimens compacted at water contents less than optimum give a higher modulus when compared with partially saturated at optimum moisture content and fully saturated specimens.

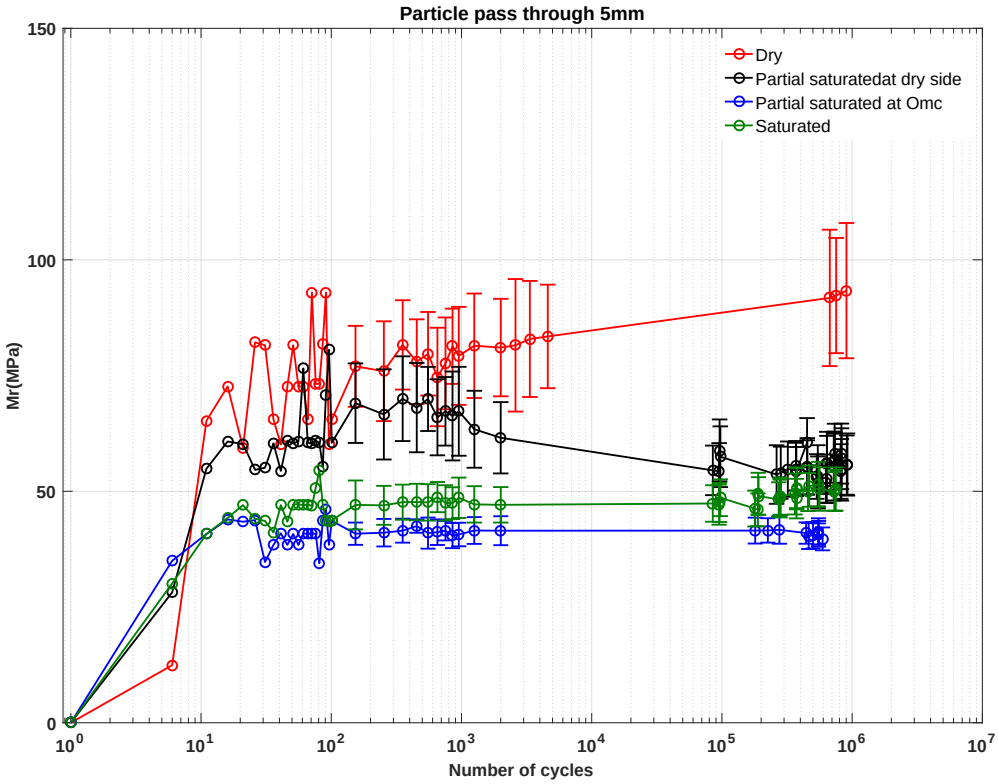

Figure 4.3: Resilient modulus with different water conditions for particles < 5 mm, 4 Hz

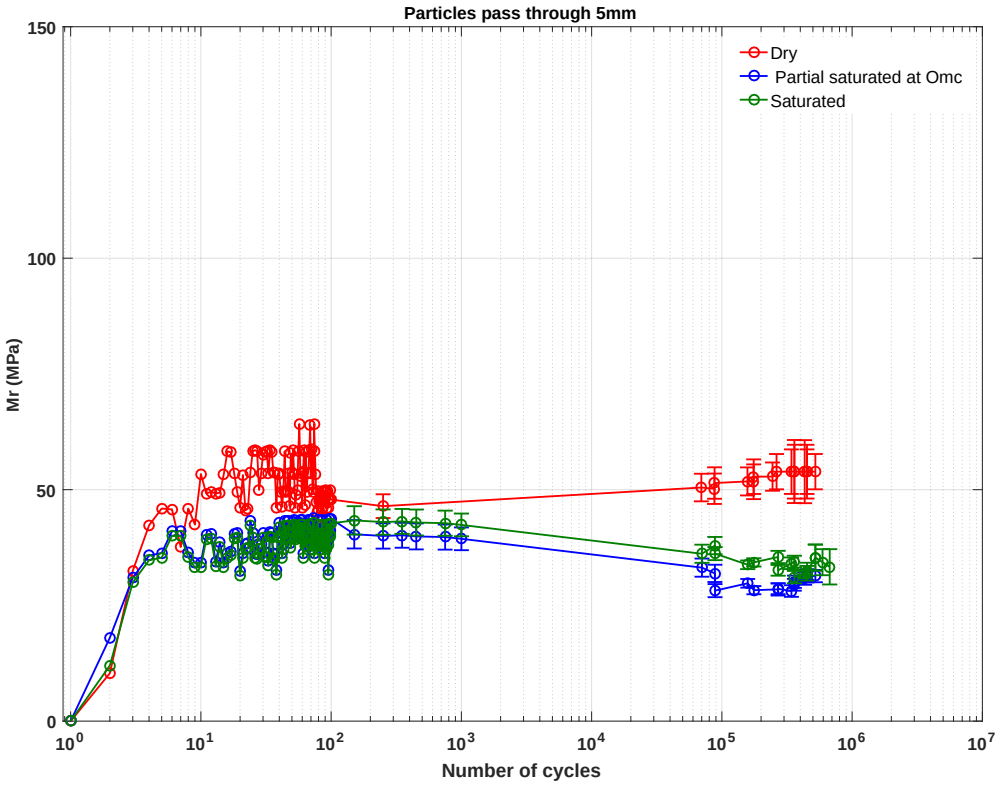

Figure 4.4: Resilient modulus with different water conditions for particles < 5 mm, 1 Hz

To more closely examine the variations in each moisture content condition on the resilient modulus, Mr verses number of cycles is plotted for each condition at different particle size and load frequency as seen in Figures 4.11–4.14 and discussed in Section 4.4.

4.2 Permanent deformation

Geotechnical designs for railway substructures will commonly have to include the calculation of settlement. The fact that cyclic loading leads to increased permanent deformation compared with static loading, must be accounted for in the design. Under the axial strain applied in the testing, plastic strains occur.

Cumulative strain has been plotted against number of cycles for varying conditions to characterize the settlement rate for mudrock colliery spoil. The results show, as expected, that deformation increases with the number of cycles. However, there appears to be no equilibrium for the cumulative strain for each case as was found in the resilient modulus behaviour. There is a step in strain at the beginning of each test due the initial compaction. This then leads to a slow increase which appears linear on a log scale.

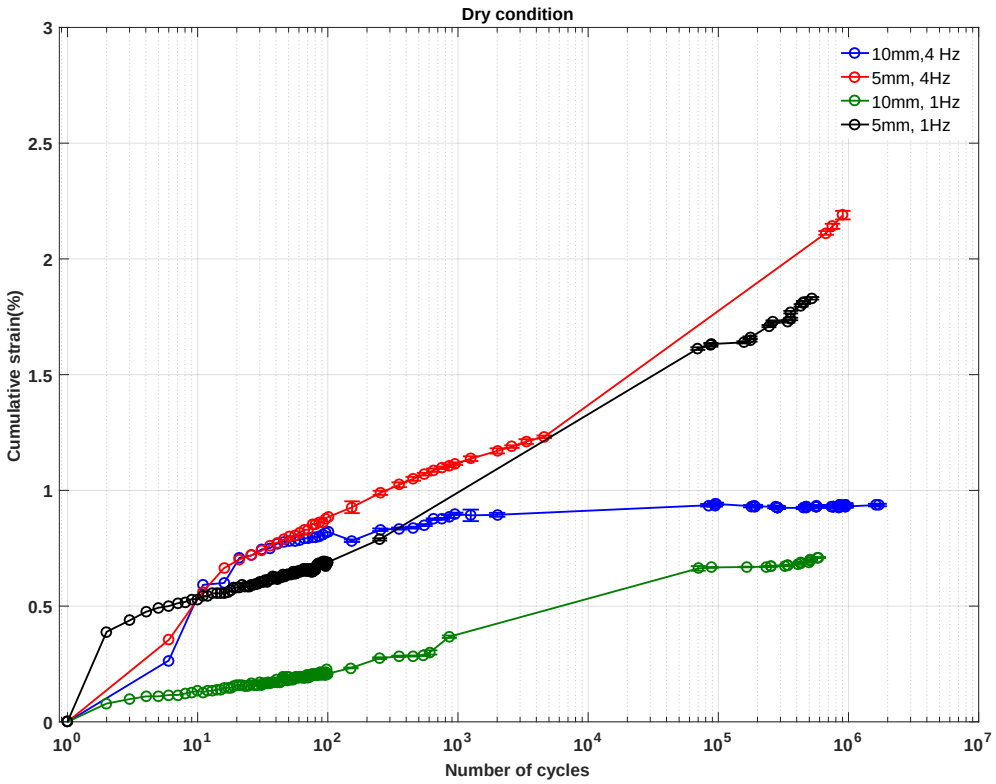

Figure 4.5: Cumulative strain under dry conditions for varying particle sizes and frequencies

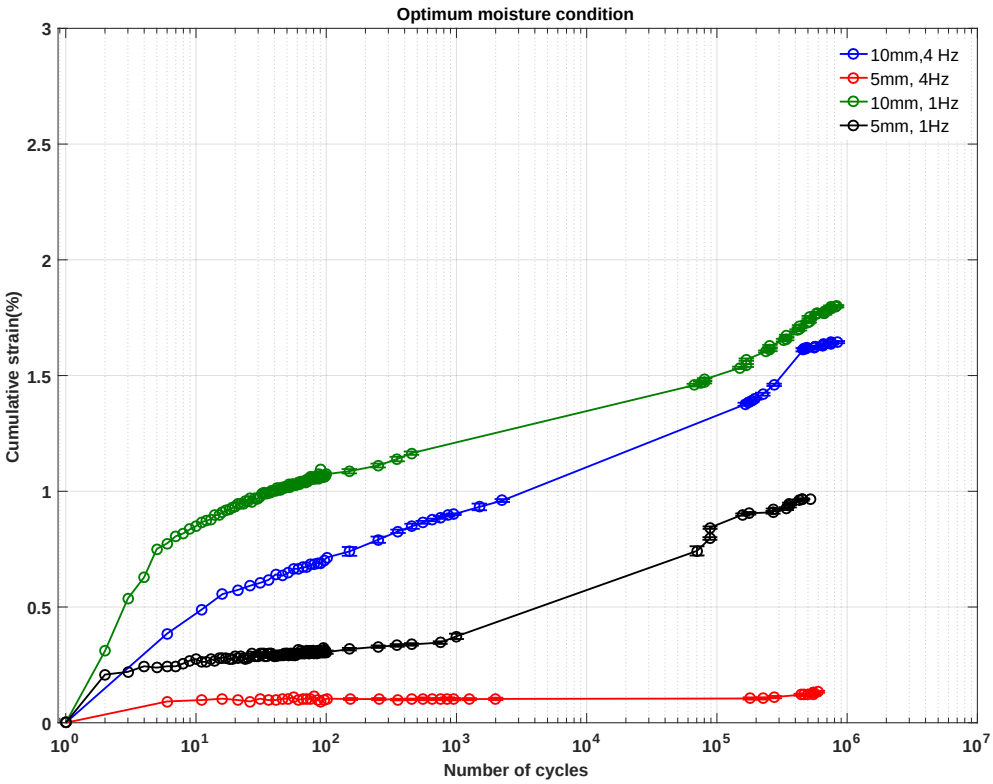

Figure 4.6: Cumulative strain at OMC for varying particles sizes and frequencies

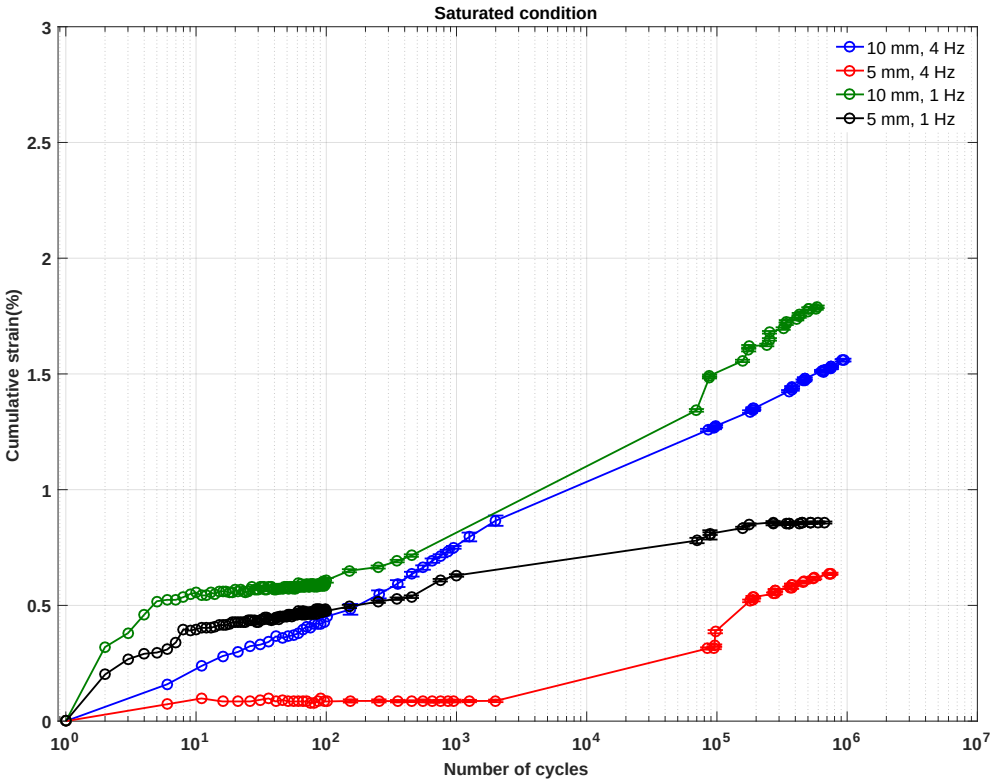

Figure 4.7: Cumulative strain in saturated conditions for varying particle sizes and frequencies

Cumulative strain for dry conditions are shown in Figure 4.5. In this figure, different dry specimens are compared for both particle sizes < 10 mm and < 5 mm and load frequencies of 1 and 4 Hz. It can be seen that increase in the fines content causes an increase in the rate of settlement, with the higher frequencies also developing higher cumulative strains. The maximum strain for each specimen for particles < 5 mm and < 10 mm subjected to 4 Hz and 1 Hz are: 2.25, 1.1, 1.8, 0.7% respectively.

Figure 4.6 shows the results of the specimens compacted at the optimum moisture content. Again, the cumulative strain increases linearly with the log number of cycles. In the tests with moisture present the rate of strain is higher for those tests with larger particles (< 10 mm) and lower load frequencies. Thus, the maximum strain at the end of each test for particles < 5mm and < 10 mm subjected to 4 Hz and 1 Hz are: 0.134, 1.64, 0.98, 1.75% respectively. The results for the saturated tests are shown in Figure 4.7. For each test the B-value was in the range 0.95–0.97. The results show the same pattern that displayed in Figure 4.6 for partially saturated at OMC test. The maximum strain at the end of each test was: 0.65, 1.6, 0.88, 1.65% respectively. Water present in the soil matrix could develop into excess pore pressures, causing an increase in the deformation induced due to the dynamic loading. It can be seen that vertical stress induced by axial cyclic loading not completely recover to the initial state, the initial axial stress and confining pressure were assumed as mention in the Table 3.5. The cumulative strain increases with increased number of cycles. The results show that residual strains are built up under each single stress loading and compounded which lead to the total deformation observed. On the other hand, at the particle level, rearrangement of the soil skeleton with presence of water would lead to an increase the stiffness. Furthermore, the big particles might break due to the cyclic loading, this phenomenon leads to deterioration and densification which causes an increase in stiffness as a result of increase number of cycles.

4.3 Effect changing of inundation water condition

Specimens were compacted at optimum moisture content for particles passing through a 5 mm sieve and subjected to 10^5 cycles. The specimen was then saturated to a B-value $= 0.95$ and next subjected to another 10^5 cycles in the same stress state. Figure 4.8 shows a rapid change occurred for the stiffness of soil after the water content change due to volume change and dissipation of water pressure after applying load. The cumulative strain increased sharply from 1.2–1.39% (Figure 4.9). The purpose of this test was to explore the effect of changing water content during the life time of the foundation. A potential explanation for this is that the loading prior to inundation leads to a reduction in the voids and the water ingresses to fill all the pores in the specimen and to cover the

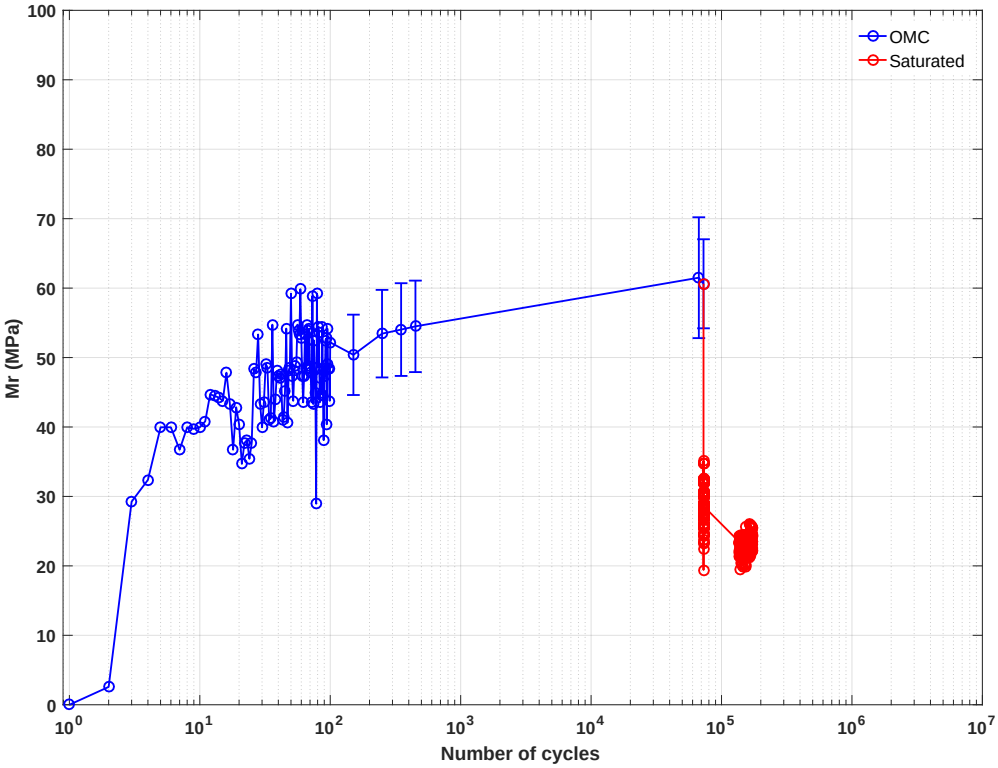

Figure 4.8: Resilient modulus before and inundation of water condition

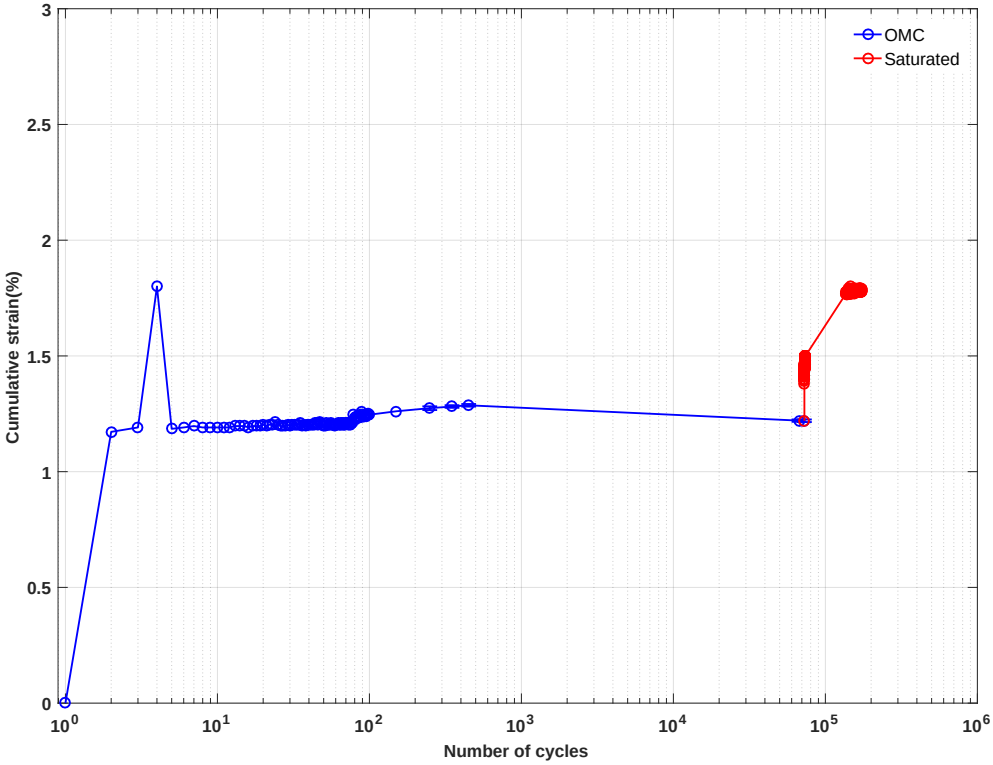

Figure 4.9: The rate of deformation before and inundation of water condition

outer surface of the particles due to capillary action that occur on the microfissures on the surface of the particles. This could lead to the softening and collapse of the outer edge of the individual particles at points where the saturated edges of adjacent particles contact, causing degradation as seen in the slaking tests (Nahazanan, 2010).

4.4 Interpretation and discussion of the results

Mudrock is a type of material which can be classified as either a soil or a rock depending on its behaviour. Four different conditions have been taken in consideration in this chapter, dry, fully saturated and partially saturated (including compacted specimen at optimum moisture content and compacted at dry side). The resilient modulus for mudrock is not constant, with its characteristics being dependant on many factors. In this chapter the impact of water content at different particle size distributions and load frequency is emphasized.

Commonly, soil consists of different phases depending on the degree of saturation (Figure 4.10). Firstly, soil in a dry state: in this condition the soil specimen consist of two phases, solid grains and pores between the grains full of air, matric suction is increased in this case as the water content approach to zero, means the pore pressure is zero and the total stresses are equal to the effective stresses. The matric suction effect in this case is neglected as it does not generate any volume change (Fredlund and Rahardjo, 1993). The collated results for the dry case are shown in Figure 4.11.

A saturated soil exists if voids completely fill with water, and the stress state is equal to the effective stress as commonly expressed in the formula below:

$$\sigma' = \sigma - u \tag{4.1}$$

Where: σ' = Effective stress, σ = Total stress, u = Pore pressure.

In the saturated stress state the total normal stress applied is equal to the pore water pressure. During cyclic pore water pressures develop and that leads to a reduction in soil strength in cases where the water is not free to flow (Figure 4.12). However, the permeability estimated for the soil using Hazen's method is classified as a medium pervious, meaning the low permeability obstructs the free drainage of water. The volume change occurring in saturated specimens would be due to the drainage of water, while in the partially saturated conditions, volume change could happen in water and air.

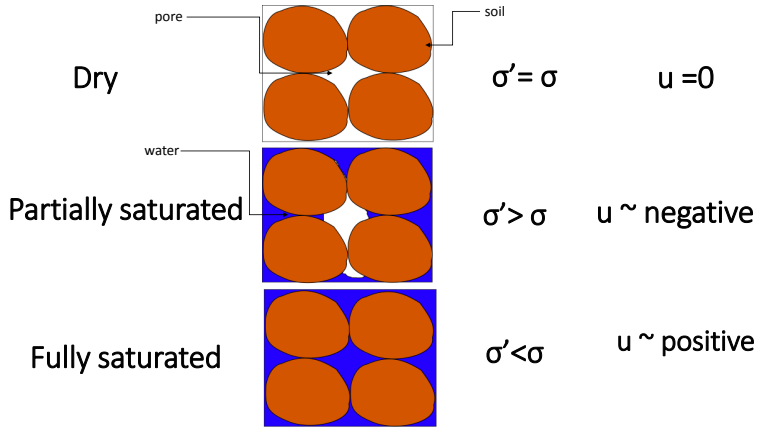

Figure 4.10: Phase relationship diagrams, with varying saturation conditions

The soil structure of mudrock has a subgrain system of voids because of micro cracks and fissures. These pores could form between the grains and within the grains. There will exist both macropores and micropores with both water and air being able to be absorbed into the micropores as well as the macropores. In partially saturated conditions the soil has three phases: air, water, and solid. The interface surface between air and water leads to the surface tension of water creating a meniscus (Figure 4.10).

The difference between the pore air pressure and pore water pressure is known as the soil suction. This type of suction caused by capillary action within the soil matrix is known as matric or capillary suction. Suctions are set up at inter-granular contacts by the air/water interface and create a normal force holding the grains together. As saturation takes place the suction forces are destroyed, allowing the particles structure to collapse.

The dry case is seen to exhibit a higher stiffness. Hence, under cyclic loading the soil has a higher resilient modulus. In this non-uniform grain structure of the mudrock the particles can move as a mass of unattached particles. During cyclic loading, the individual particles direct themselves relativity to each other within the specimen causing rotation of the contact surfaces to resist the major principal stress (Oda and Konishi, 1974).

In Figure 4.11 the results of dry condition at different particle size tested under 1 and 4 Hz are displayed. It can be seen that highest stiffness appears for soil passing through 10 mm and 4 Hz load cycles. The specimens under 4 Hz show high scatter compared with the specimens tested under 1 Hz and the stiffness increases linearly with the number of cycles. This is because of the rapidly applied stress. Under low frequencies the soil exhibits a slight increase in stiffness which is seen to be dependant on the percentage of fines.

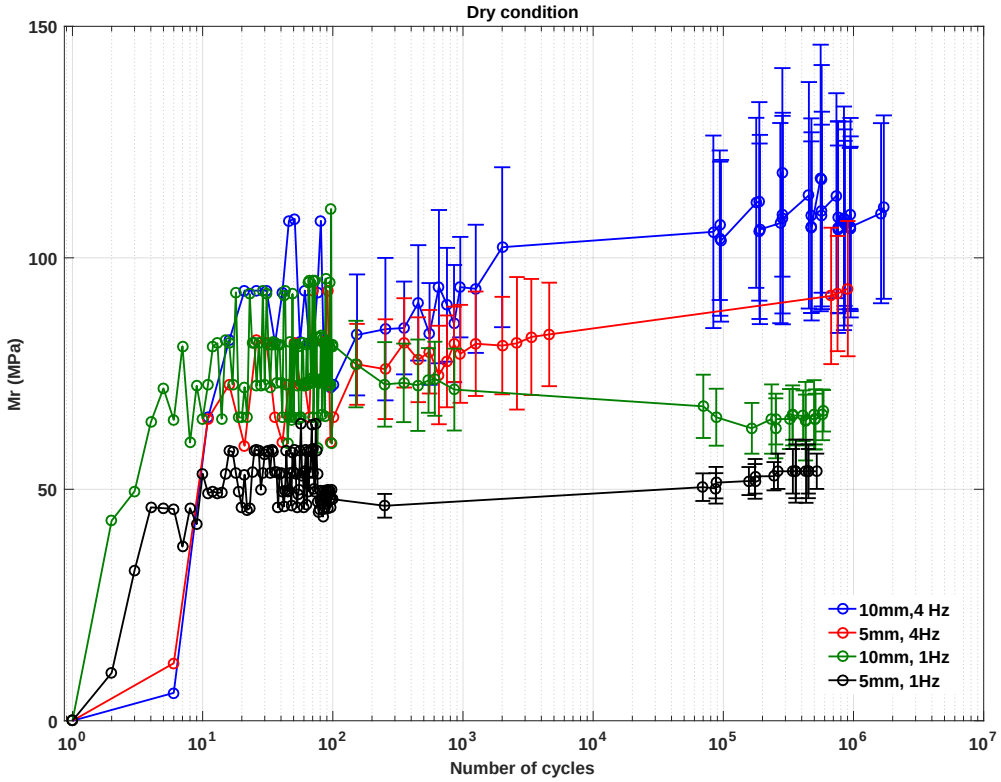

Figure 4.11: Resilient modulus in dry conditions

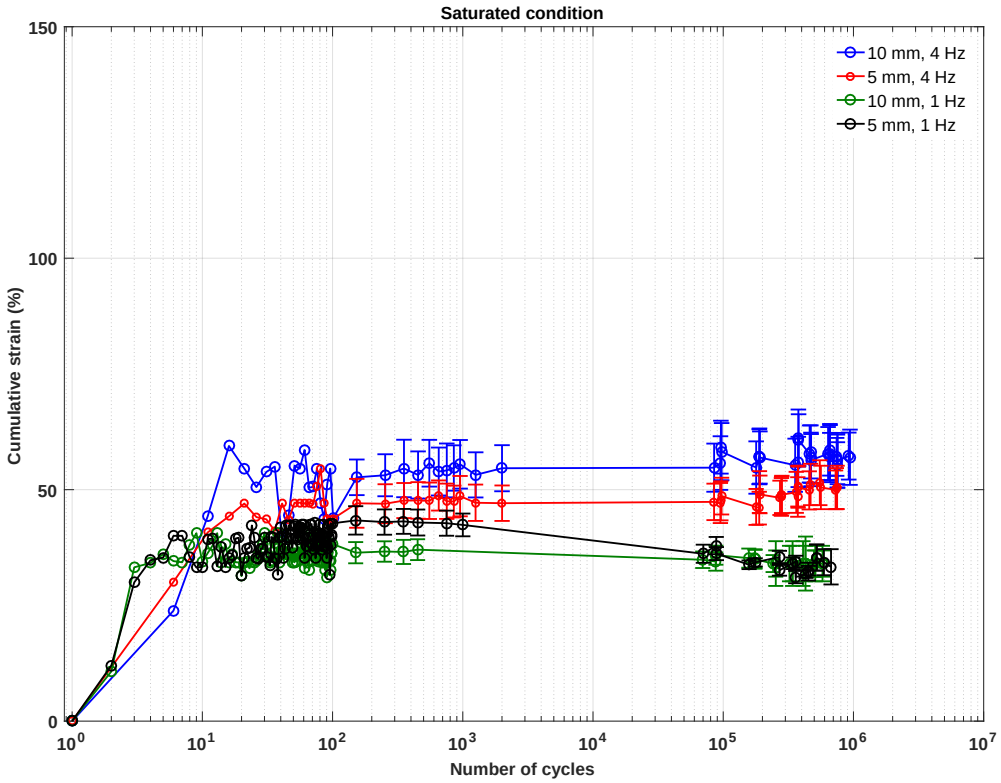

Figure 4.12: Resilient modulus in fully saturated conditions

The fines will fill the voids between the bigger particles hence, the movement of particles will be constricted and the stiffness will be reduced.

In Figure 4.12 due to the saturation of the specimen it is likely that particle breakage will be reduced as the voids all full of water. Saturation is hence seen to reduce the strength of the specimens. However, saturated mudrock specimens exhibit similar behaviour to partially saturated specimens. It may be that the breakage of mudrock which occurs during compaction or cyclic loading leads to the reduction in strength and gradually became constant. In addition, rearrangement of particles induced by repeated loading, volume reduction and densification will occur. At higher load frequencies, more energy may be lost within the specimen, generating internal forces between particles which leads to breakage of the particles. This would then explain the deformation trends as the soil becomes denser and stiffer, the equilibrium state would also depend on the water content of the specimen.

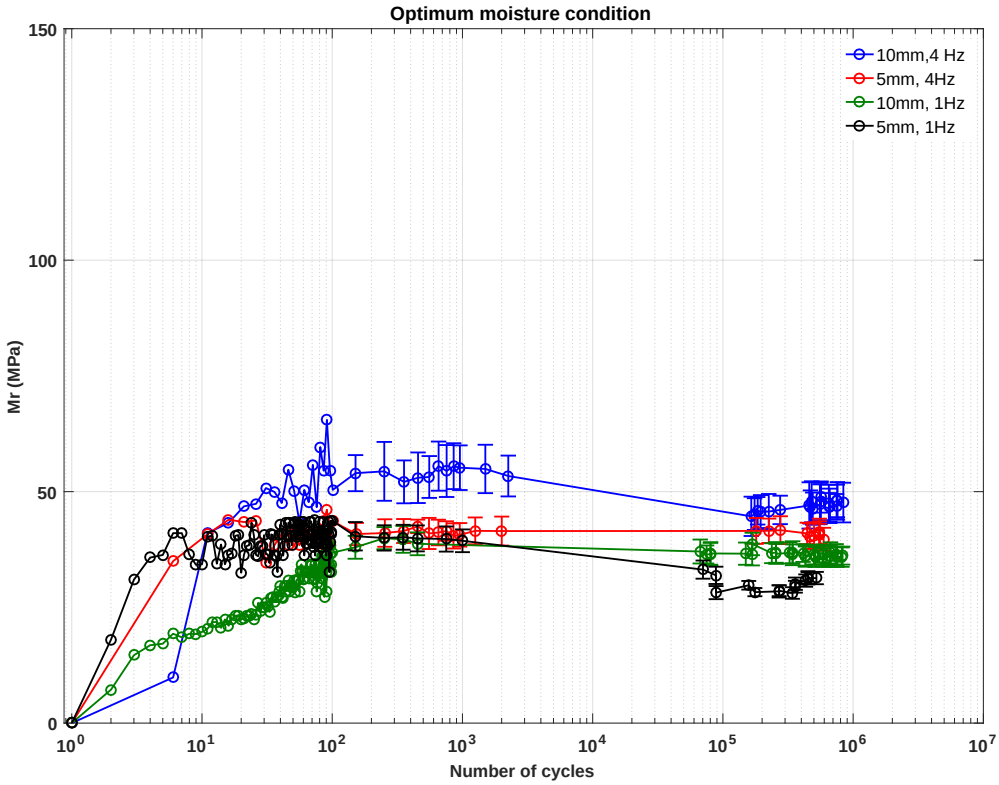

Figure 4.13: Resilient modulus in partially saturated conditions at OMC

It has been reported by Lee and Farhoomand (1967) and Lade et al. (1996) that bigger particles have larger planes of weakness due to laminations and flaws, and that well-graded soils have fine particles trapped between bigger particles. These fine particles will reduce the amount of voids and form low-stress particle contacts or will increase the total number

of particle contacts which would act to minimize the effect of crushing.

Figure 4.13 shows the results of the partially saturated specimens. This figure shows the same pattern of behaviour as exhibited in Figure 4.12 with the particle size distribution and load frequency having a minor effect on the development of the resilient modulus in each specimen. In partially saturated specimens, suction tends to force the particles together and this can be attributed to extra stability at inter-particle contacts. Increase water content toward the saturated state leads to reduction in the suction until it becomes zero and that leads to decrease the effective stress. It can be observed that resilient modulus in the fully saturated specimens are slightly higher than in the partially saturated at optimum moisture content specimens. This shows that the matric suction is only likely to play a minor role in the the generation of stiffness.

If the soil compacted at lower degree of saturated tends to absorb water from the surrounding area to achieve stability. The resilient strain will increase, thus reducing the resilient modulus (Seed et al., 1967). Compacted soil with a higher degree of saturation, tend to lose its moisture. The subsequent suction increase makes the soil specimen stiffer and result in a higher resilient modulus as shown in the data when comparing the partially saturated at OMC and fully saturated cases.

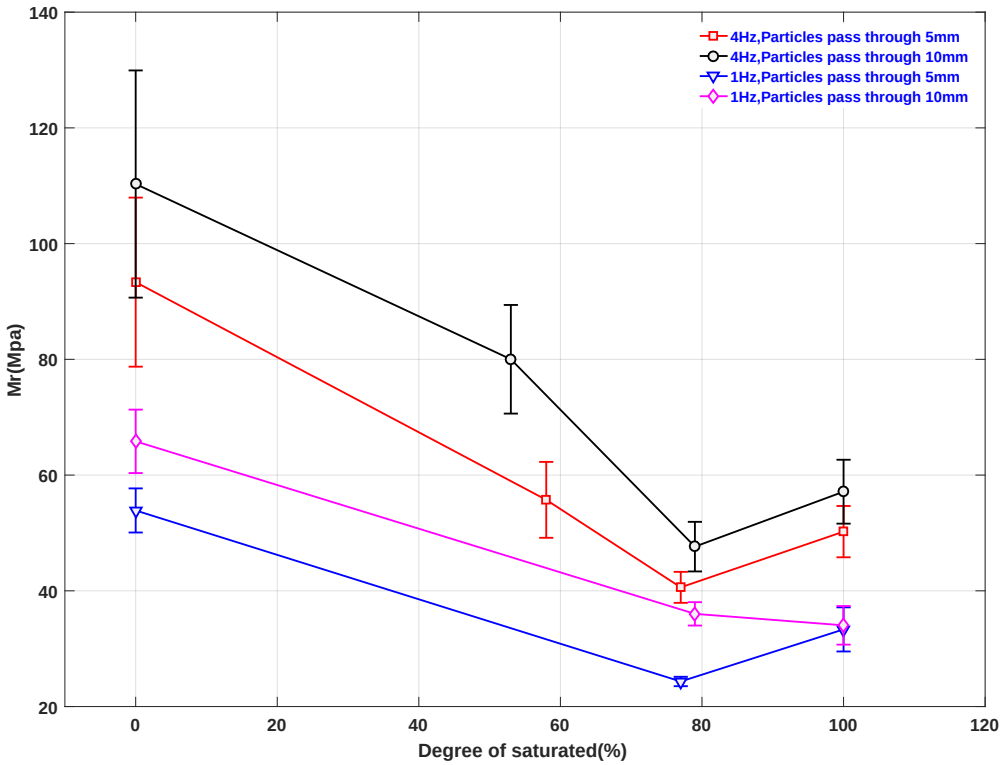

Figure 4.14: The effect of water content on the resilient modulus

To allow a deeper analysis of the impact of water content, particle size and frequency on the resilient modulus, the Mr value for each test at 5×10^5 cycles has been plotted in Figure 4.14. This clearly shows that the long-term resilient modulus increases due to decreases in the moisture content, and increases in the maximum particle size or loading frequency.

First of all, is worth remembering that the strength of the larger particles is lower than that of the smaller particles due to a large possibility of an existence of defects and flaws such as laminations. And in wet condition the particles will absorb the water leads to more collapse, leading to an increase in the the stiffness as the process of densification stabilises the structure of the specimen.

Table 4.1: Maximum recorded cumulative strains

	Maximum cumulative strain (%)			
	$<$ 5 mm / 4 Hz	$<$ 10 mm / 1 Hz	$<$ 5 mm /4 Hz	$<$ 10 mm / 1 Hz
Dry	2.25	1.1	1.8	0.75
Dry side	0.75	1.48	0.128	0.40
OMC	0.134	1.64	0.99	1.75
Saturated	0.65	1.6	0.88	1.67

In terms of permanent deformation, it builds up after each load cycle and adding to the total strain until the end of test. The end of test cumulative strains are collated in Table 4.1. It can be seen that the cumulative strain varied under the same loading condition dependant on water content and load frequency, however there is no clear relationship between the variables. During all tests the initial stress ratio was constant. The largest cumulative strain was recorded in the dry specimen for particles passing through a 5 mm sieve tested at 4 Hz. The lowest recorded value was in the OMC specimen for the $<$ 5 mm particles tested at 4 Hz also.

One of the major factors which affects the settlement for mudrock colliery spoil is water recharge. As the water content increases the pore pressure increases and reduces the effective stress, and the friction between particles. There are softening and dispersing of the outer parts of the particles themselves. Thus, the particles will slip against each other causing collapse of the specimen (Blanchfield, 1998). Wetting condition might cause crushing at inter-particle contacts as the particle strength reduces (Terzaghi, 1960). In addition, the volume of soil will be reduced because of the collapse of the soil structure and that depends on the magnitude of the total applied stress at time of wetting. This behaviour was seen for the current specimens in Section 4.3.

4.5 Summary

It has been reported by many studies that the significant factors affecting the resilient modulus of a soil are water content and particle size distribution, as they have a combined effect. As set out in the test programme the aim of this study is to examine these effects by conducting tests with different water contents and two sets of particle size distributions.

The physical state of the soil (represented by water content and particle size distribution) was exposed to the effect of seasonal water change that would cause changes in the mechanical properties of the subgrade layer. Simulation for such situations have been done in the laboratory. The specimens were compacted at optimum moisture content and maximum dry density and then saturated prior to testing (if required). The results indicate that increases in water content causes significant decrease of resilient modulus, with the difference decaying between the optimum moisture content and saturated cases. This agrees with the work of Thom and Brown (1987), Kamal et al. (1993) and Lekarp et al. (2000).

Larger particles size distributions used are poorly-graded and the smaller are well-graded, and the rate of settlement depends on the fines content, with all the tests with water present showing that the larger particles displayed a greater cumulative strain. From the observation of the results it can be seen that the partially saturated at optimum moisture content specimens showed a similar behaviour to the fully saturated specimens with minor differences in the resilient modulus.
From the testing conducted, the long-term resilient modulus was found to increase due to:

- decreases in the moisture content;
- increases in the maximum particle size and
- increases in the loading frequency.

Chapter 5

The effect of stress state on the performance of mudrock

The main objective for this project is to investigate the impact of the initial stress conditions and dynamic stress on the permanent deformation performance of the soil under different physical conditions. Structural performance of the railway track strongly depends on the level of stress that is transmitted to the ground and this must be reduced to an acceptable level to minimise deterioration in the subgrade soil. This chapter presents the results of two studies. The first is a study on the behaviour of mudrock under same confining pressure and vertical load under different cyclic stress and load frequency. The second is to study the effect of changing vertical load, cyclic stress and confining pressure as well as load frequency.

5.1 Effect of cyclic loading and moisture content

In this section, specimens have been tested at the same confining pressure and vertical stress whilst varying the magnitude of the cyclic loading. The purpose of these tests are to define the effect of cyclic loading stress on the stiffness. In each case unless stated otherwise the cyclic frequency is 4 Hz. Testing under 1 Hz has been conducted and will be discussed in Section 5.4. Resilient modulus and cumulative strain are plotted against number of cycles to determine their effect in turn. The results are categorised according to the stress conditions applied, to simplify the interpretation of the results. Specimens were also tested with different water contents to assess the effect.

5.1.1 Dry conditions

Figure 5.1 plots the resilient modulus for two compacted specimens at relative densities of 75% for particles < 10mm, and 78% for particles < 5mm. The soils were compacted dry and had a vertical stress applied of 20–24 kPa representing both ballasted and ballastless construction (Table 3.5). To simulate the conditions under the track a constant confining pressure of 18 kPa was applied. The results show that an increase in the cyclic stress, increases the resilient modulus noticeably under the same confining stress, in the case of a dry soil. Figure 5.1 shows an initial stiffening over the first ≈100 cycles, with a plateau being reached in both conditions up to around 5000 cycles. The specimens with higher cyclic stress reached higher resilient modulus. The specimen with a cyclic stress of σ_{cyclic} = 40 kPa developed a modulus of 80 MPa, with the lower σ_{cyclic} = 20 kPa specimen developing 50 MPa. After this plateau the modulus of the 40 kPa increased to 110 MPa, whereas the 20 kPa specimen showed a more modest increase to 60 kPa up to 10^6 cycles.

Similarly, Figure 5.2 reveals that the performance of specimens for particles < 5 mm behave in the same pattern with a general tendency to be less stiff when compared with the larger particles. It can be also seen that the specimens tested with σ_{cyclic} = 40 kPa increase linearly with increase number of cycles, and exhibit less scatter in resilient modulus, for a 10^6 cycles application without resting.

Cumulative strain for the specimens was measured and is given in Figures 5.3 and 5.4. For the particles < 10 mm there is a modest initial increase in the cumulative strain which reaches equilibrium at 2×10^5 cycles in the σ_{cyclic} = 40 kPa case, with an overall strain of 0.93%. With σ_{cyclic} = 20 kPa, cumulative strain increased to a maximum of 0.8% at same confining pressure.

For Figure 5.4 shows the cumulative strain increase for both cyclic stress cases against number of cycles. The cumulative strain for the specimen with σ_{cyclic} = 40 kPa is much higher than the specimen with σ_{cyclic} = 20 kPa. The strain for both specimens does not reach an equilibrium with the maximum strain recorded being 2.3% and 1.3% for the 40 kPa and 20 kPa cases respectively. It is worth noting that the specimens with smaller particles show higher deformations. This may be due to the higher internal stress levels generating greater particle breakage which induces higher changes in void ratio and hence strain (Lade et al., 1996).

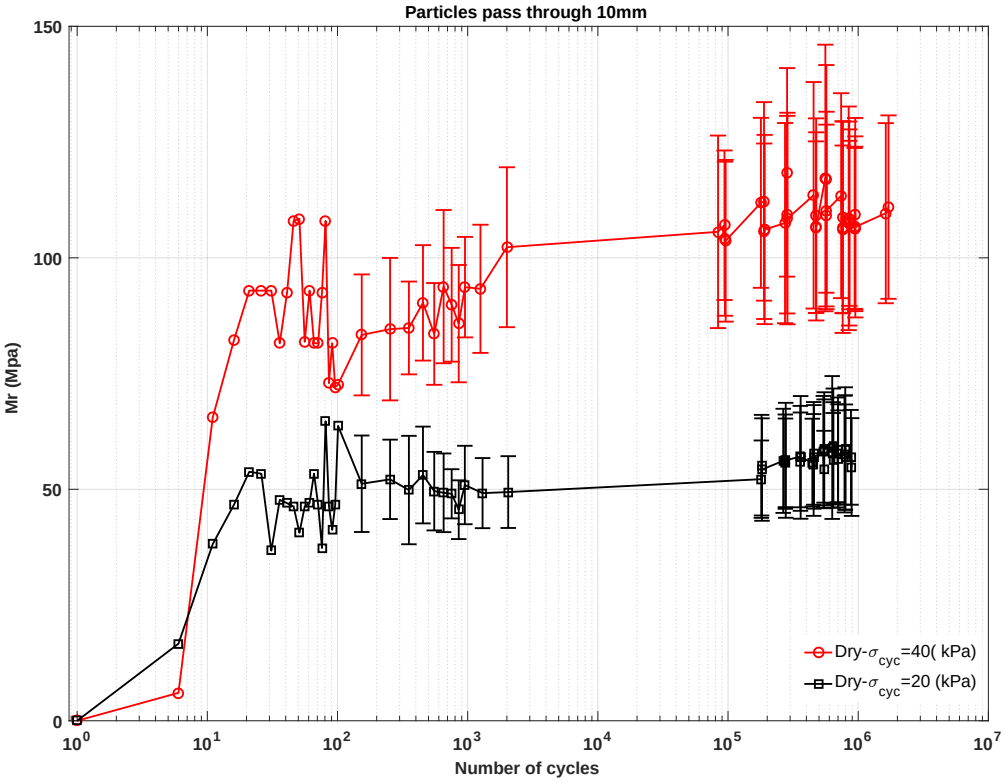

Figure 5.1: Resilient modulus in dry state, varying cyclic stress, particles < 10 mm

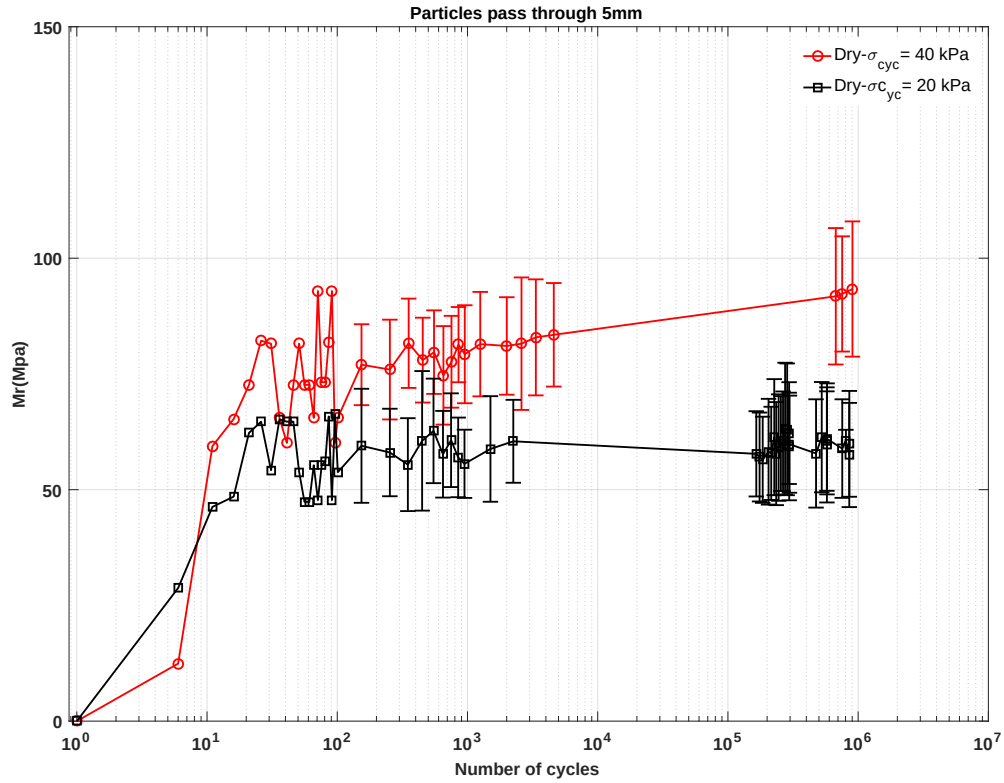

Figure 5.2: Resilient modulus in dry state, varying cyclic stress, particles < 5 mm

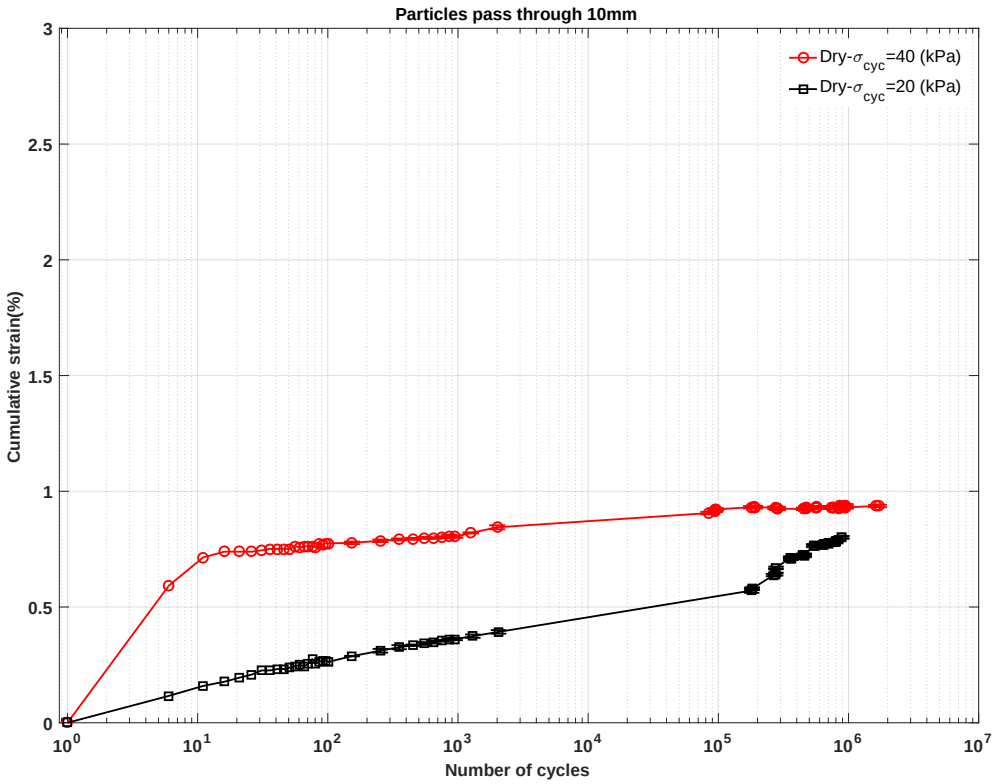

Figure 5.3: Cumulative strain for dry state, varying cyclic stress, particles < 10 mm

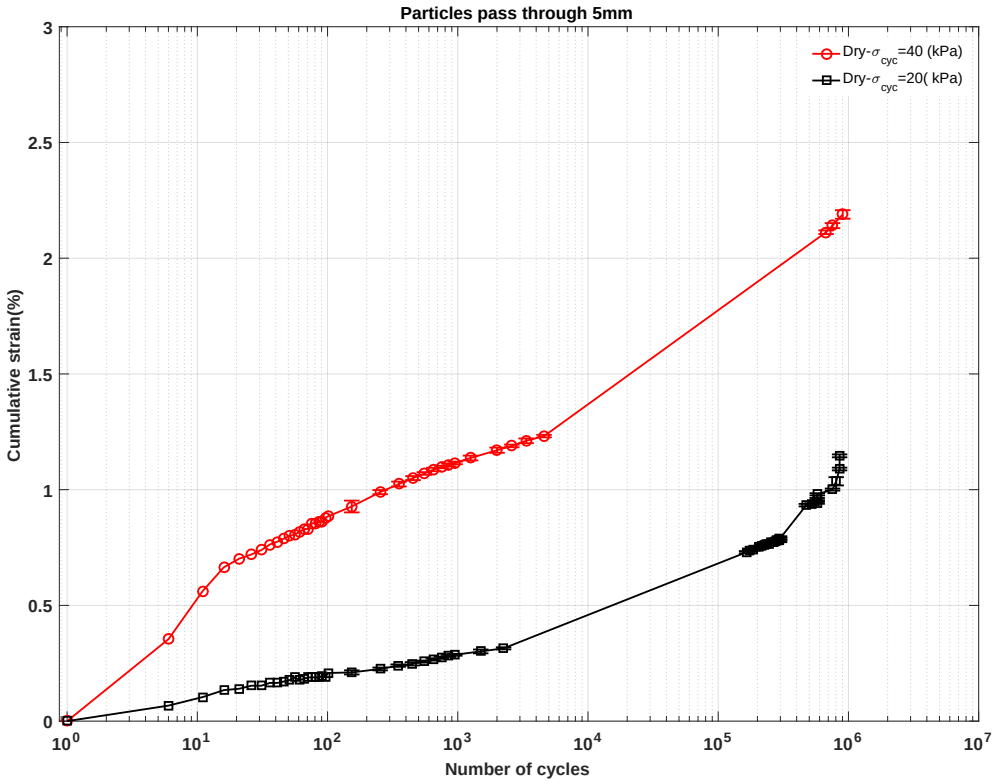

Figure 5.4: Cumulative strain for dry state, varying cyclic stress, particles < 5 mm

5.1.2 Partially saturated at dry side of OMC

In this case the soil was compacted at a moisture content less than the optimum moisture content which is on the dry side of compaction curve. The evolution of the resilient modulus over $\approx 10^6$ cycles is shown in Figures 5.5 and 5.6. In Figure 5.5 a linear increase in Mr with number of cycles can be seen in the $\sigma_{cyclic} = 40$ kPa specimen. It can be also seen that in the specimen with $\sigma_{cyclic} = 20$ kPa, more scatter in the Mr over first 50 cycles, which reduces at $\approx$150 cycles, to be similar to the scatter seen in the other specimens.

In Figure 5.6 the behaviour of the specimen with particles less than 5 mm shows that in these conditions the resilient modulus is independent of the cyclic stress applied. The resilient modulus for the specimen with $\sigma_{cyclic} = 40$ kPa is marginally higher than the specimen tested with $\sigma_{cyclic} = 20$ kPa. The equilibrium values reached were 55 and 48 MPa respectively.

To summarize, the resilient modulus for specimens compacted on the dry side for particles passing through 10 mm and 5 mm show the same trends as seen in the dry state in respect of relative magnitudes. However, there is a lesser trend for the gradual increase in Mr as seen in the dry state. The only specimen which exhibited this behaviour was the $<$ 10 mm specimen tested under $\sigma_{cyclic} = 40$ kPa. In general terms it could be argued that the resilient modulus for specimens containing smaller particle sizes exhibit a lower stiffness, and there is a minor difference in stiffness between the specimen subjected to $\sigma_{cyclic} = 40$ kPa and $\sigma_{cyclic} = 20$ kPa (with the exception of the $<$ 10 mm, $\sigma_{cyclic} = 40$ kPa specimen).

Figures 5.7 and 5.8 show the development of cumulative strain for the same conditions. The trends seen are very similar to those seen in the dry state, with cumulative strain increasing with the number of cycles for both stress states. As was seen previously the specimens with $<$ 5 mm particles experience much higher cumulative strain. The magnitude of the final cumulative strains for the specimens with $\sigma_{cyclic} = 40$ kPa where 0.4% and 0.15%. Whilst with $\sigma_{cyclic} = 20$ kPa were 1.49% and 0.75% respectively.

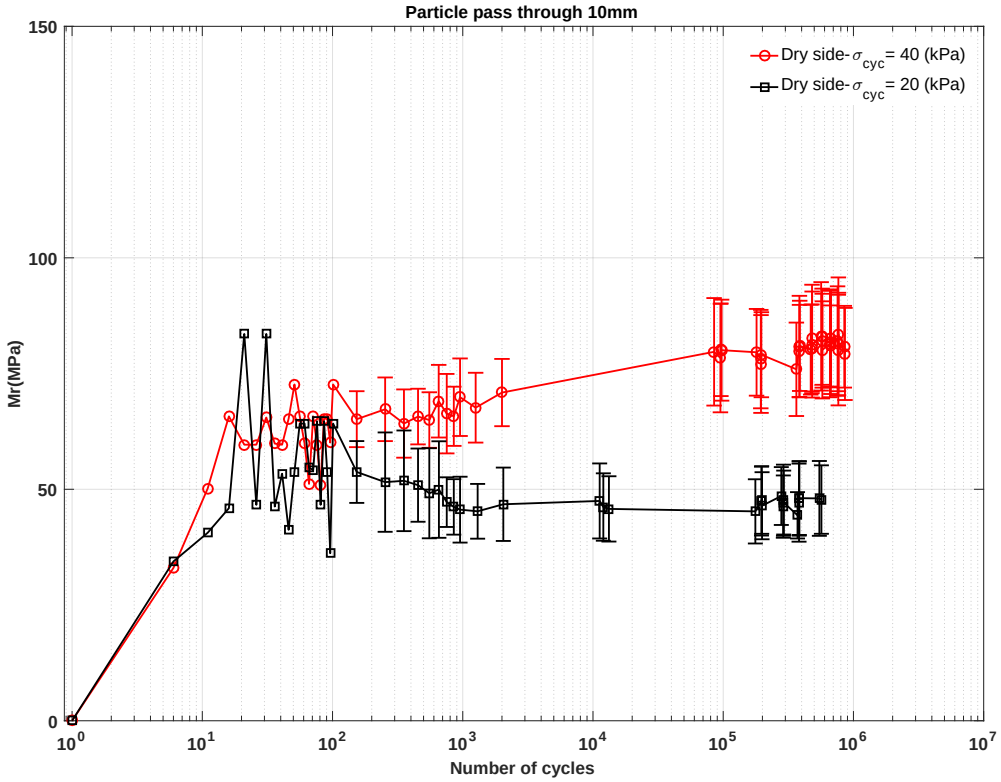

Figure 5.5: Resilient modulus for dry side condition and varying cyclic stress, particles < 10 mm

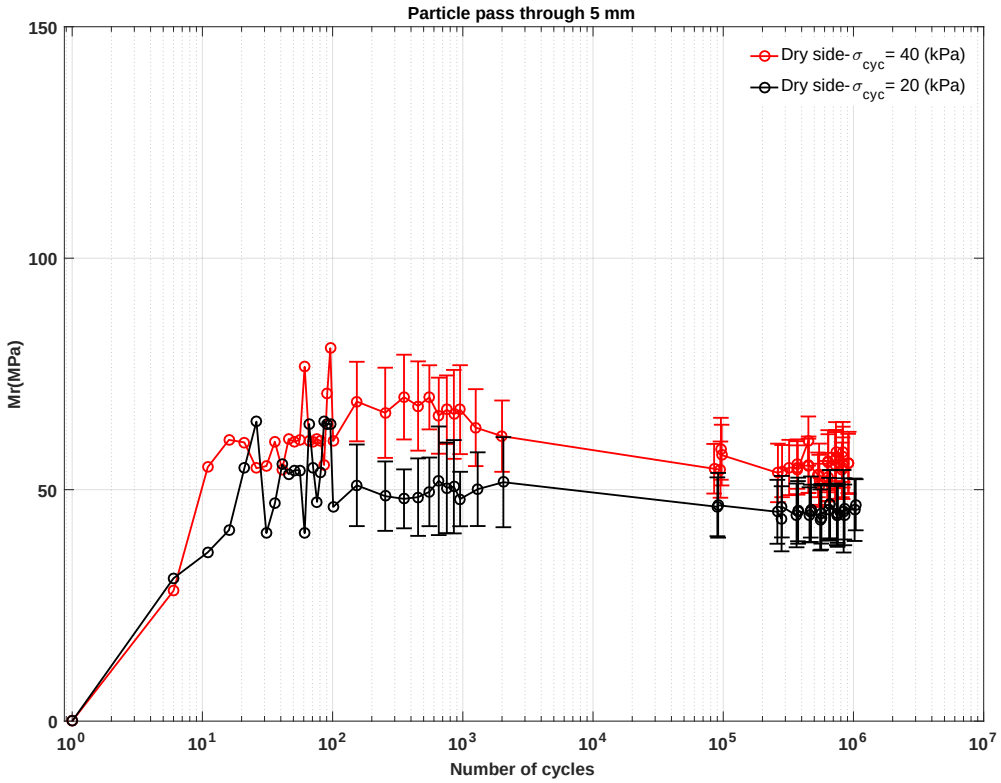

Figure 5.6: Resilient modulus for dry side condition and varying cyclic stress, particles < 5 mm

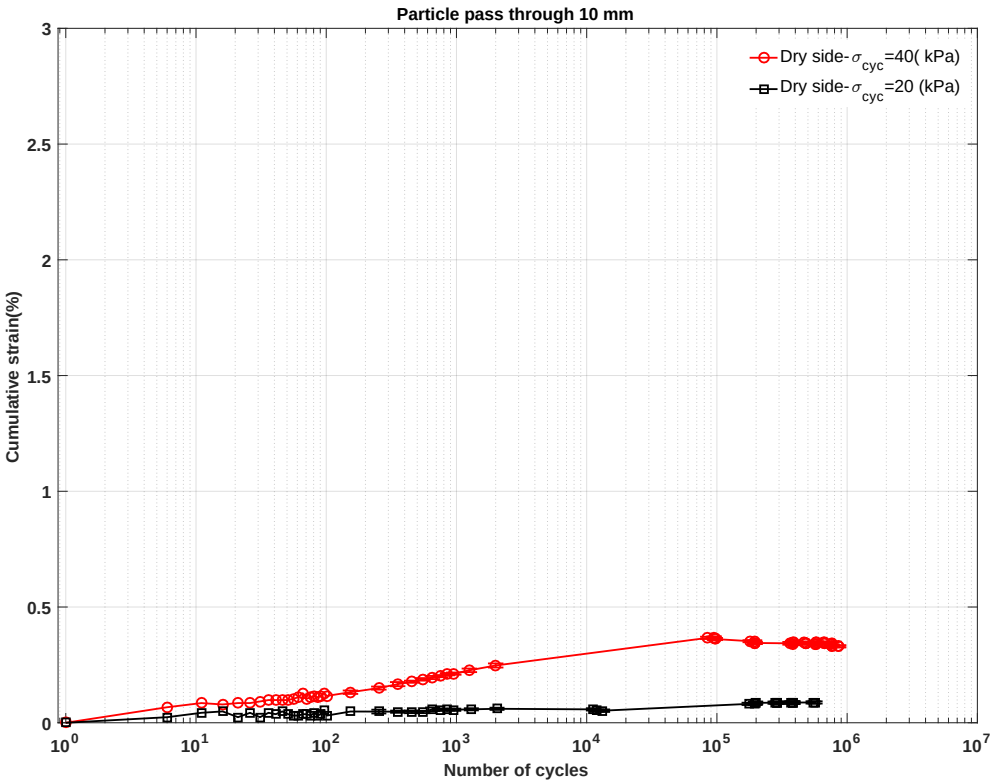

Figure 5.7: Cumulative strain for dry side state, varying cyclic stress, particles < 10 mm

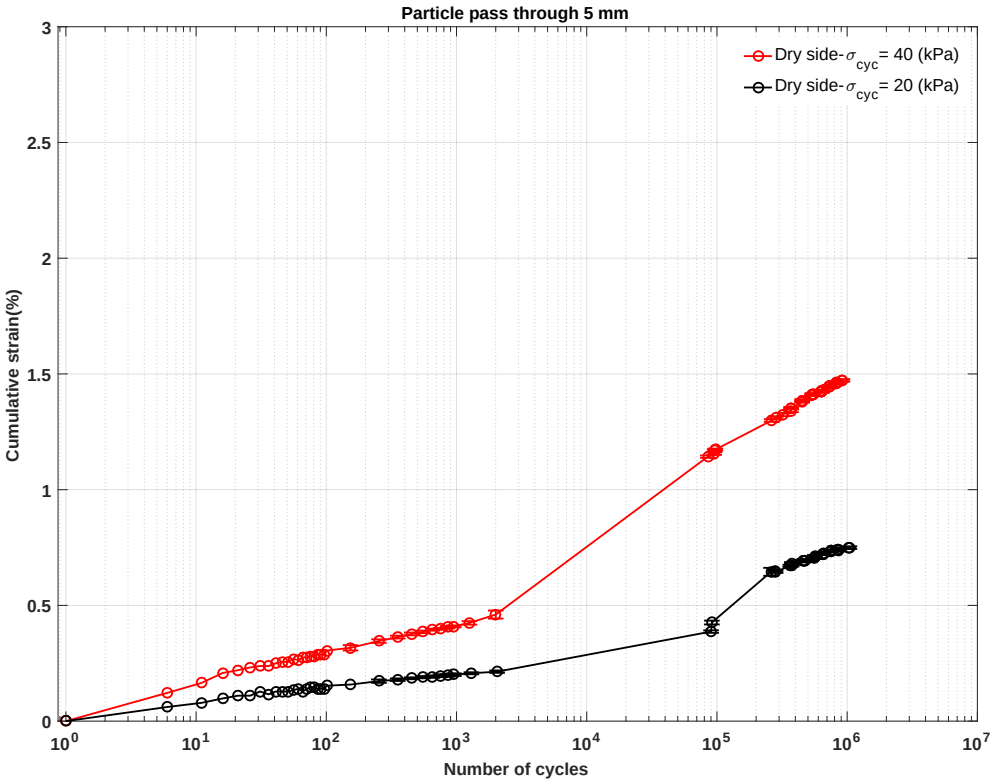

Figure 5.8: Cumulative strain for dry side state, varying cyclic stress, particles < 5 mm

5.1.3 Partially saturated at optimum moisture content

Figures 5.9 and 5.10 show the resilient modulus for specimens compacted at the optimum moisture content for particles passing through 10 mm and 5 mm sieves respectively. The results show that all the specimens exhibit a similar resilient modulus with very little effect of changing the cyclic stress or the maximum particle size. Scatter in the data is slightly more pronounced over the first ≈100 cycles for the < 10 mm specimen with σ_{cyclic} = 20 kPa, but this reduces with further cycles. These slight fluctuations are probably due to the breakage of particles during the test. At the optimum moisture content all the specimens reached equilibrium at ≈1000 cycles. In conclusion, the different stress states and particle sizes make minor changes to the exhibited stiffness for specimens compacted at the optimum moisture content.

The cumulative strains shown by the specimens are plotted in Figures 5.11 and 5.12, the results appear similar to the cases mentioned above. The cumulative strain for both particles sizes increases with an increase in the number of cycles. The maximum strain was seen in the < 10 mm specimen tested under σ_{cyclic} = 40 kPa, developing 1.6%. For the same stress the specimen with particles < 5 mm showed a small reduction in the strain to 1.4%. Whilst, the cumulative strain with the lower σ_{cyclic} = 20 kPa developed to 0.39% and 0.23% for both specimen passing through 10 mm and 5 mm respectively. The general trend shows that specimens with particles less than 10 mm in size exhibit slightly higher strains than specimens with particles less than 5 mm size. The more pronounced effect is the reduction in strain seen when reducing the cyclic stress which was seen in specimens with both particle sizes.

5.1.4 Saturated conditions

Similarly, the results under saturated conditions are shown in Figures 5.13 and 5.14, the results reveal that increasing the deviatoric stress under saturated conditions again makes little difference to the resilient modulus. Again, specimens reached equilibrium at ≈1000 for all tests. The resilient moduli at 8×10^5 cycles were 56.5 kPa and 54.7 kPa (< 10 mm) and 50.5 kPa and 49.0 kPa (< 5 mm), for the σ_{cyclic} = 40 kPa and σ_{cyclic} = 20 kPa specimens respectively.

The cumulative strain in Figure 5.15 and 5.16 indicate for same trend the cumulative strain with no plateau in the data being reached. The specimen subjected to σ_{cyclic} = 40 kPa reached a maximum 1.53% deformation. The maximum strain for the specimen with particles passing through 5 mm was 0.43% under the same cyclic stress. For specimens tested under σ_{cyclic} = 20 kPa, the maximums strains reached were 0.092%, and 0.24% for the < 10 and < 5 mm specimens respectively.

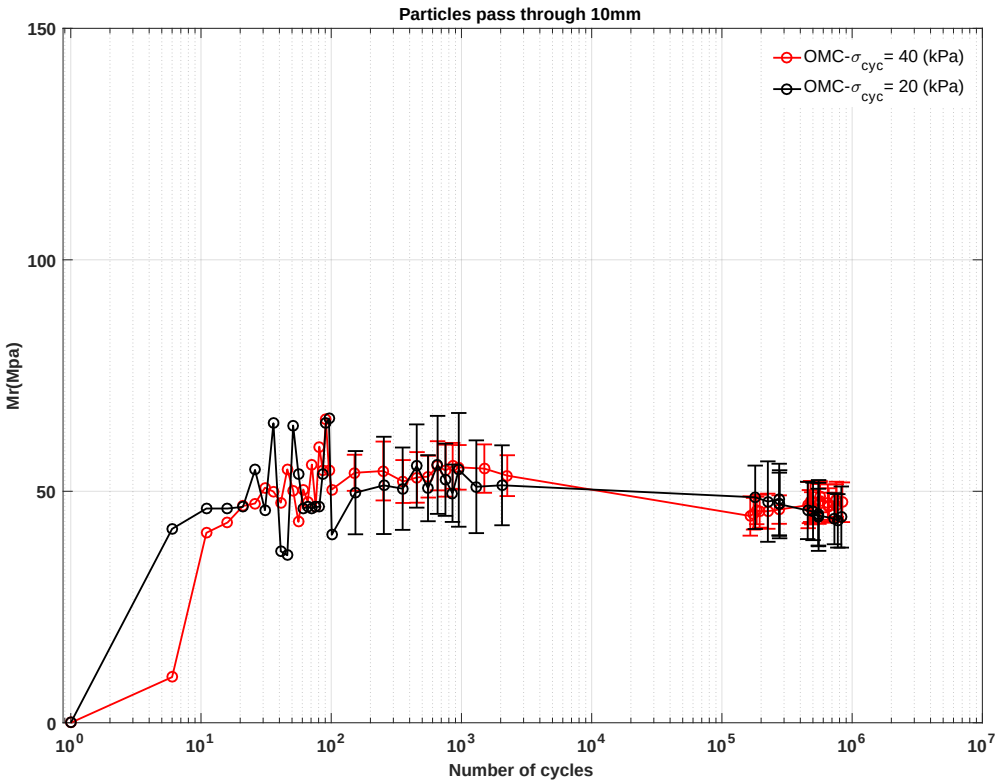

Figure 5.9: Resilient modulus for OMC condition, varying cyclic stress, particles < 10 mm

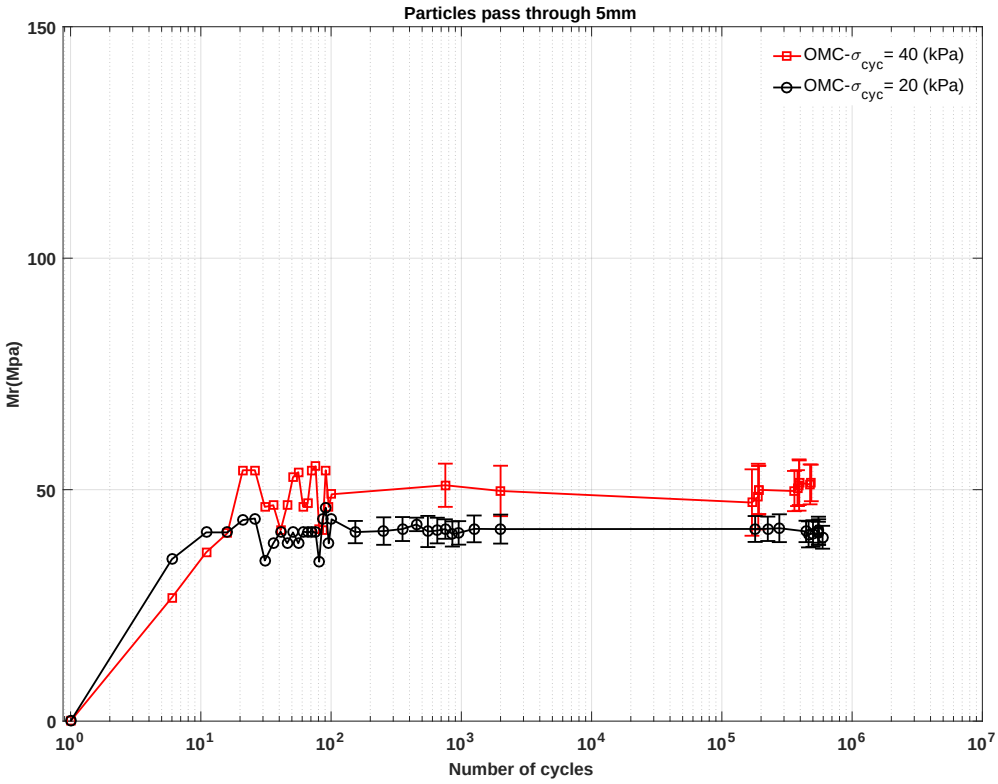

Figure 5.10: Resilient modulus for OMC condition, varying cyclic stress, particles < 5 mm

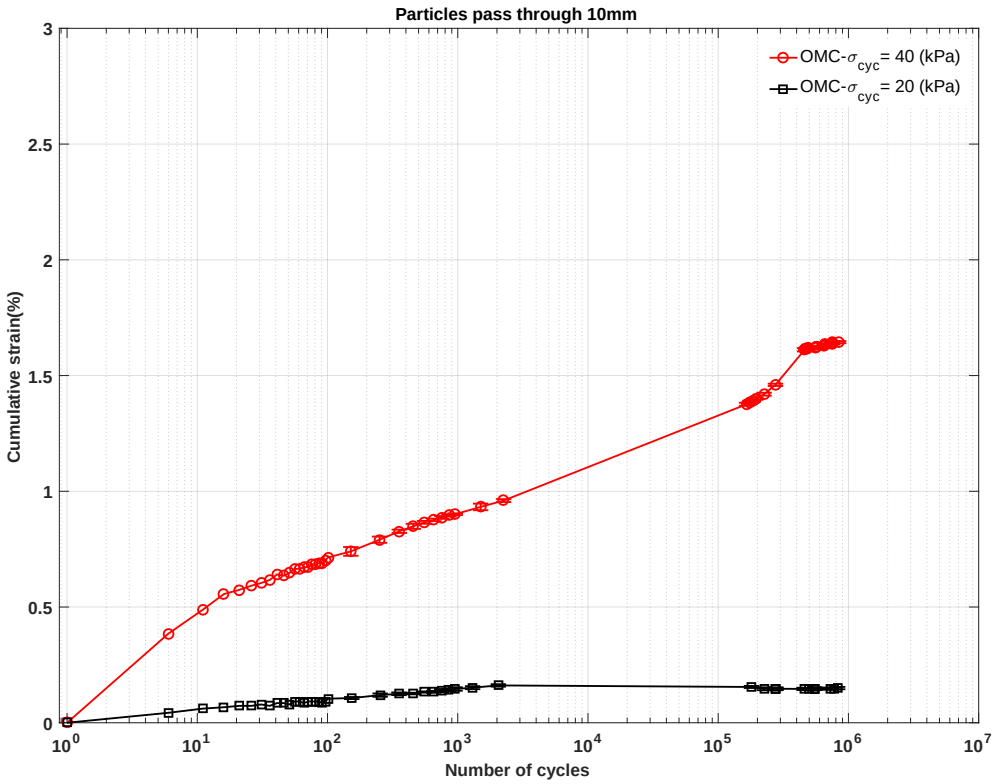

Figure 5.11: Cumulative strain for OMC state, varying cyclic stress, particles < 10 mm

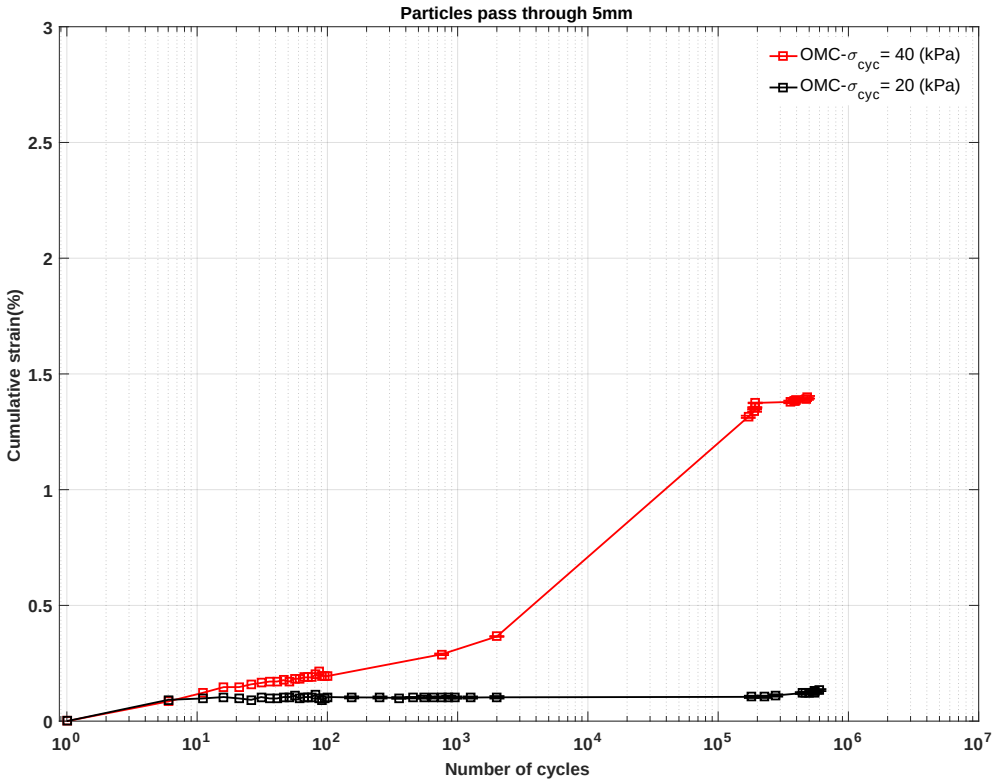

Figure 5.12: Cumulative strain for OMC state, varying cyclic stress, particles < 5 mm

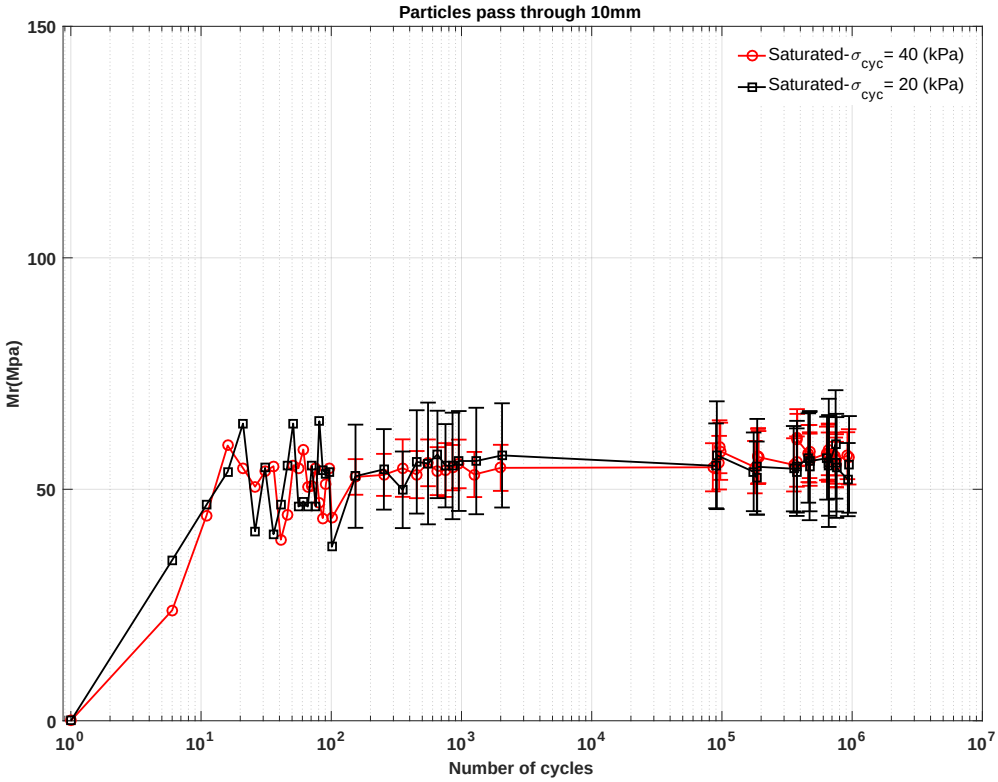

Figure 5.13: Resilient modulus for saturated condition, varying cyclic stress, particles < 10 mm

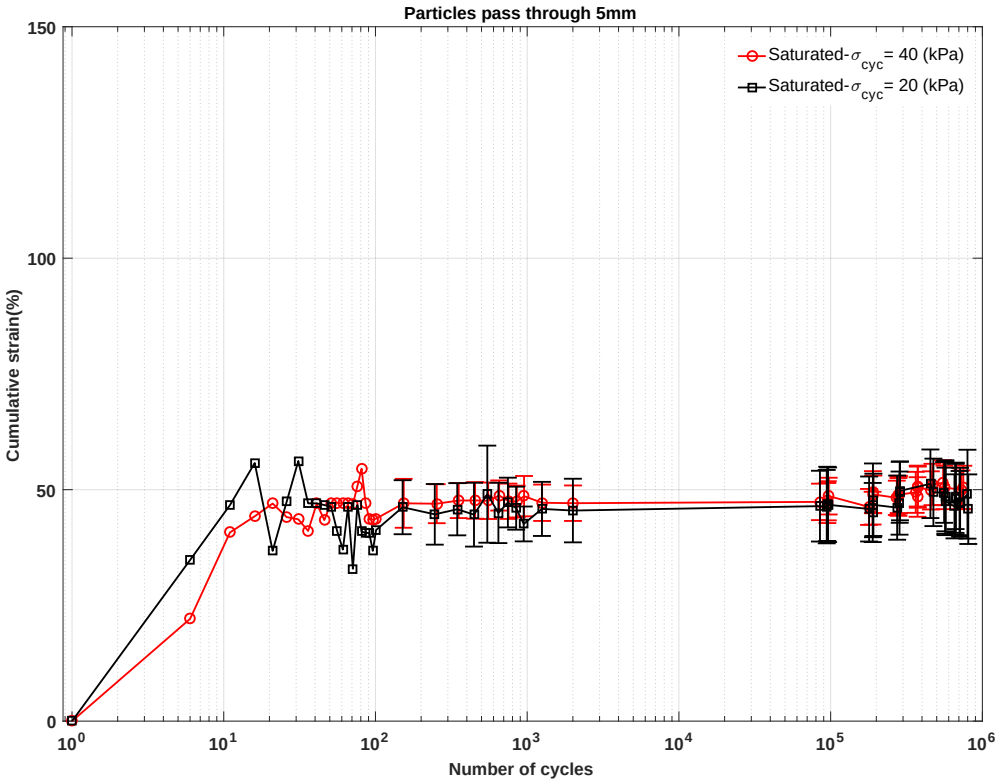

Figure 5.14: Resilient modulus for saturated condition, varying cyclic stress, particles < 5 mm

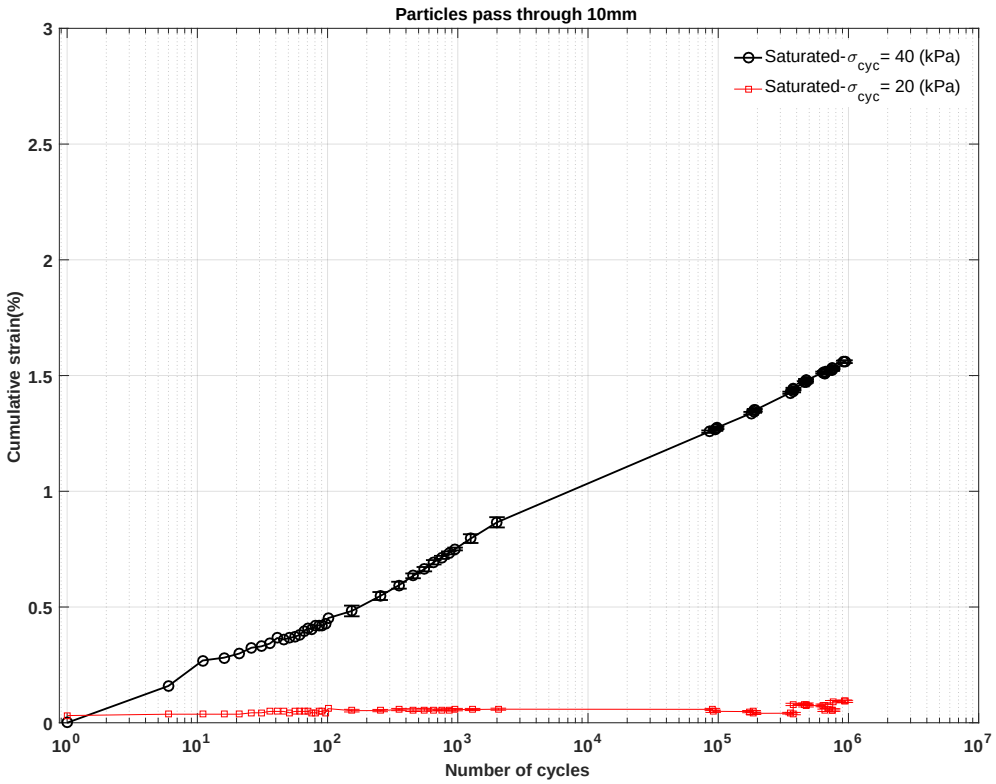

Figure 5.15: Cumulative strain for saturated state, varying cyclic stress, particles < 10 mm

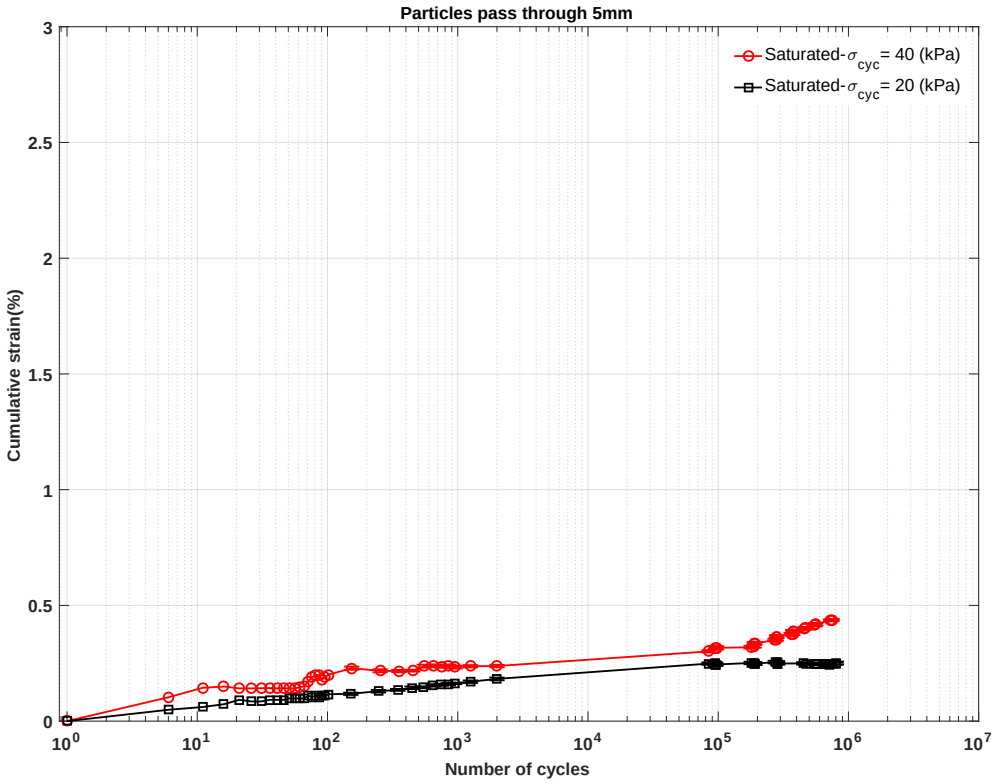

Figure 5.16: Cumulative strain for saturated state, varying cyclic stress, particles < 5 mm

5.1.5 Interpretation and discussion of the results

In this discussion, stress state is defined as the changing of the cyclic loading whilst keeping the confining pressure and vertical stress constant. Many tests have been conducted showing the influence of cyclic stress on the resilient modulus. High stress level and cyclic loads have a beneficial effect on the stiffness of mudrock by increasing the Mr. However, for the specimens that were tested at optimum moisture content and fully saturated, the results show a minor difference between both stress states. It can be expected that the cyclic loading changes the strength and stiffness of soil dependent on the moisture content of the soil. In dry conditions the rearrangement of particles has taken place hence, the resilient modulus increases with increased deviatoric stress. This effect of deviatoric cyclic stress is minimal for specimens in saturated or optimum moisture content conditions. Partially saturated soils are able to hold water between pores depending on the magnitude of the negative pressure or suction in the pores. This soil suction pulls particles together leading to an increase in stability and strength. However, with further increases in water content the suction will reduce and strength will change (Peterson, 1988).

The growth of deformation is described by the cumulative strain. The response characteristics are similar to those seen in the stiffness results, indicating that the cyclic development of the deformation might objectively be characterized by the cyclic stress. The fine particles fill the space between bigger particles cannot be neglected the friction. However, in the testing beyond the OMC, particularly in the saturated condition, the specimens with small particles show less deformation due to the generation of internal suctions. Hence, in the saturated condition, finer particles have a positive effect on the structure of the soil. Generally, all the specimens tested at $\sigma_{cyclic} = 20$ kPa show low deformation.

5.2 The effect of track type induced stress states

The tests in the previous section were conducted at constant confining pressure and different cyclic stress levels, as simulating the stress distribution for ballasted and ballastless at 1 m depth in the subgrade (see Table 3.5 on page 51). The stress distribution has a significant influence on the soil until a depth of 2 m for ballastless track construction. Thus, in this section the confining pressure is increased to $\sigma_c = 27$ kPa whilst the cyclic loading is decreased, mimicking the conditions at 2 m depth for ballasted ($\sigma_{cyclic} = 30$ kPa) and ballastless ($\sigma_{cyclic} = 10$ kPa) track types. Two different water content conditions, partially saturated at optimum moisture content and fully saturated have been chosen to evaluate the effects.

5.2.1 Partially saturated at optimum moisture content

Figure 5.17 plots the results for four compacted specimens at maximum dry density and optimum moisture content for particles < 10 mm. The results show that an increase in cyclic stress and confining pressure, leads to increases the resilient modulus. The specimen tested under σ_{cyclic} = 30 kPa and σ_c = 27 kPa exhibits an initial stiffening over the first ≈100 cycles and the highest overall Mr of 68 MPa. The specimen with a cyclic stress of σ_{cyclic} = 10 kPa showed an overall decrease in modulus to 36 MPa. There is a fluctuation of the resilient modulus in all specimens between 200–10^4 cycles, likely due to the breakage of particles, after which the soil behaves more stably. Similarly, Figure 5.18 reveals that the performance of specimens for particles passing through 5 mm behave in the same manner with a general tendency to be less stiff when compared with the larger particles. It can be also seen that the specimens tested with σ_{cyclic} = 30 kPa and σ_{cyclic} = 10 kPa equilibrium being reached in both conditions at around ≈10^3 cycles, leading to a modulus of 53 Mpa and 30 MPa respectively at 10^6 cycles.

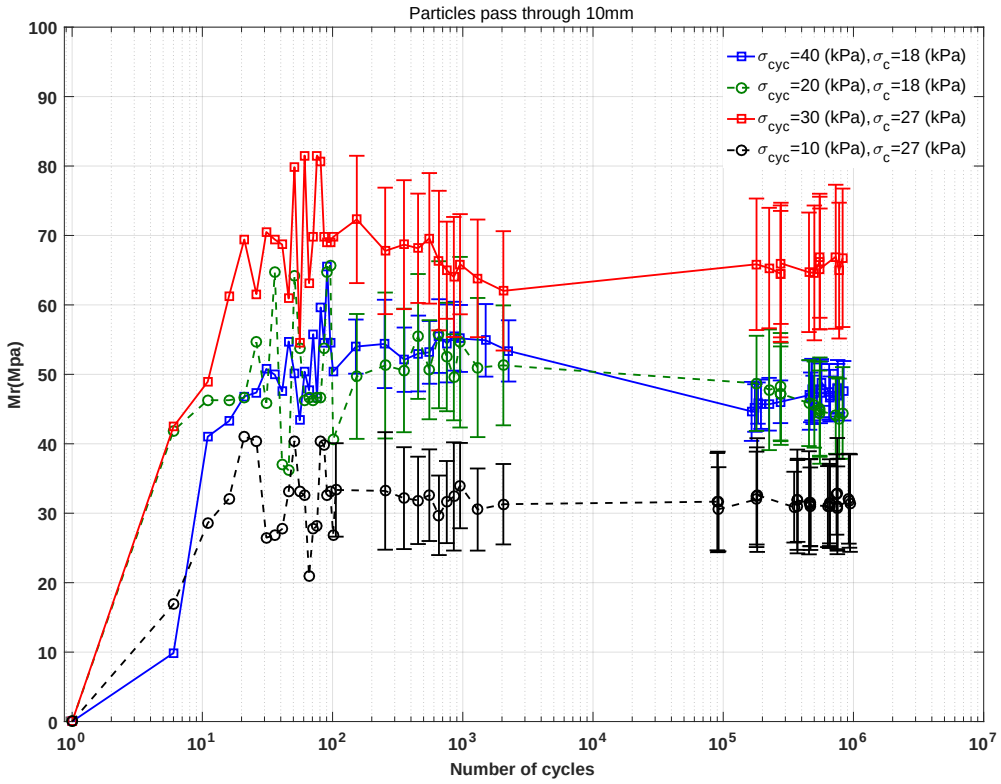

Figure 5.17: Effect of confining pressure on stiffness for OMC state, particles < 10 mm

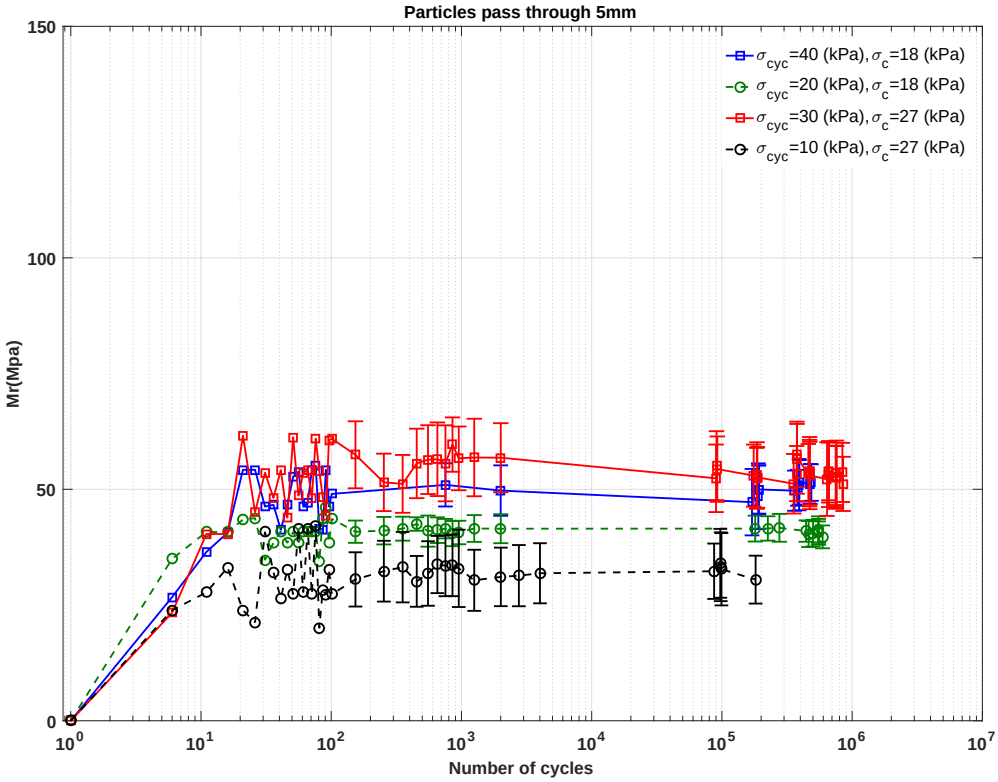

Figure 5.18: Effect of confining pressure on stiffness for OMC state, particles < 5 mm

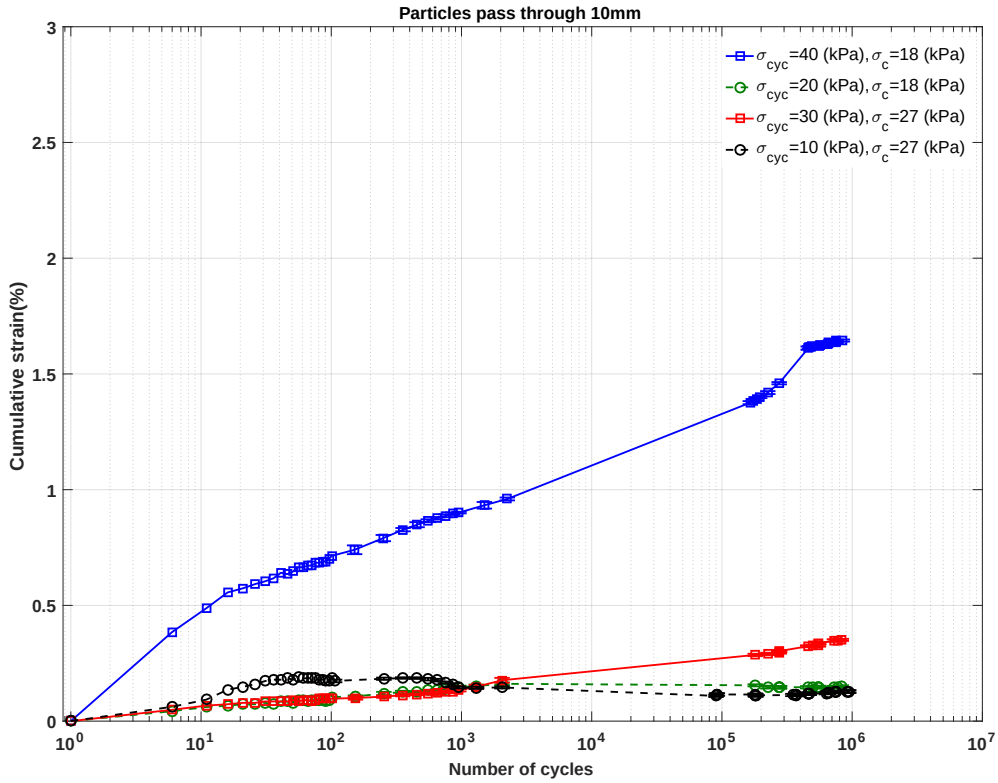

Figure 5.19: Effect of confining pressure on deformation for OMC state, particles < 10 mm

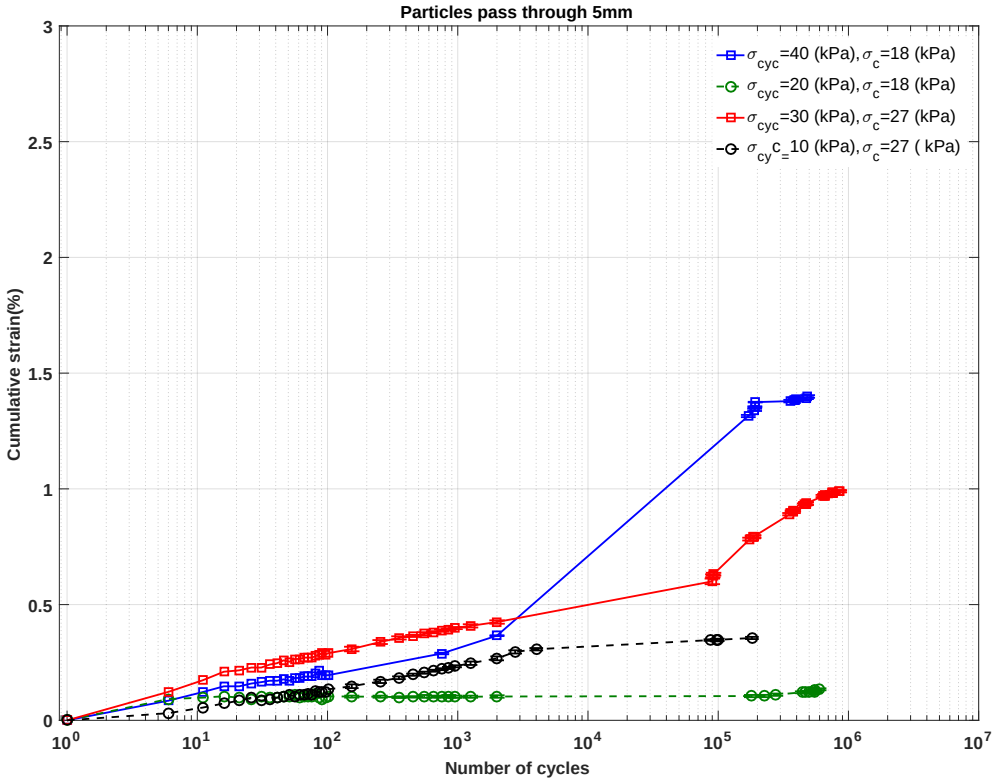

Figure 5.20: Effect of confining pressure on deformation for OMC state, particles < 5 mm

Cumulative strain for these specimens are evaluated and displayed in Figures 5.19 and 5.20. The rate of deformation with increase confining pressure and decrease cyclic loading are very low for both figures, with a modest increase for all but the dry specimen in the < 5 mm specimens. The specimens under the lowest cyclic stress for each depth showed the lowest cumulative strain.

5.2.2 Saturated conditions

Figure 5.21 plots the results for four compacted specimens at maximum dry density and optimum moisture content and then saturated prior to conducting the cyclic test. The results show that an decrease in cyclic stress and confining pressure, does not effect the resilient modulus for specimen $\sigma_{cyclic} = 30$ kPa. However, for the specimen with $\sigma_{cyclic} = 10$ kPa and $\sigma_c = 27$ kPa an initial stiffening over the first ≈100 cycles reduces to a modulus of 32 MPa. There is a plateau between 300–1500 cycles, then soil approaches equilibrium giving a lower than average resilient modulus of 35 MPa.

Figure 5.22 shows that the performance of specimens for particles passing through a 5 mm sieve. For the specimen tested under a $\sigma_{cyclic} = 30$ kPa a slightly higher resilient modulus was reached (58 MPa) when compared with the specimens tested previously

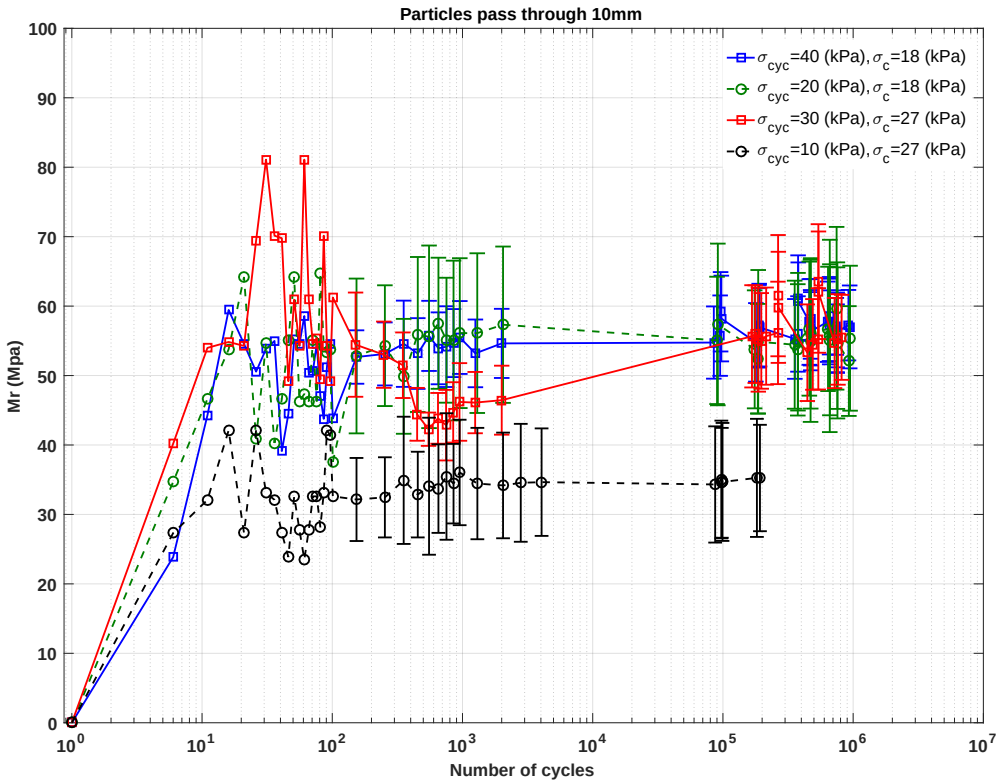

Figure 5.21: Effect of confining pressure on stiffness for saturated state, particles < 10mm

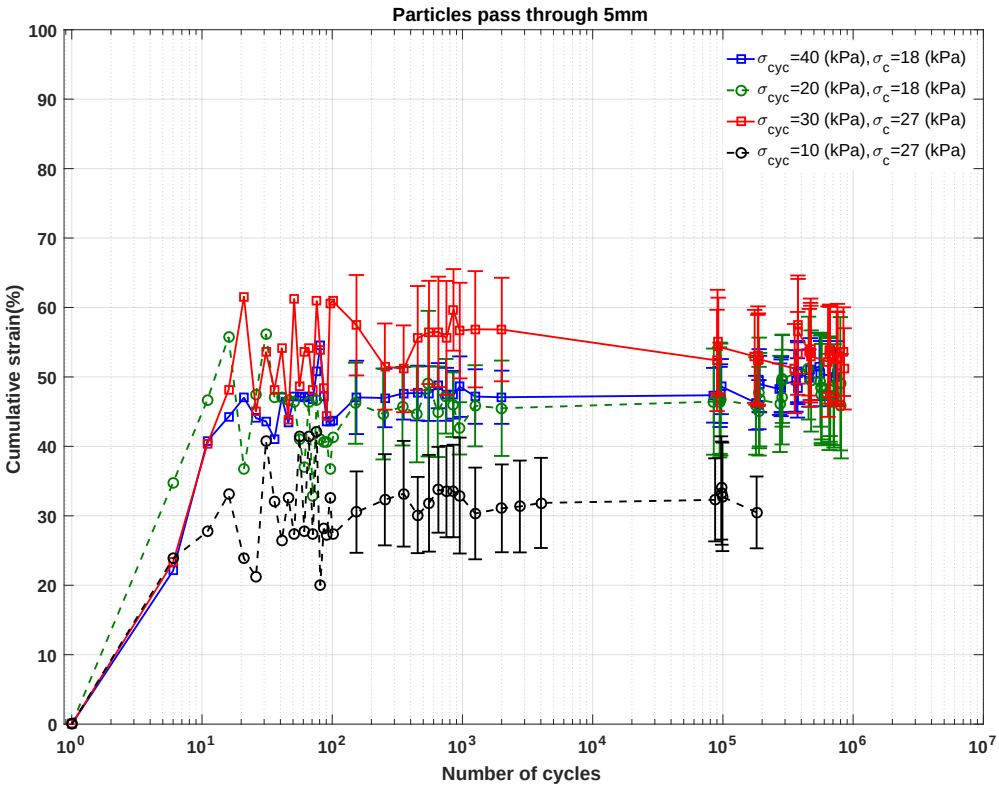

Figure 5.22: Effect of confining pressure on stiffness for saturated state, particles < 5mm

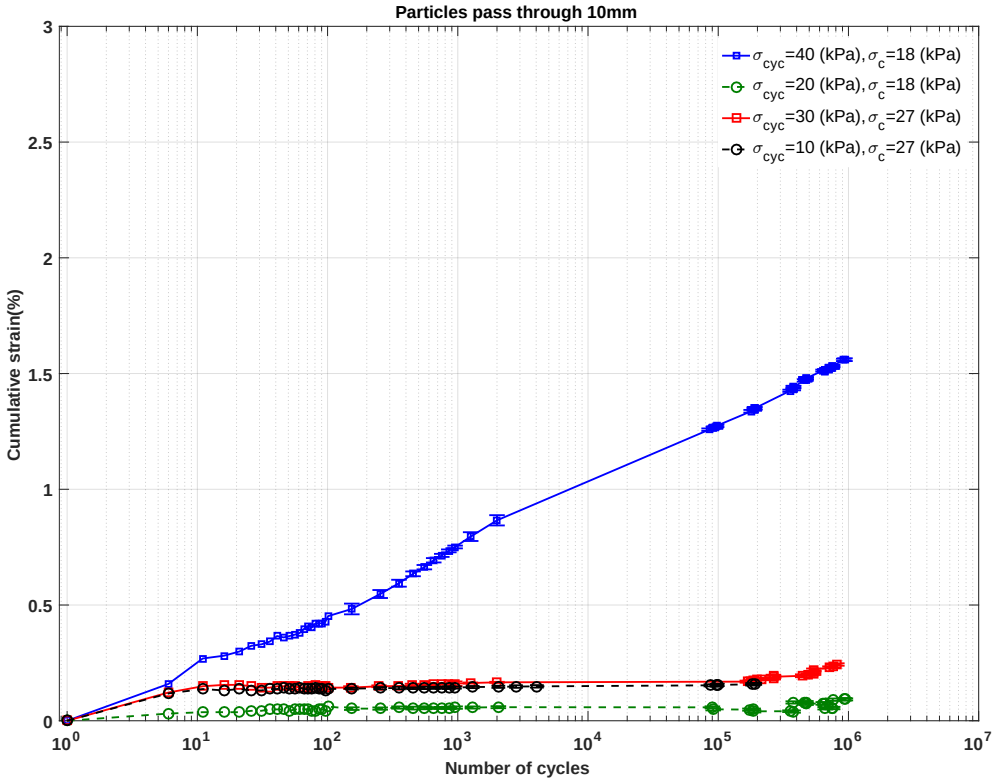

Figure 5.23: Effect of confining pressure on deformation for saturated state, particles < 10mm

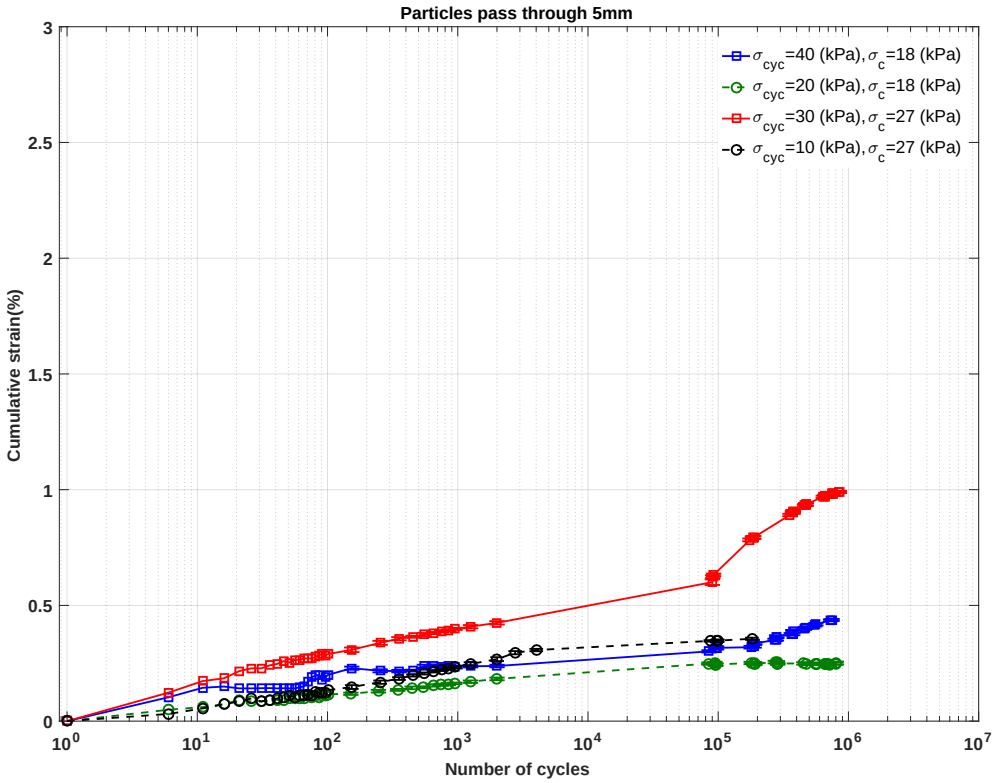

Figure 5.24: Effect of confining pressure on deformation for saturated state, particles < 5mm

(σ_{cyclic} = 40 kPa & 20 kPa). It can be also seen that the specimen tested under σ_{cyclic} = 30 kPa and σ_c = 27 kPa exhibited a plateau being reached up to around ≈1000 cycles at which point there is a gradual decay to the final value of Mr of 53 MPa. The σ_{cyclic} = 10 kPa specimen reached a plateau after a similar number of cycles but maintained this modulus throughout the test having a Mr of 30 MPa at 2×10^5 cycles.

Similarly, cumulative strain for those specimens are evaluated and displayed in Figures 5.23 and 5.24. The rates of deformation with increase in confining pressure and decrease in cyclic loading are very low in Figure 5.23. The only notable variation from the previously discussed trend is that of < 5 mm, σ_{cyclic} = 30 kPa specimen which had double the cumulative strain of the other specimens. As for the partially saturated case, there seems to be no notable correlation between stress state and cumulative strain.

5.3 Effect of varying cyclic loading and confining pressure

In this section variable stress distributions are applied to specimens tested under the optimum moisture content and fully saturated states, to further assess the impact of stress state on resilient modulus. Resilient modulus will be plotted versus number of cycles, and also cumulative strain will be discussed with various of q_{max} which is the maximum deviatoric stress.

5.3.1 Partially saturated at optimum moisture content

In Figures 5.25 and 5.26 vertical stress, combined with increased confining pressure and a decrease the cyclic loading leads to an increase in resilient modulus for all specimens. This increment depends on stress ratio. In Figure 5.25 shows low Mr for curve of 90 kPa of deviatoric stress with stable stiffness over ≈10^5 cycles. It could be argued that cyclic stress cycling over the yield surface for this material causes degradation of soil under even small cyclic stresses. In the q_{max} = 80 kPa test a slightly higher Mr is seen than at q_{max} = 70 kPa. Most curves reach equilibrium over the first ≈1000 cycles.

Figure 5.26 shows the plots for the specimens with particles < 5 mm. The same trends in behaviour can be seen as specimen q_{max}= 80 kPa shows the highest stiffness, reaching 58 MPa at 5×10^5 cycles. Whilst the specimen tested under q_{max} = 70 kPa shows a resilient modulus developing to 55 MPa for the same number of cycles. The resilient modulus for the specimen with q_{max}= 60 kPa reducing to 52 MPa. The specimen that cyclic out the yield of stress gives maximum stiffness being reached to 36 MPa which is marginally higher than that tested with particles less than 10 mm size.

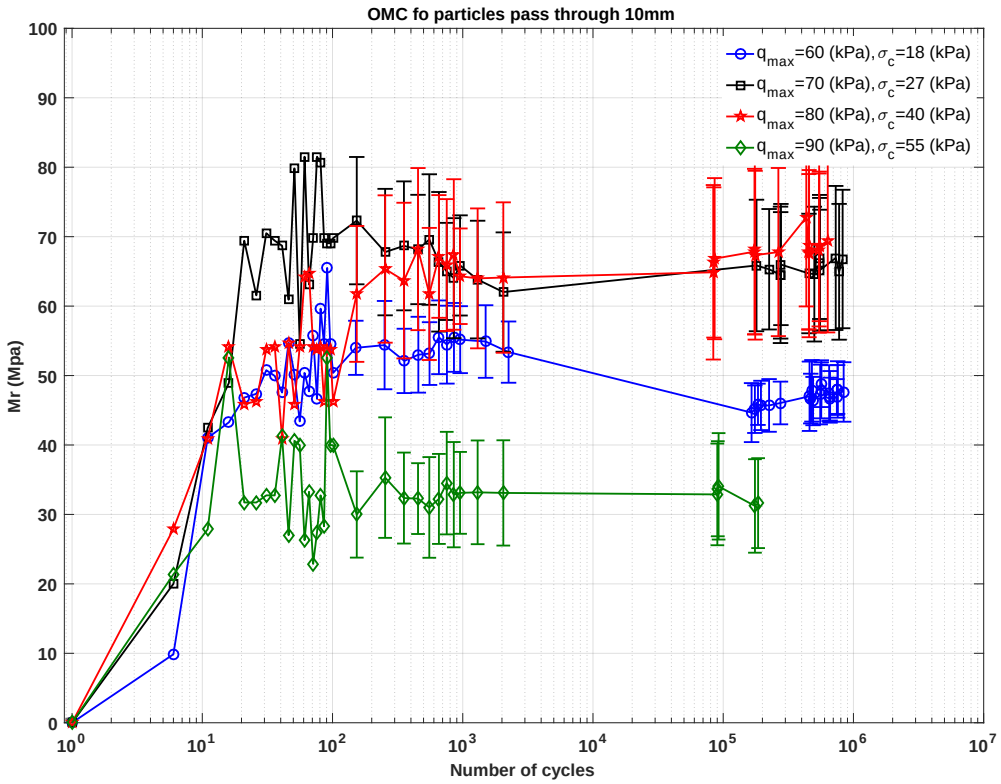

Figure 5.25: Resilient modulus for saturated conditions, varying stress state, particles < 10 mm

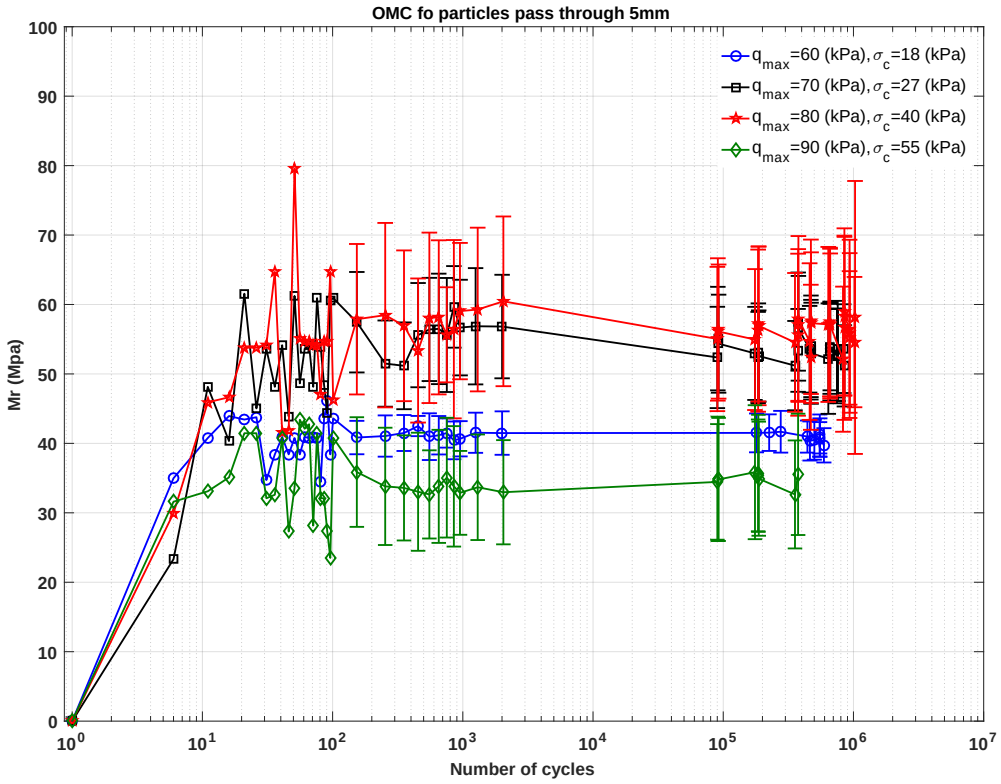

Figure 5.26: Resilient modulus for saturated conditions, varying stress state, particles < 5 mm

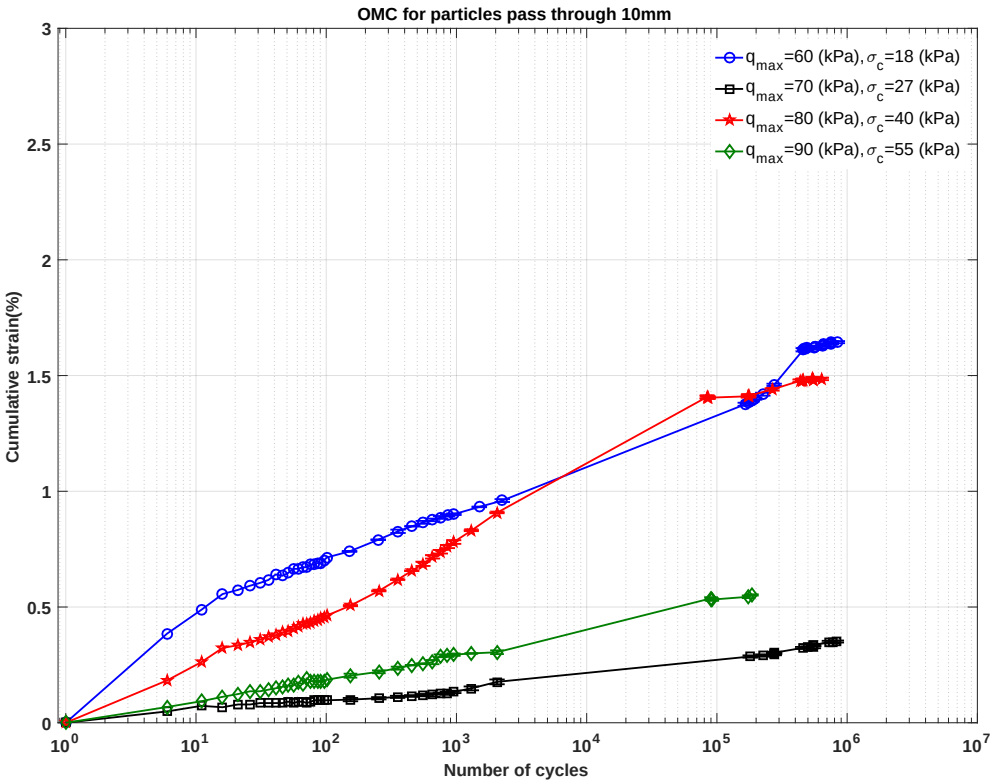

Figure 5.27: Deformation for saturated conditions, varying stress state, particles < 10 mm

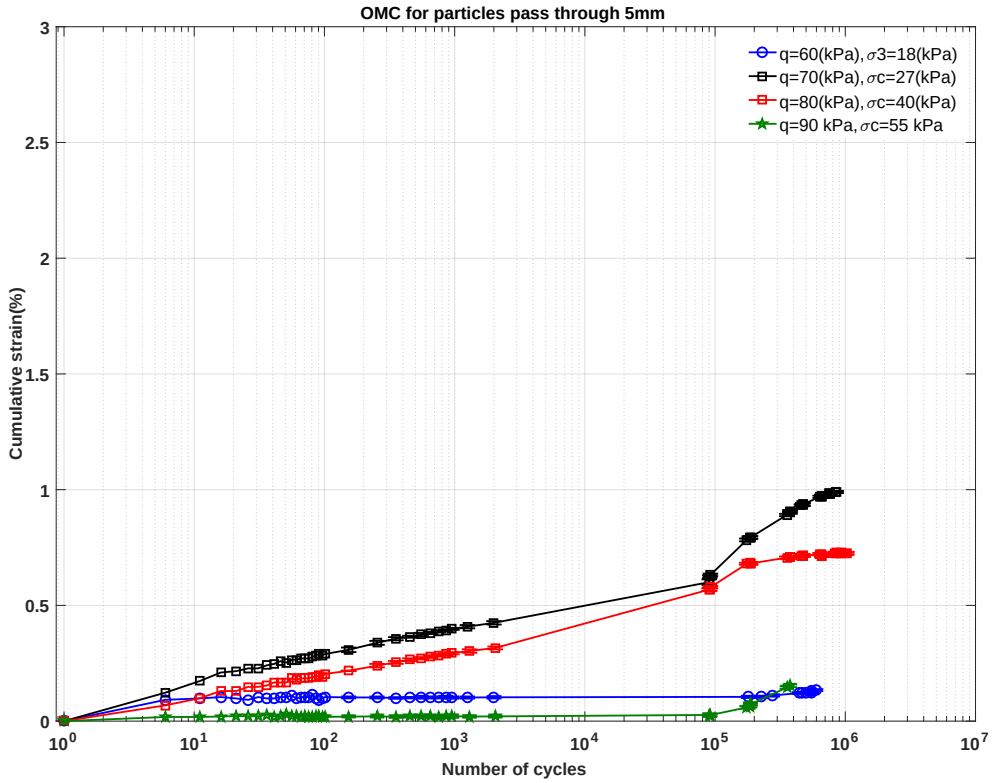

Figure 5.28: Deformation for saturated conditions, varying stress state, particles < 5 mm

Deformations for specimens under these stress states are shown in Figures 5.27 and 5.28. A linear trend of increasing cumulative strain with increasing log number of cycles is seen in both figures. For the $<$ 10 mm specimens the cumulative strain reached at $\approx 2{\times}10^5$ was 1.48% for q_{max} = 60 kPa, 0.3% for q_{max} = 70 kPa, 1.48% for q_{max} = 80 kPa, and 0.55% for q_{max} = 90 kPa. For particles less than 5 mm size, the strain being developed was 1.45%, 0.7%, 0.65%, and 0.15% respectively at the same number of cyclic loading for the same q_{max} levels respectively. The highest deformation was seen in both figures at q_{max} = 60 kPa.

5.3.2 Saturated conditions

In saturated conditions the specimens behave similarly to those tested under OMC conditions, with slightly less stiffness seen in all stress states. Figure 5.29 shows that increased vertical stress combined with increased confining pressure causes a slight increase in resilient modulus for σ_c = 40 kPa. Nevertheless, soil becomes less stiff at q_{max} = 90 kPa. As has been seen previously the effect of reducing the maximum particle size to 5 mm keeps the same pattern of behaviour but with a lower resilient modulus (Figure 5.30).

Correspondingly, the results of cumulative strain are shown in Figure 5.31 and Figure 5.32. The maximum recorded cumulative strains in the $<$ 10 mm tests were 1.52%, 1,2%, 0.53%, and 0.53% for the q_{max} = 60, 70, 80 and 90 kPa tests respectively, and 0.69%, 1.2% and 0.15% for q_{max} = 60, 80 and 90 kPa tests respectively in the $<$ 5 mm tests. To conclude, for both conditions tested the deformations show the same trends with moderate increases with number of cycles.

5.4 Effect of varying stress state and load frequency

In this section the resilient modulus for mudrock under 1 Hz is examined to assess whether the stress states looked at in the preceding sections will be also affected by frequency. It was seen previously that Mr increases with increased cyclic stress. The results for resilient modulus are shown in Figure 5.33 and Figure 5.34. For the specimens at the same confining pressure, the stiffness being developed is higher for a higher applied deviator stress. In general it can be observed that soil tested under lower load frequencies produce a lower resilient modulus. Tests were conducted under fully saturated conditions.

Figure 5.34 plots the resilient modulus for particle passing through 5 mm. Most of the tests reach an early equilibrium, with no notable increase with increasing number of cycles. The exceptions are the slight increase in Mr for the q_{max} = 45 kPa specimen and the gradual decrease seen in the q = 60 kPa test after the plateau at ≈1000 cycles. As seen previously the increase in deviatoric stress to 70 kPa causes an increase in the stiffness

recorded.

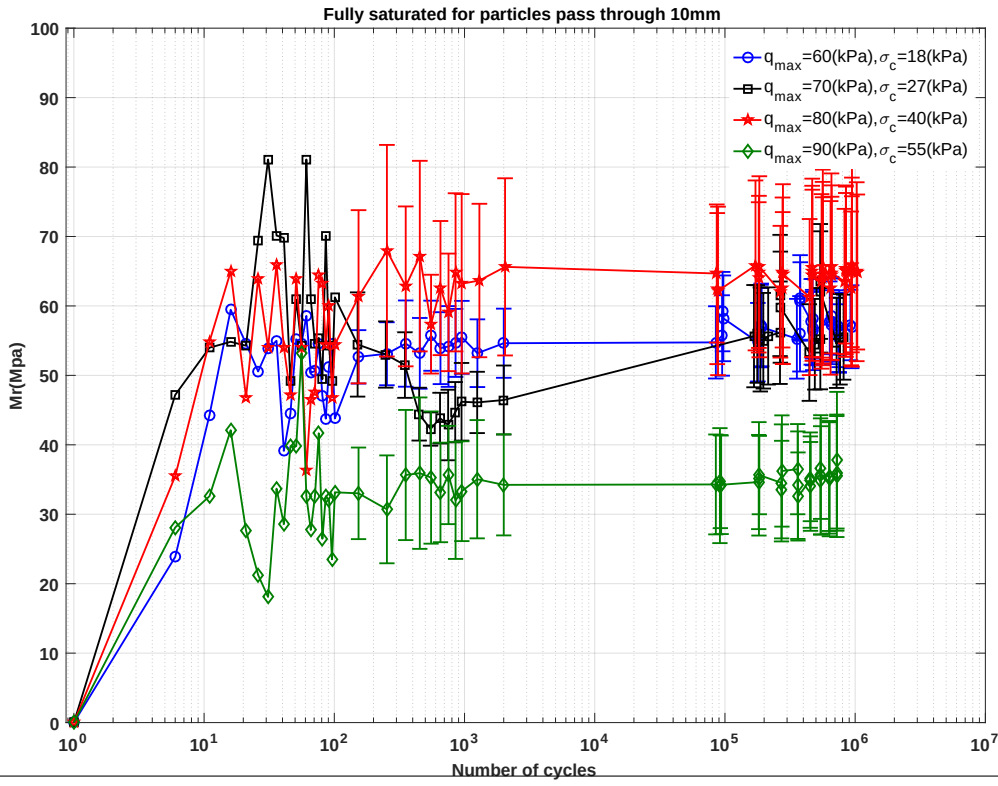

Figure 5.29: Resilient modulus for saturated conditions, varying stress state, particles < 10 mm

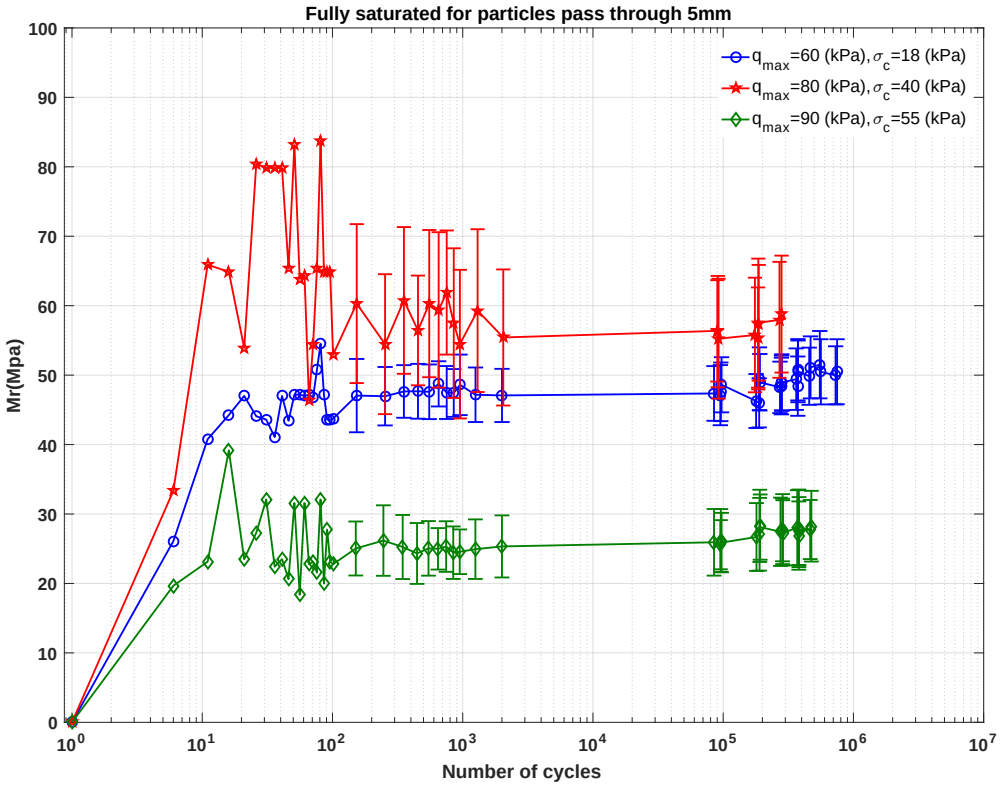

Figure 5.30: Resilient modulus for saturated conditions, varying stress state, particles < 5 mm

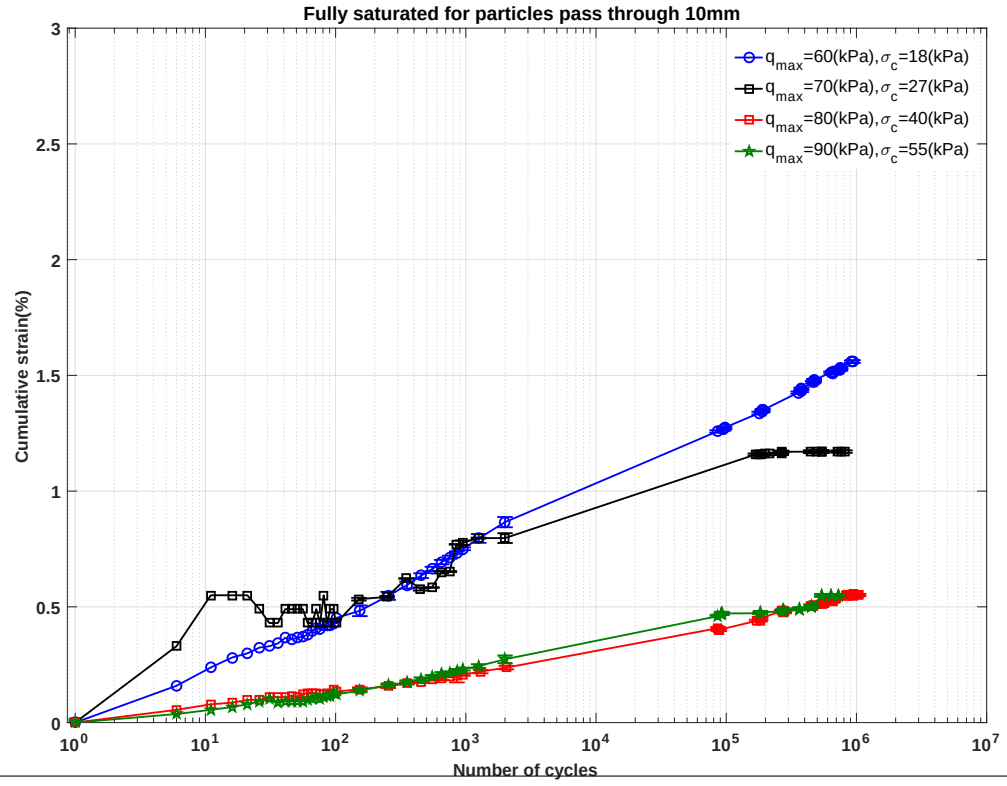

Figure 5.31: Deformation for saturated conditions, varying stress state, particles < 10 mm

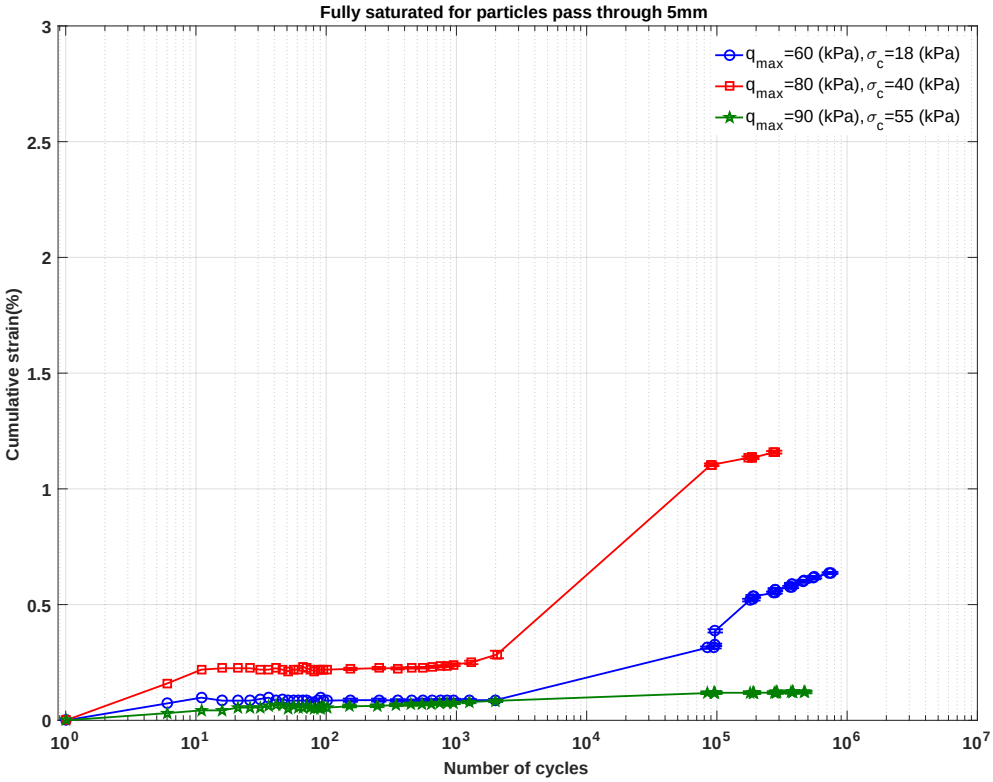

Figure 5.32: Deformation for saturated conditions, varying stress state, particles < 5 mm

The resilient modulus at 5×10^5 cycles for the < 10 mm specimens were 32, 67.8, 36 and 76.622 MPa at $q_{max} = 45$, 55, 60, 70 kPa respectively and in the < 5 mm specimens 28, 43.8, 34.3 and 58.7 MPa respectively (for the same values of q_{max}).

The plots of cumulative strain are shown in Figures 5.35 and 5.36. The specimen deformation increases linearly with increased number of cycles with the lower confining stress in each case leading to increased cumulative strain.

There was a slight increase in settlement for the specimen tested under $q_{max} = 70$ kPa when compared with the $q_{max} = 55$ kPa specimen given that the confining stress was constant. When soil is exposed to repeated loading which exceed the failure envelope the soil become less stiff. It is believed that if the loading is within the yield surface, soil will behave elastically and the resilient modulus should reach an equilibrium with an increasing number of cycles without failure.

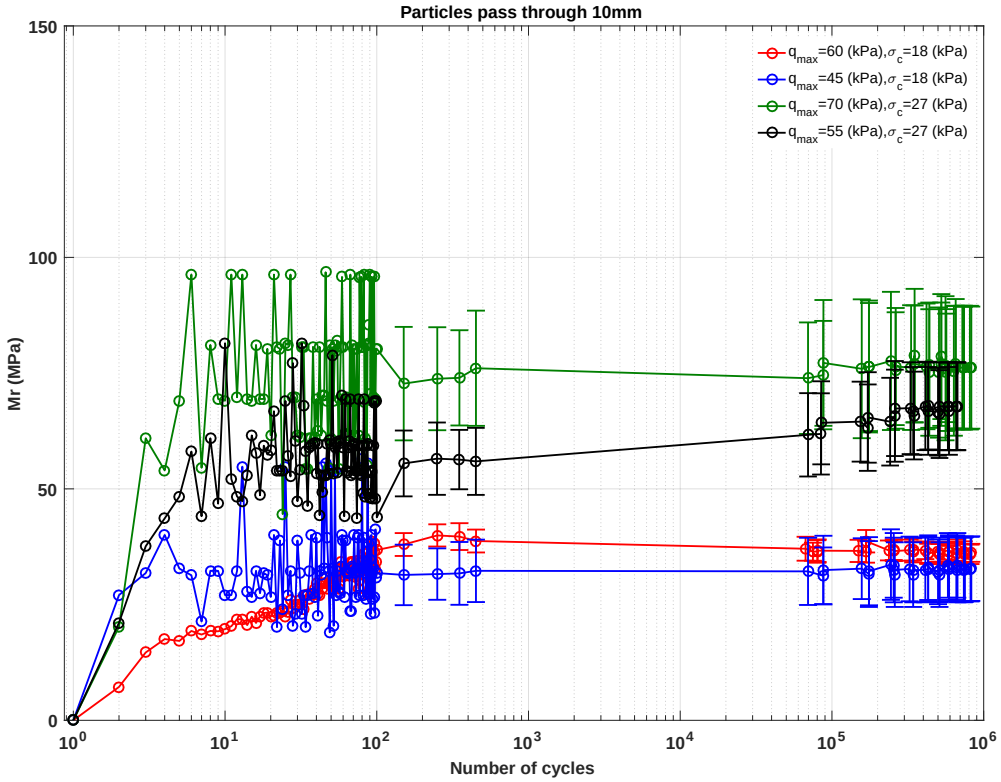

Figure 5.33: Resilient modulus for saturated conditions, particles < 10 mm, 1 Hz

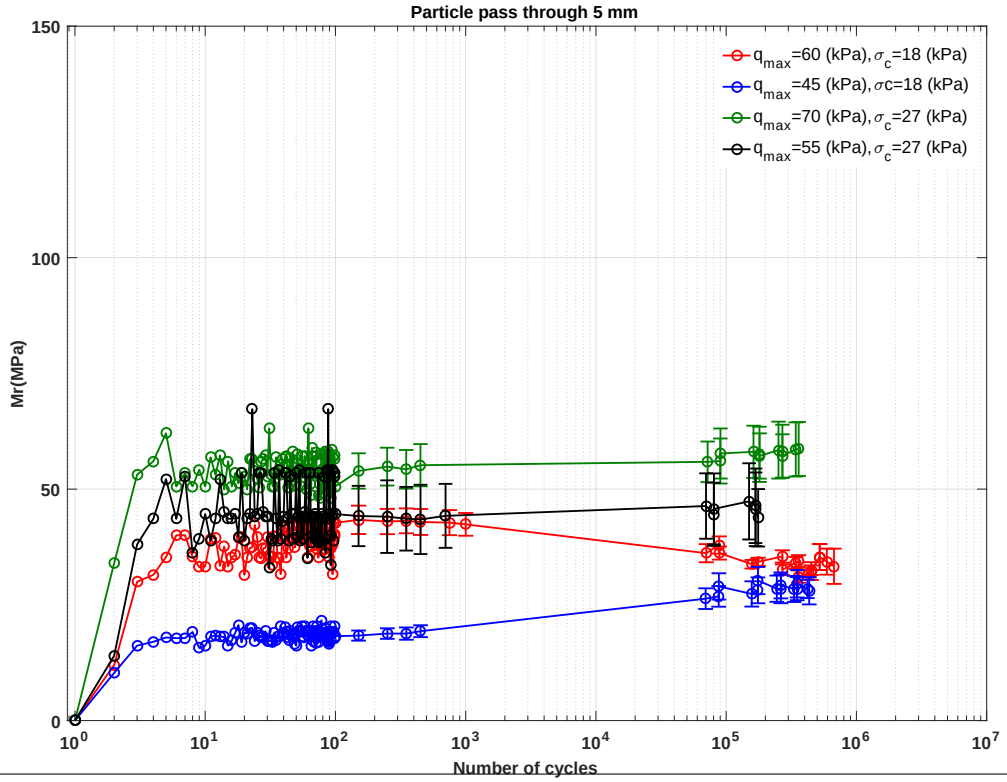

Figure 5.34: Resilient modulus for saturated conditions, particles < 5mm, 1 Hz

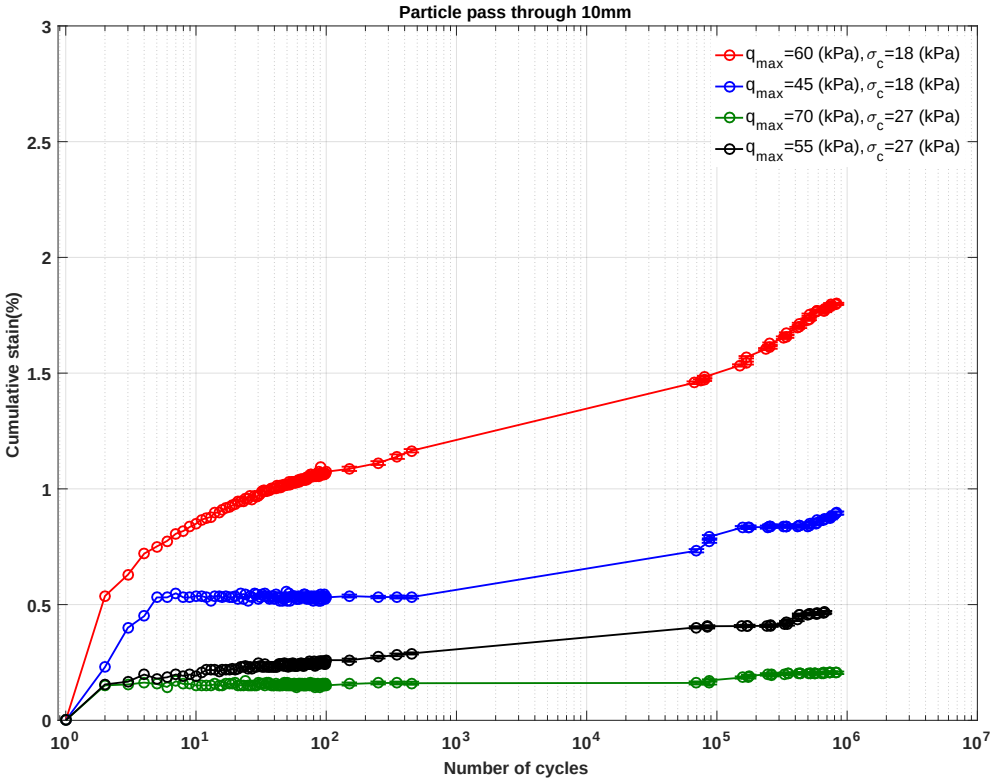

Figure 5.35: Deformation for saturated conditions, particles < 10mm, 1 Hz

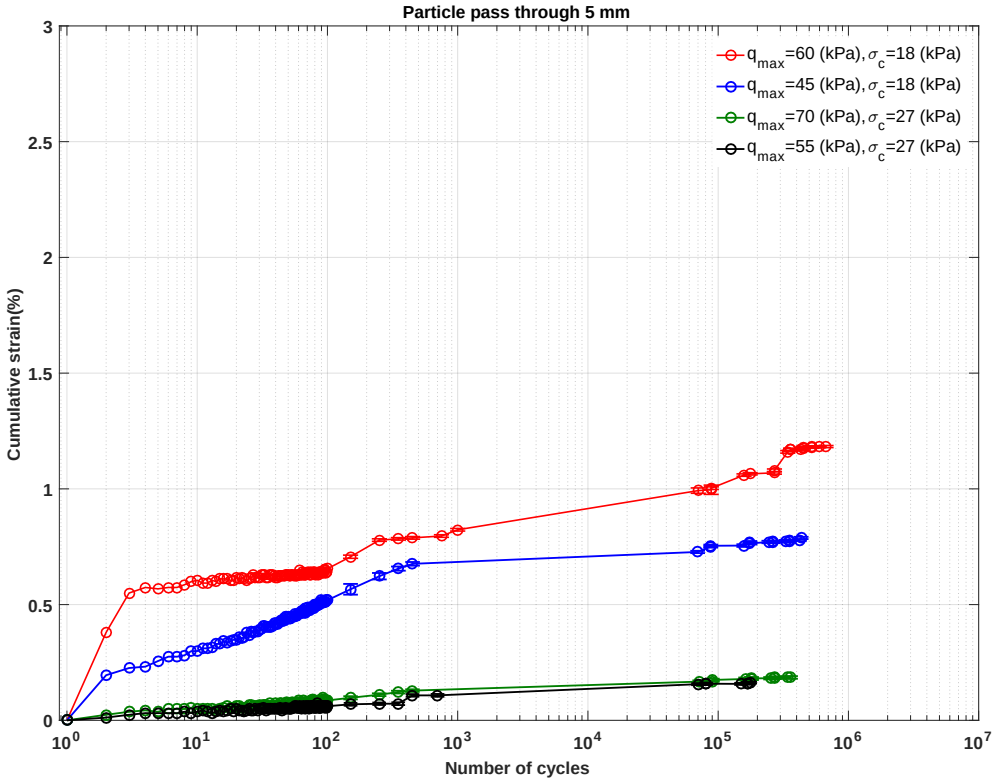

Figure 5.36: Deformation for saturated conditions, particles < 5mm, 1 Hz

5.5 Interpretation and discussion of the results

The focus of this chapter is to characterize the Mr in terms of changing stress state. The resilient modulus indicates the distribution of stress and strain for the soil system. Several studies pointed that Mr significantly relates to the physical properties of soil. Based on the results of the tests in this chapter it can be said that an increase in cyclic deviatoric stress with a constant confining pressure will act to increase resilient modulus. A similar trend was seen in the three different soil conditions dry, partially saturated and fully saturated.

To better illustrate the trends in the data, the peak resilient modulus for all tests are compared using stress ratio (σ_{cyc}/p') and are plotted versus the Mr attained at 5×10^5 cycles in Figures 5.37 and 5.38. The stress ratio was varied from 2.14 to 0.154 as noted previously in Table 3.5 (page 51). With high-stress ratios ($\sigma_{cyc}/p' > 1$) the resilient modulus is relatively stable. In this region the particle size affected the stiffness of soil for 1 Hz and 4 Hz frequencies by reducing the Mr 4% and 11% respectively for a reduction in the maximum particle size from 10 to 5 mm. In this region it can also be seen that the Mr is higher for increased load frequency.

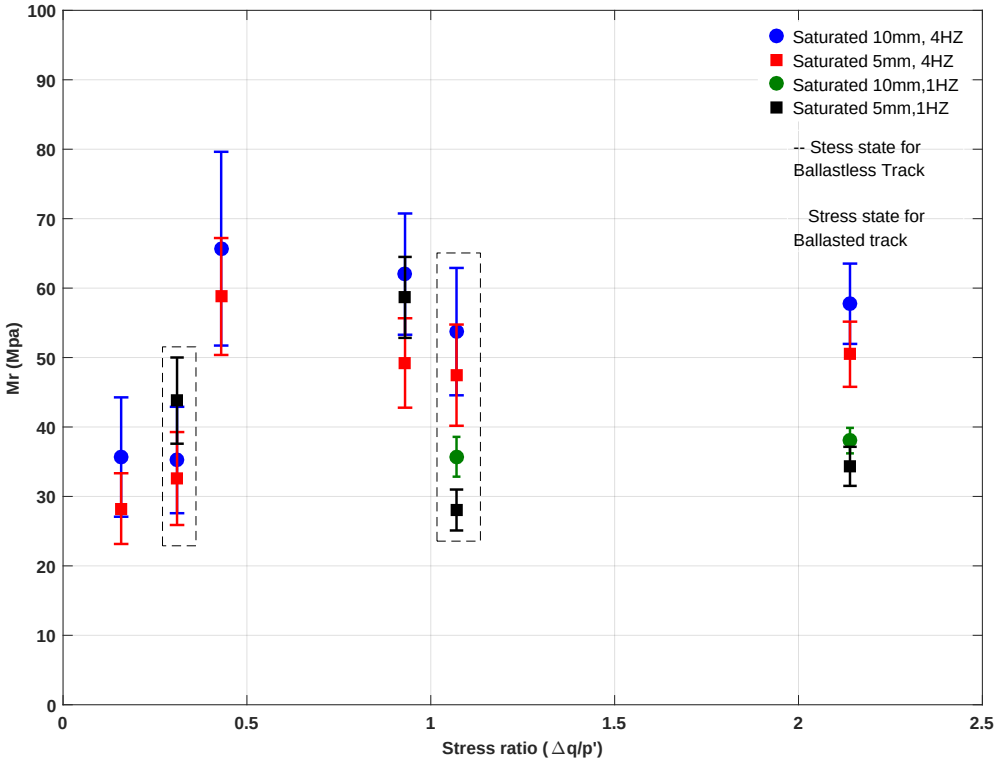

Figure 5.37: Development of resilient modulus with varying stress ratio in saturated condition

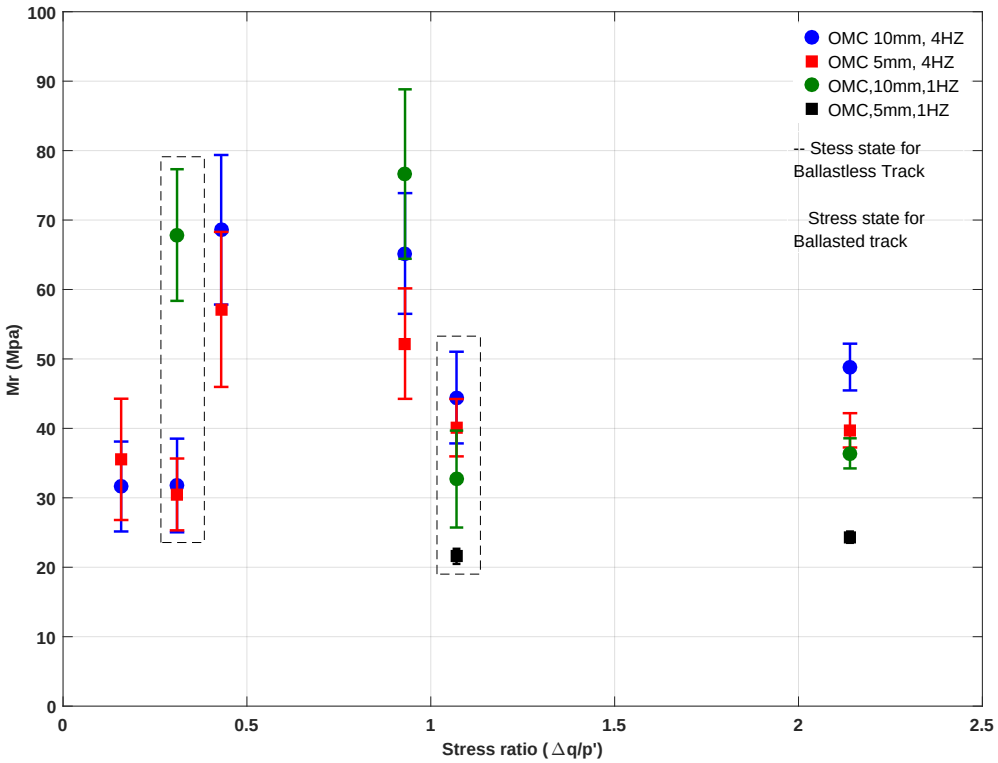

Figure 5.38: Development of resilient modulus with varying stress ratio in OMC conditions

For stress ratios between 0.4 and 1 the performance improved as the stiffness was higher in all like-for-like tests. The highest stiffness of any test was developed in the 1 Hz under OMC conditions for particles < 10mm. For stress ratios below 0.4 all the specimens exhibited low resilient moduli.

General speaking, the resilient modulus increases with a decrease in stress ratio until reaching $\sigma_{cyc}/p' = 0.31$ at which point the specimens became less stiff for any given moisture content condition. In addition, decreasing stress ratio under the same confining pressure leads to decrease in resilient modulus stress ratio (see results at $\sigma_{cyc}q/p' = 1.07$ and 0.31).

The value of resilient modulus for mudrock classify as a good modulus according to the classification that found in for track and subgrade modulus (Ahlf, 1975). The results indicate that an increasing cyclic deviatoric stress leads to an increase in stiffness (Mr). Thus, a stiffer subgrade combines with higher deviator stress. Nevertheless, this does not mean a stiffer layer would behave badly due to higher cyclic deviator stress because the performance of soil not only depends on stress state but also on the strength of soil. From the comparison between ballasted and ballastless stress distributions it was shown that the resilient modulus for ballasted systems was larger than that in ballastless due to the deviator stress being higher. As the increment of strength much higher than an increase in deviator stress (Li, 1994).

Conversely, settlement of the railway track is the main cause of deterioration, which entirely depend on the dynamic effect (Nguyen Gia et al., 2011). Cyclic stress significantly impacts on the soil dynamic performance and that generates the permanent deformation. In the saturated conditions, the B-value was 0.95-0.96, guaranteeing the specimens were close to saturation.

The permanent deformation increases with the increasing number of cycles to approach the equilibrium state in some cases. Stress ratio is influenced by the progress of deformation, some high-stress ratios improves the ability of soil to resist further strain. Large cumulative strains can lead to a significant failure. There are many factors that control deformation which is reflected in the settlement of railways. The possible reason for this deformation based on the number of cycles, physical state and stress state. Number of cycles that show development of cumulative strain until this progress ceases to reach the stable state. The cumulative strain was found to increase with increases in cyclic stress when the confining stress was held constant as can be seen in the figures within this chapter. It can be said that reducing stress ratio at the same confining pressure reduces the settlement rate. Many researchers have found that deviator stress ($\sigma_1 - \sigma_3$) is the main stress affecting the cumulative stain, increasing deviator stress leads to an increase in cumulative strain (Seed et al., 1955; Monismith et al., 1975). Some research has indi-

cated that an increase in moisture content will increase the plastic strain (Edil and Motan, 1979). The cumulative strain for mudrock shows that increase deviatoric stress increases the cumulative strain under the same physical state. However, the relationship between Mr and cumulative strain is not constant for the mudrock in this study. It is vital to understand how increasing cyclic stress combined with increases in the confining pressure change the behaviour of the soil and the exhibited cumulative strain for the same physical conditions.

Saturated and partially saturated specimens with two particle size distributions have been tested. The cumulative strain generally shows an increase with increasing number of cycles, when the cyclic stress state is higher the cumulative strain also increases. Particle breakage is mainly effected by the stress level, the magnitude of the stress and stress path and also time. The particles are likely to break when they are larger due to the fact that these particles contain more laminations. Increasing particle angularity has the same effect as the stress can condense along there narrow dimension and also along contact angular points causing points of fracture. However, by increasing the density the amount of breakage decreases. With more particles surrounding each other, the average force contact tends to decrease. Water can act to soften the surfaces causing increased breakage as well. In the dry state the stiffness was higher for particles passing through 10 mm and increased linearly with increase number of cycles. Whilst specimens subjected to 1 Hz load frequency showed an increasing stiffness until the equilibrium state is reached at $\approx 2 \times 10^5$ cycles. Furthermore, more scatter of the data during the cyclic test can be noticed for dry test due to the vibration movement of the particles which is inherent in cyclic loading. It can be concluded that stress ratio has a remarkable influence on the resilient modulus in both particle size distribution of specimens.

5.6 Summary

Different levels of confining stress and vertical stress have been applied to specimens to mimic the stress distribution created below the axles of high speed trains. The effect of cyclic loading has been discussed and found that resilient modulus increases with the decrease of the cyclic loading. The stress distributions that are induced below ballasted and ballastless track structures have been estimated from the literature and specimens have been tested under the same stress states in the laboratory. The results were compared and found that mudrock subjected to the stress distribution for a ballastless system had a modest decrease in stiffness of around 6% than seen in the ballasted stress state. However, increasing deviatoric stress and confining pressure led to a decrease of the stiffness of the ballastless track to around 54%. In addition, it found that the resilient modulus for

specimens with the smaller maximum particle size decreased by around 17% than in the ballasted stress state for the dry condition, with the difference becoming less increases to the degree of saturation.

In the final part this chapter the effect of changing of stress distribution on the resilient modulus was highlighted. The results showed that stiffness increases with a decrease in the stress ratio σ_{cyc}/p' until the maximum at 0.43 (higher deviatoric stress is reached). The Mr then decays by around 50–55% for stress ratios down to 0.134.

Chapter 6

General discussion

Subgrades are required to provide a stable railway foundation. The subgrade consists of natural ground and fill material. This chapter summarises the work done to estimate the performance of mudrock material, as it is important to consider its use and to evaluate its suitability to be a subgrade material under future high speed railway tracks. Experiments have been conducted to measure the appropriateness of the mudrock material. A discussion of experimental results are explained below in relation to the aim of this research. In this project, 54 specimens were tested under various water content and stress state state conditions as shown in Table 3.6 on page 62.

6.1 Material selection and properties

Mudrock colliery spoil has been analysed as it represents a potential subgrade of the railway track structure for HS2. This material is a common feature in ex-coal mining areas such as South Yorkshire. Details of the route of HS2 (at the time of project startup) are shown in Figure 1.1 (p 2), with the detailed description of the material being contained in Section 3.1 on page 32. In order to investigate the behaviour of such material under high speed railway triaxial cyclic tests were utilised to understand the engineering properties govern the performance of the subgrade layers. The resilient modulus plays a significant role in the analysis and design of structures track under the cyclic loading that is generated due to passing trains. In addition, cumulative strain is essential to predict the long-term strains which allow the prediction of the performance of the track system.

Disturbed specimens were tested, as these best represent the expected compaction on site during track construction. Figure 3.2 shows the particle size distributions of the specimens tested. The maximum particle size was taken as 10 mm have been compacted and tested due to the suitability of disturbed specimens for testing in the triaxial cell (dimensions: 100 mm diameter and 200 mm length). Table 6.1 shows the engineering

properties of mudrock for the current study and the properties that were obtained from previous studies. The Atterberg limits were close to the values that were found in all previous studies. The specific gravity is close to the material that utilised in Blanchfield (1998) and Nahazanan (2010).

Table 6.1: Engineering properties of mudrock in recent research

	O'Neill (2007)	Blanchfield (1998)	Nahazanan (2010)	Current study
Liquid limit (%)	34	36.6	35	34.5
Plastic limit (%)	20	21.3	21	20.5
Plasticity index (%)	14	15.3	14	14
Specific gravity	2.52	2.75	2.75	2.75
Maximum dry density (Mg/m^3)	-	1.63–2.02	1.539	2.04
Optimum moisture content (%)	-	9–16	-	11.5

6.2 Characterization of soil stiffness

Geotechnical design of track foundation needs to take into account the stiffness of the soil and the expected deformation. Any foundation design of track should consider three major issues: avoid issues caused by the increased loading frequency, avoid or limit track maintenance, and minimise the possibility of excessive deformation and failure. In this project, attention has been paid to the characterisation of mudrock that is assumed to be a subsoil for HS2. The main objective of this research was to estimate the resilient modulus during long-term cyclic tests, and the long-term deformation and critically the factors which effect these values.

All specimen tests were conducted with the application of a haversine load wave with constant amplitude at frequencies of 1 and 4 Hz. The experimental tests were conducted by simulating the in-situ conditions on the material of study to determine the actual mechanical behaviour of the mudrock backfill under cyclic loading. The resilient modulus during the cyclic for such material was shown to increase linearly, and in some conditions equilibrium was reached. From slaking tests conducted the soil was shown to have a medium durability, as it has the ability to degrade under the present water and by the compaction effect which was applied during the preparation of the specimens. This phenomenon has a positive influence on soil. With the increase number of cycles the soil increases in density which increases the number of contacts between particles and reduces the void ratio.

Lower moisture content specimens exhibited a higher cyclic resistance than other specimens. A decrease in the cyclic stress also led to increasing stiffness, but this effect was

found to be dependent on stress state. The resilient modulus for mudrock backfill in this study can be classified as 'medium' according to the classification system used by Li et al. (2002) that is given in the table below:

Table 6.2: Classification of resilient modulus, Li et al. (2002)

Soil type	Resilient modulus (MPa)	Compressive strength (kPa)
Soft	7–28	34–103
Medium	28–69	103–207
Stiff	69–138	207–345

6.3 Characterization of cumulative strain

Cumulative strain plays a significant role in the calculation of settlement, which can lead the failure of the foundation design. The cumulative strain for mudrock shows high variation due to the degradation of the mudrock particles during the tests. The cumulative strain that was generated during the cyclic tests is indicative of the probable settlement of the track. There are many issues which contribute to the deformation in mudrock, such as the relocation of the particles, wetting that causes the degradation and also breakage that is induced due to compaction and the cyclic loading. Hence, the cumulative strain in this study is classified as a fair to good condition for the design of foundations. Inundation of mudrock has a significant impact in terms of changing the condition of soil. In this situation the soil can experience a sudden volume loss due to the addition of pore water.

Monismith et al. (1975) and Knutson et al. (1977) presented an empirical model to estimate the settlement which is shown in Equation below:

$$\varepsilon_p = A(N)^b \tag{6.1}$$

Where: ε_p = cumulative plastic strain (%), N = number of cycles, and A and b are calculated in Table 6.3.

Application of this equation to the data produced in the current research is shown in Table 6.3. The exponents A and b have been estimated by taking the log for both figure axes (on a plot of cumulative strain versus number of cycles) and then linear regression was used to quantify A and b as function of N. As can be seen that the data has high variation and that this variation increases with increased water content. Due to the variation in results fitting a single parameter model will always have limitations to enable good predictions for such a soil, but the upper bounds could be used to predict worst case scenarios for future designs.

Table 6.3: Parametrisation of the predictive model for cumulative strain

Soil state	A	b
Dry	1.62–1.68	0.87–0.78
Dry side	1.55–2.95	0.16–0.41
OMC	5.21–1.46	0.74–0.09
Saturated	9.68–1.48	0.58–0.139

6.4 Effects of the track type

Performance of the track depends on the stress situation and the soil properties. Increasing axial loads and train speed increase inevitably the number of problems. The tests were conducted in order to simulate subgrade foundation material under repeated train load under two track systems: ballasted and ballastless. The stress distribution for both track types have been mimicked in the laboratory and the effect on stiffness evaluated. The resilient modulus under the stress state of ballasted showed a higher stiffness at 2 m. The cumulative strain that are induced from the ballasted stress state are higher than that seen for the ballastless track with slight increase with the increase of small particles. Ballasted is a widely used track type in the UK.

An alternative track system is a ballastless track which is capable of reducing the about of maintenance required by 10–30% when compared with ballasted track. Ballasted track showed more suitability for use in design in terms of the stiffness generated in the subgrade. However, the stress state for ballastless produces less settlement, due to the cumulative strain being dependent mainly on the deviatoric stress. This is particularly the case for the smaller particles as bigger particles are more capable to breakage and densification with further cycles. This conclusion agrees with the previous work done by Seed et al. (1955), Monismith et al. (1975) and Brown et al. (1975).

6.5 Future design

To make good use of the results of the cyclic triaxial tests for the possible use of mudrock as a subgrade, it is necessary to take into account the traffic weight, maintenance schedule and allowable values of elastic and plastic deformations of the subgrade to determine the appropriate parameters and structure of the subgrade.

Subgrade soil properties of each layer is the most important factor that influences the track modulus when compared with the other track components (Li et al., 2002). Design of an adequate track railway should prevent subgrade progressive shear failure and excessive plastic deformation. These problems cause excessive track maintenance. In this research

the mudrock under repeated load shows improvement during the cyclic loading. However, the resilient modulus is only classified as medium stiffness and strength and should be designed with accordingly.

Track should avoid being built on the soft or medium subgrades because these kinds of subgrade can have two possible problems: excessive plastic strain and progressive shear failure. These problems will lead to the deterioration of the track. In order to reduce the major maintenance and rehabilitation cost, it is necessary to control the material quality, physical state and load distribution. When the soil approaches the saturated state the fines percentage negatively affected the stiffness of the soil. As a consequence the drainage conditions must be taken into consideration to protect the subgrade layer stiffness. The cumulative strain for the mudrock is categorised between good and fair for settlement performance. In this case, maximum effort should be made in the preparation and compaction of the mudrock to prevent the subgrade exhibiting excessive plastic deformations and limit the total cumulative strain of subgrade layers to below an allowable level for the design period.

For acceptable foundation performance of the material, it would be necessary to maintain the margin between the shear failure surface and the cyclic stress imposed at the depth which the material it to be used. Cyclic deviator stresses are lower in ballastless track types than in ballasted as the thickness of the first layer is higher and this will spread the stress distribution and reduce the stress. According to the slaking test and compaction particle size distribution data the results show that breakage leads to an increase in fines content after compaction. The permeability hence also can be affected which could lead to the soil not meeting the design requirements. Filter materials could be used in this case to maintain drainage in the soil. Seepage tests must be conducted in this case under the same conditions as in the field to prove the final performance of drains, and hence guarantee track performance.

Chapter 7

Conclusion and recommendations for future work

The current study has investigated the use of mudrock for use as a subgrade beneath the upcoming development in the UK of high speed rail 2 (HS2). This study required investigating the long-term performance under cyclic loading. The main conclusions of this work are listed below and are followed by recommendations for future work.

7.1 Conclusions

7.1.1 Material of study and the apparatus

- The engineering properties of the material are representative of a mudrock colliery spoil in the UK. Classification tests showed good agreement with previous studies.
- Triaxial cyclic loading was an appropriate apparatus to achieve the aim of this project. Repeated tests gave repeatable results which meant the result of specimens that were subjected to triaxial cyclic loading could be trusted.

7.1.2 Effect of water content

Water content plays a significant role in terms of the performance of the mudrock specimens. Its effects are listed below:

- The experimental results show a strong relationship between the resilient modulus and water content. An increase in water content decreases the resilient modulus for all particle size distributions and water contents tested.

- Dry mudrock showed the highest resilient modulus. Dry specimens also showed the most in-test scatter which was attributed to the relocation of the particles during the cyclic loading.
- Water content has a significant effect on the resilient modulus, as an increase in degree of saturation causes a decrease in the stiffness of the soil.
- Unsaturated soil conditions with smaller particle size show higher resilient modulus than the saturated state.
- It has been shown that the application of cyclic loading can lead to a considerable increase in stiffness.
- Inundation of the soil after loading caused a sharp drop in resilient modulus and sharp increase in settlement. This phenomenon has been linked in previous work to the degradation of the mudrock into clay.

7.1.3 Effect of stress state and load frequency

Track structure subgrades are exposed to different levels of stress that are produced from the train passing, and these are dependent on track type and depth of interest as well as train speed. Stress states were determined from the literature to represent the conditions below ballasted and ballastless track types, to allow the performance of mudrock to be studied. The effect of the stress states induced in the laboratory are listed below:

- Soil stiffness improved during cyclic loading, as it is became stiffer due to the breakage and rearrangement of the particles under repeated loading.
- This increase in the resilient modulus was found to depend on the stress state.
- The effects of increasing the deviatoric stress on the resilient modulus showed that, changing vertical stress combined with an increase the confining pressure caused an increase in the stiffness.
- Resilient modulus increased with a decrease in cyclic loading magnitude (with the stress distributions estimated from the track type, for the same soil conditions and the same confining pressure). In addition, smaller particles showed a higher cumulative strain under same confining pressure.
- A similar trend was recorded for cumulative deformation that was induced due to repeated loading.
- Permanent deformation at lower cyclic stresses is small.

- Load frequency has a positive impact on stiffness. As frequency changed from 4 Hz to 1 Hz a decrease in the stiffness was seen in commensurate tests.

7.2 Recommendations for future work

The following recommendations are listed below based on the results of this research:

- It is worth studying the effect of changing the confining stress on the stiffness of mudrock while keeping other components of stress constant. This may aid in the future development of a long-term constitutive model for the behaviour of mudrock.
- Static triaxial testing after cyclic testing to assess the effect of the loading on soil strength. This would allow the development of a model which could link the resilient modulus, number of cycles and compressive strength.
- Effect of a wider range of particle size distributions on the stiffness of mudrock should be investigated, enabling natural specimens to be tested (this would require a larger triaxial cell). Such tests would be more representative of materials in their natural state.
- As the frequency impacted on the resilient modulus and the settlement, rest periods between sets of cycles for mudrock would be worth investigating to more realistically simulate the real-world loading. In this test schedule would better simulate drainage conditions around particle contacts that must govern the rate of cumulative strain generation.
- According to the UK weather condition, the subgrade will have water draining downwards through it at several points of the year. Its worth to investigate the effect of wet/dry cycles on resilient modulus and cumulative strain.

There are also some specific requirements for the testing apparatus which should be considered in future work:

- To use a more advanced apparatus with the capability to capture every single cycle.
- To compare drained and undrained testing with the inclusion of a pore water pressure check.
- To measure the volume change by using an LVDT, hence giving more information about breakage particle and possible dilation during testing.

Bibliography

ABAQUS (2005). Version 6.5. *Users Manual, Providence, Rhode Island, USA*.

Ahlf, R. E. (1975). M/w costs: How they are affected by car weights and the track structure. *Railway track and structures*, 71(3).

Andrei, D., Witczak, M., Schwartz, C., and Uzan, J. (2004). Harmonized resilient modulus test method for unbound pavement materials. *Transportation Research Record: Journal of the Transportation Research Board*, (1874):29–37.

ASTM (2013). *2699 Standard Test Method for Research Octane Number of Spark-Ignition Engine Fuel*. ASTM.

Barksdale, R. D. (1972). Laboratory evaluation of rutting in base course materials. In *Presented at the Third International Conference on the Structural Design of Asphalt Pavements, Grosvenor House, Park Lane, London, England, Sept. 11-15, 1972.*, volume 1.

Bian, X., Jiang, H., Cheng, C., Chen, Y., Chen, R., and Jiang, J. (2014). Full-scale model testing on a ballastless high-speed railway under simulated train moving loads. *Soil Dynamics and Earthquake Engineering*, 66:368–384.

Bishop, A. and Wesley, L. (1975). A hydraulic triaxial apparatus for controlled stress path testing. *Geotechnique*, 25(4):657–670.

Blanchfield, R. (1998). *Volume change characteristics of opencast coal mine backfill.* PhD thesis, University of Sheffield.

Brecciaroli, F. and Kolisoja, P. (2006). Deformation behaviour of railway embankment materials under repeated loading: literature review. *Ratahallintokeskuksen julkaisuja. A*.

Brown, S. (1996). Soil mechanics in pavement engineering. *Geotechnique*, 46(3):383–426.

Brown, S., Lashine, A., and Hyde, A. (1975). Repeated load triaxial testing of a silty clay. *Geotechnique*, 25(1):95–114.

Burland, J. and Maswoswe, J. (1982). Discussion on in situ measurements of horizontal stress in overconsolidated clay using push-in spade-shaped pressure cells. *Géotechnique*, 32(2):285–286.

Carrera, A., Coop, M., and Lancellotta, R. (2011). Influence of grading on the mechanical behaviour of stava tailings. *Géotechnique*, 61(11):935.

Carrier III, W. D. (2003). Goodbye, hazen; hello, kozeny-carman. *Journal of geotechnical and geoenvironmental engineering*, 129(11):1054–1056.

Collins, R. (1976). Method for measuring the mineralogical variation of spoils from british collieries. *Clay Minerals*, 11(1):31–50.

Cripps, J. and Taylor, R. (1981). The engineering properties of mudrocks. *Quarterly Journal of Engineering Geology and Hydrogeology*, 14(4):325–346.

Czerewko, M. A. and Cripps, J. C. (2006). The implications of diagenetic history and weathering on the engineering behaviour of mudrocks. In *10th IAEG International Congress: Engineering Geology for Tomorrow's Cities. Paper*, number 118.

Dawson, A., Thom, N., and Paute, J. (1996). Mechanical characteristics of unbound granular materials as a function of condition. *Gomes Correia, Balkema, Rotterdam*, pages 35–44.

Dhakal, G., Yoneda, T., Kato, M., and Kaneko, K. (2002). Slake durability and mineralogical properties of some pyroclastic and sedimentary rocks. *Engineering Geology*, 65(1):31–45.

Dick, J. and Shakoor, A. (1992). Lithological controls of mudrock durability. *Quarterly Journal of Engineering Geology and Hydrogeology*, 25(1):31–46.

Dobbs, M., Culshaw, M., Northmore, K., Reeves, H., and Entwisle, D. (2012). Methodology for creating national engineering geological maps of the uk. *Quarterly Journal of Engineering Geology and Hydrogeology*, 45(3):335–347.

Donohue, S., O'Sullivan, C., and Long, M. (2009). Particle breakage during cyclic triaxial loading of a carbonate sand. *Géotechnique*, 59(5):477–482.

Drumm, E., Boateng-Poku, Y., and Johnson Pierce, T. (1990). Estimation of subgrade resilient modulus from standard tests. *Journal of Geotechnical Engineering*, 116(5):774–789.

Dumbleton, M. J. and West, G. (1966). Studies of the keuper marl: mineralogy.

Duong, T. V., Cui, Y.-J., Tang, A. M., Dupla, J.-C., Canou, J., Calon, N., and Robinet, A. (2016). Effects of water and fines contents on the resilient modulus of the interlayer soil of railway substructure. *Acta Geotechnica*, 11(1):51–59.

Edil, T. B. and Motan, S. E. (1979). Soil-water potential and resilient behavior of subgrade soils. *Transportation Research Record*, (705).

Esveld, C. (2001). Modern railway track.

Feeley, A. (1994). UTM-5P, universal testing machine, hardware reference manual. *Industrial Process Controls Limited, Boronia, Australia.*

Franklin, J. and Chandra, R. (1972). The slake-durability test. In *International Journal of Rock Mechanics and Mining Sciences & Geomechanics Abstracts*, volume 9, pages 325–328. Elsevier.

Fredlund, D., Bergan, A., and Wong, P. (1977). Relation between resilient modulus and stress conditions for cohesive subgrade soils. *Transportation Research Record*, (642).

Fredlund, D. G. and Rahardjo, H. (1993). *Soil mechanics for unsaturated soils.* John Wiley & Sons.

Gräbe, P. and Clayton, C. (2009). Effects of principal stress rotation on permanent deformation in rail track foundations. *Journal of Geotechnical and Geoenvironmental Engineering*, 135(4):555–565.

Gräbe, P. J. (2002). *Resilient and permanent deformation of railway foundations under principal stress rotation.* PhD thesis, University of Southampton.

Hanazato, T., Ugai, K., Mori, M., and Sakaguchi, R. (1991). Three-dimensional analysis of traffic-induced ground vibrations. *Journal of geotechnical engineering*, 117(8):1133–1151.

Head, K. H. and Epps, R. (1986). *Manual of soil laboratory testing*, volume 3. Pentech Press London.

Hicks, R. G. and Monismith, C. L. (1971). Factors influencing the resilient response of granular materials. *Highway research record*, (345).

Higuchi, T. (2002). *Liquefaction and cyclic failure of low plasticity silt.* PhD thesis, University of Sheffield, Department of Civil and Structural Engineering.

Hveem, F. N. (1955). Pavement deflections and fatigue failures. Technical report.

Indraratna, B., Ionescu, D., and Christie, H. (1998). Shear behavior of railway ballast based on large-scale triaxial tests. *Journal of geotechnical and geoenvironmental Engineering*, 124(5):439–449.

Kamal, M., Dawson, A., Farouki, O., Hughes, D., and Shaat, A. (1993). Field and laboratory evaluation of the mechanical behavior of unbound granular materials in pavements. *Transportation Research Record*, pages 88–88.

Kempfert, H. and Hu, Y. (1999). Measured dynamic loading of railway underground. In *Proc., 11th Pan-American Conf. on Soil Mechanics and Geotechnical Engineering*, pages 843–847. International Society for Soil Mechanics Brazil.

Knutson, R., Thompson, M., Mullin, T., and Tayabji, S. (1977). Ballast and foundation materials research program. phase iv. materials evaluation study. Technical report.

Lackenby, J. (2006). Triaxial behaviour of ballast and the role of confining pressure under cyclic loading.

Lade, P. V., Yamamuro, J. A., and Bopp, P. A. (1996). Significance of particle crushing in granular materials. *Journal of Geotechnical Engineering*, 122(4):309–316.

Lee, K. L. and Farhoomand, I. (1967). Compressibility and crushing of granular soil in anisotropic triaxial compression. *Canadian geotechnical journal*, 4(1):68–86.

Lekarp, F. (1999). *Resilient and permanent deformation behavior of unbound aggregates under repeated loading*. PhD thesis, Institutionen för infrastruktur och samhällsplanering.

Lekarp, F., Isacsson, U., and Dawson, A. (2000). State of the art. i: Resilient response of unbound aggregates. *Journal of transportation engineering*, 126(1):66–75.

Li, D. (1994). Railway track granular layer thickness design based on subgrade performance under repeated loading. *Journal of Geotechnical Engineering*, 120(6):939–957.

Li, D., Hyslip, J., Sussmann, T., and Chrismer, S. (2002). *Railway geotechnics*. CRC Press.

Li, D. and Selig, E. T. (1996). Cumulative plastic deformation for fine-grained subgrade soils. *Journal of geotechnical engineering*, 122(12):1006–1013.

Li, D. and Selig, E. T. (1998). Method for railroad track foundation design. i: Development. *Journal of Geotechnical and Geoenvironmental Engineering*, 124(4):316–322.

Liu, E.-L., Chen, S., Lai, Y., Wei, W., and Fu, Z. (2016). Particle breakage of artificially crushable materials subject to drained cyclic triaxial loading. *Soil Dynamics and Earthquake Engineering*, 89:262–268.

Liu, J. and Xiao, J. (2009). Experimental study on the stability of railroad silt subgrade with increasing train speed. *Journal of Geotechnical and Geoenvironmental Engineering*, 136(6):833–841.

Madshus, C. and Kaynia, A. (2000). High-speed railway lines on soft ground: dynamic behaviour at critical train speed. *Journal of Sound and Vibration*, 231(3):689–701.

Marsal, R. (1967). Large-scale testing of rockfills materials. *Journal of the Soil Mechanics and Foundation Engineering Division, ASCE*, 93:27–44.

McDowell, G., Bolton, M., and Robertson, D. (1996). The fractal crushing of granular materials. *Journal of the Mechanics and Physics of Solids*, 44(12):2079–2101.

Meca, J. B. (2005). *Rate effects of rapid loading in clay soils.* PhD thesis, University of Sheffield.

Monismith, C. L., Ogawa, N., and Freeme, C. (1975). Permanent deformation characteristics of subgrade soils due to repeated loading. *Transportation Research Record*, (537).

Moossazadeh, J. and Witczak, M. W. (1981). Prediction of subgrade moduli for soil that exhibits nonlinear behavior. *Transportation Research Record*, (810).

Morgan, J. (1966). The response of granular materials to repeated loading. *Australian Road Research Board Proc.*

Morgenstern, N. R. and Eigenbrod, K. D. (1974). Classification of agrillaceous soils and rocks. *Journal of Geotechnical and Geoenvironmental Engineering*, 100(Proc Paper 10885 Proceeding).

Nahazanan, H. (2010). *The compression of mudrock fills.* PhD thesis, University of Sheffield.

Nguyen Gia, K., Goicolea Ruigómez, J. M., and Gabaldón Castillo, F. (2011). Dynamic effect of high speed railway traffic loads on the ballast track settlement.

Oda, M. and Konishi, J. (1974). Microscopic deformation mechanism of granular material in simple shear. *Soils and foundations*, 14(4):25–38.

O'Neill, M. A. (2007). *Creep settlement of opencast mine backfill*. Sheffield Hallam University (United Kingdom).

O'Reilly, M. P., Brown, S. F., et al. (1991). *Cyclic loading of soils: from theory to design*. Blackie and Son Ltd.

Pappin, J. and Brown, S. (1980). Resilient stress-strain behaviour of a crushed rock. In *Proceedings, International Symposium on Soils Under Cyclic and Transient Loading, Swansea, Great Britain*, volume 1, pages 169–177.

Peterson, R. W. (1988). Interpretation of triaxial compression test results on partially saturated soils. In *Advanced Triaxial Testing of Soil and Rock*. ASTM International.

Potter, P. E., Maynard, J. B., and Depetris, P. J. (2005). *Mud and mudstones: Introduction and overview*. Springer Science & Business Media.

Powrie, W. (2013). *Soil mechanics: concepts and applications*. CRC Press.

Powrie, W., Priest, J., and Clayton, C. (2008). Recent research on railway track sub-base behaviour. In *Advances in Transportation Geotechnics: Proceedings of the International Conference held in Nottingham, UK, 25-27 August 2008*, page 37. CRC Press.

Powrie, W., Yang, L., and Clayton, C. R. (2007). Stress changes in the ground below ballasted railway track during train passage. *Proceedings of the Institution of Mechanical Engineers, Part F: Journal of Rail and Rapid Transit*, 221(2):247–262.

Prakash, S. (1981). *Soil dynamics*. McGraw-Hill New York.

Priest, J. and Powrie, W. (2009). Determination of dynamic track modulus from measurement of track velocity during train passage. *Journal of geotechnical and geoenvironmental engineering*, 135(11):1732–1740.

Proctor, R. (1933). Fundamental principles of soil compaction. *Engineering News-Record*, 111(13).

Rainbow, A. (1987). Minestone fill in reinforced earth abutments. *Highways and transportation*, 34(6):25–31.

Seed, H., Mitry, F., Monismith, C., and Chan, C. (1967). Factors influencing the resilient deformations of untreated aggregate base in two-layer pavements subjected to repeated loading. *Highway Research Record*, (190).

Seed, H. B. and Chan, C. (1958). Effect of stress history and frequency of stress application on deformation of clay subgrades under repeated loading. In *Highway Research Board Proceedings*, volume 37.

Seed, H. B., Chan, C., and Lee, C. E. (1962). Resilience characteristics of subgrade soils and their relation to fatigue failures in asphalt pavements. In *International Conference on the Structural Design of Asphalt Pavements. SupplementUniversity of Michigan, Ann Arbor*.

Seed, H. B., Chan, C. K., and Monismith, C. L. (1955). Effects of repeated loading on the strength and deformation of compacted clay. In *Highway research board proceedings*, volume 34.

Shackel, B. (1974). Repeated loading of soils a review. In *International Journal of Rock Mechanics and Mining Sciences & Geomechanics Abstracts*, volume 11, page A220. Pergamon.

Stewart, H. E. (1982). The prediction of track performance under dynamic traffic loading.

Taylor, R. (1988). Coal measures mudrocks: composition, classification and weathering processes. *Quarterly Journal of Engineering Geology and Hydrogeology*, 21(1):85–99.

Taylor, R. and Garrard, G. (1984). Design shear strengths for uk coarse colliery discards. In *Proceedings of a Symposium on Reclamation, Treatment Utilisation of Coal Mining Wastes, Durham, England*, pages 34–1.

Taylor, R. and Smith, T. (1986). The engineering geology of clay minerals; swelling, shrinking and mudrock breakdown. *Clay Minerals*, 21(3):235–260.

Taylor, R. and Spears, D. (1970). The breakdown of british coal measure rocks. 7(5):481–501.

Taylor, R. and Spears, D. (1981). Laboratory investigation of mudrocks. *Quarterly Journal of Engineering Geology and Hydrogeology*, 14(4):291–309.

Terzaghi, K. (1960). From theory to practice in soil mechanics: selections from the writings of k. terzaghi. Technical report, Wiley.

Thom, N. and Brown, S. (1988). The effect of grading and density on the mechanical properties of a crushed dolomitic limestone. In *Australian Road Research Board (ARRB) Conference, 14th, 1988, Canberra*, volume 14.

Thom, N. and Brown, S. F. (1987). *Effect of moisture on the structural performance of a crushed-limestone road base*. Number 1121.

Thompson, M. R. and Robnett, Q. L. (1976). Resilient properties of subgrade soils. Technical report.

Wood, D. M. (1980). Laboratory investigation of the behaviour of soils under cyclic loading: A review. Technical report.

Yang, L., Powrie, W., and Priest, J. (2009). Dynamic stress analysis of a ballasted railway track bed during train passage. *Journal of Geotechnical and Geoenvironmental Engineering*, 135(5):680–689.

Zaman, M., Chen, D.-H., and Laguros, J. (1994). Resilient moduli of granular materials. *Journal of Transportation Engineering*, 120(6):967–988.